Molecular Mechanisms of Golgi Structure Alterations during Stress

by

Stephen C. Ireland

A dissertation submitted in partial fulfillment
of the requirements for the degree of
Doctor of Philosophy
(Molecular, Cellular, and Developmental Biology)
in The University of Michigan
2020

Doctoral Committee:

Professor Yanzhuang Wang, Chair
Professor Robert Fuller
Professor John Kuwada
Professor Haoxing Xu

"A little learning is a dangerous thing. Drink deep, or taste not the Pierian spring; There shallow draughts intoxicate the brain and drinking largely sobers us again."

-Alexander Pope, "An Essay on Criticism" (1709)

Stephen C. Ireland

scirelan@umich.edu

ORCID iD: 0000-0002-1498-2864

To my parents.

Acknowledgements

I owe a debt of gratitude to many individuals for helping me complete a doctoral program at The University of Michigan. I would like to thank each of them for their help, which has been so gratifying along the way.

First, I would like to thank my advisor Yanzhuang Wang. I had not originally intended to work in Wang's lab, and if I am being honest I had initially wanted to rotate in his lab more to learn the techniques than the research itself. I arranged to interview on a lark. We "chatted" about the work I was to do and I left his office with the thought going through my head, "what just happened?". Ever since, I have always left his office feeling different sorts of things and never the same as when I went in. I'm not sure anyone else could have provided such encouragement for so long. There were many dark days especially during the first couple years when things seemed very hopeless but he always stuck it out with me. I started in his lab not knowing a thing about cell biology and I left his lab feeling like an expert in the field and knowing a lot of techniques.

I would also like to thank my dissertation committee members. In fact, both John Kuwada and Haoxing Xu were also mentors. John was my first mentor at UM and my impression was sheer awe at the depth of his knowledge and the ease at which he shared and discussed experiments. Haoxing was extremely supportive. As one example, he wrote a letter for me to present a paper I published in a previous lab and put a lot of trust in me. Edward Stuenkel

served earlier on my committee and I would like to thank him for his many suggestions. Finally, Robert Fuller, has helped me in many ways especially by encouraging me to think about finding a job, organizing the Trafficking Club, inviting me to give a talk, and for playing his great music at the GRC meetings!

I have had countless student mentors for which my thanks would be hard to understate. Kenichi Iwasaki was my first mentor. His quiet technical prowess and light-hearted camaraderie, has left a lasting impression on me. His attention to detail in the lab was astonishing. He also taught me to stop complaining about being from Michigan and that I spoke English as my first language. I would also like to thank Jiaxing Li, although we never worked together, he was a constant lunch companion where we discussed many aspects of student life on and off the campus. Xinran Li and Nirakar Sahoo were also great golfing partners outside of campus. Those guys are a lot of fun, great scientists, and role models.

I would like to thank current and past members of the Wang lab. Mingzhou Fu was my first colleague. Mingzhou taught me cell culture in a very non-threatening way and She was very professional. Michael Bekier helped me with cell culture while telling me all about his home life. Xiaoyan Zhang surprised and opened my eyes to how special wet lab work and molecular biology can be. There was a time I began to lose hope in an assay and gave her the same ingredients I had been using. Within 24 hours she was able to perform on small scale what I had written off as impossible and taught me a valuable lesson not to give up. Jie Li is one of my favorite humans. She was constantly singing which reminded me of how my mother sang when I was little. When someone is open about singing it means (to me) they have a clear conscience and a pure heart. She was always singing, writing poetry on windows in dry-erase, and putting

heart patterns in pipette boxes. That kind of rare personality on an otherwise gray day always made me thankful. Erpan Ahat, a more recent comer to the Wang lab is a fine young man.

I would also like to thank a nearly constant stream of work study undergraduates Sahal, Shaylin, Morgan, Kelly, Yoonseo and Liye. Thank you for keeping up with the lab. A special thank you to Morgan who helped with the move from the Kraus Building to the new Biological Sciences Building.

Courtney Killeen is a military veteran and briefly served as a tech in the Wang lab. I thank Courtney for making gels and for her military service.

I would like to thank three of my undergraduate researchers. Haoran, was one of my best undergraduate researchers. In return for proofreading her medical school applications, I'd like to bring my future children for free annual checkups once she becomes a pediatrician, as agreed. Dabel Emebo was way cooler than me, but then again, all of my undergraduates were. Dabel in particular was much better dressed than me. Thank you Dabel for telling me I look homeless and should shave my beard. Finally, Shun Enomoto, thank you for your help tying up some of the loose ends in my research project and working hard in the lab with almost no encouragement and oversight while I wrote the dissertation.

I would next like to thank the nice ladies in the MCDB office. Mary Carr in particular, at first intimidating with her seriousness, reminded me of the mental grit that my grandmother had. I wonder if Mary Carr can snap rattle snake necks with a single crack just like my grandmother claimed she could. Diane Durfy, who helped me apply for funding, although we didn't get it, it was a good try! Jacqueline Glebe was very helpful for ordering many of the tools used in the lab, and being patient with me. Finally, Christine Bolang was very helpful answering many of my tax-related and sometimes last minute questions.

There are many people deserving gratitude related to microscopy. Gregg Sobocinski helped me countless times. Many times Gregg and I groused together about this or that. Dana Holcomb, our Zeiss representative, went above and beyond her job description as our sales representative to help us diagnose and sometimes even fix many of our technical problems. Miles McKenna and Edwin De Feijter from Nikon were also great help to my research.

I would like to thank my friends and family. My mom, who sometimes I reported events about the PhD process, would say, "just tell me who I need to beat up." Mom has brightened my world in more ways than I can count and I owe everything to her.

Thanks also to my dad, who I talked to many many times, sometimes at great length about the PhD process, what it means, and why we subject ourselves to it, and why it is worth it. I think we always concluded it was.

William Curtiss, my grandfather, passed away during my post-graduate time at Michigan. I looked up to him a great deal. He was a pillar of family strength and desperately wanted each of his grandchildren to follow in his footsteps and become a physician. After volunteering once in a hospital, I knew I didn't at all want to be a doctor. His father had wanted him to be an oilman and the story goes, Bill had had to punch him out in order to leave the oil fields to study medicine. I explained that parallel to him about a month before he died and he finally accepted my choice. Besides, Lizzie, his granddaughter, will be a doctor soon.

My grandmother, Shirley Ireland, also passed during my graduate studies. She loved roses and was always in good spirits. She invited me to give a talk at The Rose Society of Detroit and we got along splendidly. I hope "Die Kleine" is finally content in that rose garden up yonder.

My other grandmother Margaret (Gene) Curtiss who also died while I was enrolled in MCDB, always claimed I didn't know the value of a dollar or the true value of time. Moreover, I didn't have respect for those who were bigger than me (her at the time). She looked after us a lot when I was little and was always sweet to me despite her sharp tongue.

My brother Carl is a constant source of enjoyment mostly with text messages and group texts between friends. He has also been a good role model. I guess I helped him get through the army with letters, and he's always helped me with a kind word or gesture, or a beer. I also thank him for serving in the armed forces. I am glad he didn't get his head blown off. My nephew Graham is like a beam of sunshine when I see him. Carl and Kristen have done a lot of work and helped me with my living situations in Ann Arbor making it one less thing to worry about.

Many other friends and family have been positive reinforcement. Lizzie , Emma, and Laura Hyde, all have unique and exciting lives that have given me ideas on trips to take in the future to visit them. Their mom, my aunt Cristy, is a lucky woman. Many personal friends outside of MCDB have helped to keep me sane and given me encouragement. Alison Landau, a dear friend, has accompanied me on many short weekend trips to explore different cities and these trips have kept me relatively normal and socially adjusted. Aloy Gu has been a truly lasting friend and supplied me with much of the authentic Chinese tea I have. Aloy always demands I bring my A-game into conversations and he is fun to see or speak to now and again. Andrew and Marti and their new baby, Autumn, have hosted many pleasant bonfire's that have been a welcome interlude in my studies. My friends who live far away also have been very interested in my progress and have asked me countless times "so when are you going to be done with that PhD?" which actually is a very good question because it reminded me that the PhD is not an end in and of itself.

I wish to thank all of my colleagues, friends, and family and please excuse all the times I was unavailable during my doctoral studies. Hopefully things will get better now.

Preface

I joined the MCDB department in July 2014, and the Wang lab as a graduate student on April 15, 2015. The data in this dissertation mainly came from two manuscripts developed while in the Wang lab.

Originally, there were four goals for this dissertation:

1) Develop a set of criteria for determining Golgi stress.
2) Screen a number of different stress conditions in cells using those criteria.
3) Describe a molecular mechanism of Golgi stress.
4) Perform experiments in a physiological model of Golgi stress.

Much of Chapter I is from work performed while doing a full semester rotation in the Wang lab. Conceptually, Chapter I describes the system model and discusses progress made to accomplish goals 1 and 2, i.e., to establish a robust criteria of Golgi stress and screen cell stresses using it.

The data presented in Chapter II was fundamental towards reaching goal 3, discovering a mechanism of Golgi stress.

For this project, some of the Golgi stresses discovered and our criterion for measuring them, were deeply explored to find the mechanism. An initial observation, that thapsigargin caused Golgi fragmentation was made by a former student in the Wang lab, Saiprasad

Ramnarayanan, who was a co-author on the work that was eventually published. Mingzhou Fu also made important contributions in the early stages of this work and was a co-author. After continuing this work and developing it significantly in this study, which includes a physiological model of Golgi stress, the final full research article, **Cytosolic Ca^{2+} Modulates Golgi Structure Through PKCα-Mediated GRASP55 Phosphorylation**, was published in *iScience, March 27 2020; 23, 100952*. Stephen Ireland, Sai Ramnarayanan and Yanzhuang Wang designed the project. Stephen Ireland performed the experiments for Figure 2.1C-D, 2.1E-G, 2.2A-D, 2.3A, 2.3D-H, 2.4, 2.5, 2.6, 2.7, 2.8, 2.9, 2.10, 2.11A-D, 2.12, 2.13; Saiprasad Ramnarayanan performed the experiments for Figure 2.1A-B, 2.1E-G, 2.3A-C, 2.3E-G, 2.5A-B, 2.5F-G; Mingzhou Fu performed the experiments for Figure 2.1A-B, 2.1E-G, 2.3A-C, 2.3E-G, 2.5A-B, 2.5F-G; Jianchao Zhang performed the experiments in Figure 2.11E-F; Jie Li made reagents used in Figure 2.10D-E; Dabel Emebo performed the experiments for Figures 2.2E-F. Stephen Ireland, Sai Ramnarayanan and Mingzhou Fu analyzed the data. Stephen Ireland and Yanzhuang Wang wrote the paper.

Data from Chapter III comprises a continuation of goal 3, to explore molecular mechanisms, but with a different set of stressors that had an apparently different mechanism. This chapter arose from the discovery that not all Golgi stresses lend themselves to easy characterization by the initial fragmentation criterion, namely, the use of fluorescent microscopy to score or grade fragmentation level. This manuscript includes a new way to think about Golgi stress in terms of ultrastructural and biochemical changes in the cell. Some of the important preliminary data for this work was collected by undergraduate students, Haoran Huang and Shun Enomoto. A manuscript summarizing these findings entitled **Hydrogen peroxide induces Arl1 degradation and impairs Golgi-mediated trafficking** is currently in revision in the journal

MBoC. Stephen Ireland, Haoran Huang and Yanzhuang Wang designed the project. Stephen Ireland, Jianchao Zhang and Haoran Huang performed the experiments: Stephen Ireland performed the experiment for Figure 3.1A, 3.2, 3.4, 3.5, 3.6A, 3.7; Haoran Huang performed the experiment for Figure 3.1A, 3.2, 3.3, 3.6A, 3.8; Jianchao Zhang performed the experiment for Figure 3.1B. Stephen Ireland and Haoran Huang analyzed the data. Stephen Ireland and Yanzhuang Wang wrote the paper.

Chapter IV contains concluding remarks related to what is believed to be the important central conclusions of this research study with respect to accomplishing or suitably addressing stated goals. Chapter IV, is hoped to encourage future scientists to continue the work and build upon it. The chapter concludes with a brief vignette demonstrating an important open question and possible avenue(s) for future research. In this case, Stephen Ireland designed the project. Stephen Ireland analyzed the data for Figure 4.1A. Stephen Ireland performed experiments for Figure 4.1B-E.

Table of Contents

List of Figures

Abstract

In mammals, the Golgi apparatus has a unique stacked structure that is important for its function; yet, the Golgi structure is dynamic and its structure and function changes in response to different stress conditions applied to the cell. Since Golgi functions are abnormal in stress, it implies that Golgi structure may play a critical role in human diseases.

This research project studied how the Golgi apparatus responds to stress. The study process followed in a stepwise progression: First, it was necessary to determine how the Golgi responded to endoplasmic reticulum (ER) stress; findings indicated that the Golgi is fragmented in response to thapsigargin (TG) but not to other ER stress inducers such as tunicamycin (Tm) and dithiothreitol (DTT). Since TG treatment is known to cause an increase in cytosolic calcium, it was useful to determine whether a calcium-sensitive kinase could act as the trigger of Golgi morphological change. This led to identification of protein kinase C-α (PKCα) and its substrate GRASP55 in calcium stress-induced Golgi fragmentation, and abnormal Golgi functions. More generally, cytosolic calcium is a logical trigger in the Golgi structure alteration process during stress, as it has been shown to be regulated during several cellular processes. Subsequently, this study confirmed that activating or inflammatory agents induce Golgi fragmentation and cytosolic calcium increase via a similar mechanism.

These findings are of great interest to cell biologists who are working on Golgi dynamics, membrane trafficking, cellular responses to stresses, and histamine biology.

Next, several novel findings are described where, reactive oxidative species (ROS) induce the degradation of Golgi structural proteins in the *trans*-Golgi, including Arl1, Golgin-97, and Golgin-245, and thereby impair membrane trafficking.

This work is believed to be the first systematic study of how ROS affects Golgi structure and function. It revealed the *trans*-Golgi and trafficking at the *trans*-Golgi as novel targets of ROS in cells, which may help understand the toxicity of ROS in human diseases. It also found that the degradation of Arl1, Golgin-97 and Golgin-245 is not mediated by proteasomes nor lysosomes, but rather by cytosolic proteases. This finding underscores the importance of cytosolic proteases whose importance has been often underestimated in recent studies.

During this study, some molecular tools were designed and constructed to detect Golgi calcium signals in cells using GCaMP-based sensors. The main advantage of this sensor is that the GCaMP calcium probe is covalently linked to GRASP55 on the Golgi and can directly sense and detect fluctuations of local cytoplasmic calcium in the vicinity of the Golgi. This tool is essentially a *de facto* Golgi stress sensor, which can be used by others who wish to quickly screen for compounds that reduce calcium-related Golgi fragmentation during stress.

Besides calcium imaging was an opportunity to develop another set of tools for imaging specific proteins of interest at the ultrastructural level. These sensors utilize a recombinant ascorbate peroxidase (apex) enzyme to catalytically precipitate an electron dense product in the vicinity of a cellular protein of interest. In the lab the apex gene was linked to each GRASP55 and GRASP65 with the hopes that future researchers will utilize this fusion protein to identify the precise intracellular localizations of these proteins with high resolution.

CHAPTER I

Introduction[1]

1.1 Overview of the exocytic and endocytic trafficking system

The cell is a highly ordered machine in large part due to a correctly functioning endocytic trafficking system (**Fig. 1.1**) (Glick and Nakano, 2009). For conventionally secreted proteins, newly synthesized polypeptides in the endoplasmic reticulum (ER) are folded and packaged into transport carriers. The nascent polypeptides and lipids then progress through the intermediate compartments and make their way to the Golgi apparatus (Saraste and Marie, 2018). Transport vesicles fuse and their contents begin a modification process with numerous essential surface features, including sugar and phosphate groups, as they make their way through the Golgi. Trafficking between Golgi compartments relies on a group of long coiled-coil proteins called golgins, which act as membrane tethers to capture vesicles and facilitate their fusion with the Golgi membranes (Lupashin and Sztul, 2005; Muschalik and Munro, 2018; Witkos and Lowe, 2015; Xiang and Wang, 2011).

---

[1] The data from Figure 1.4 was revised from works referenced in the corresponding figure legend and in the text related to the figure. Figure 1.6 from this chapter was modified from data originally published in *Golgi biogenesis.* Cold Spring Harb Perspect Biol, 2011. 3(10): p. a005330, with authors listed as Wang, Y. and J. Seemann.

Maturation of biosynthetic products often must be a sequential process, and there are two competing models of how this occurs; in one model enzymes are located in a systematic way within an assembly line composed of *maturing cisternae,* this is also mediated by membrane tethers (Munro, 2011). Anterograde movement through the Golgi is mediated by packaging into discrete units called COPII vesicles that coalesce to form new Golgi cisternae (McCaughey and Stephens, 2018). Retrograde travel to return cargo, Golgi enzymes, or endocytosed materials to an earlier stage of the endocytic trafficking system including the Golgi happens via COPI vesicles (Ishii et al., 2016). A third type of vesicle, clathrin-coated vesicles are destined for endosome/autophagosome via multivesicular bodies. Clathrin-coated vesicles originate from an area of the Golgi called the trans-Golgi network (TGN) and were discovered to also emerge from the plasma membrane (Mettlen et al., 2018). The Golgi cisternae, however, seem to be *stable compartments* that accept cargo via incoming COPII vesicles from the ER.

Whatever model of Golgi transport one embraces, protein products are packaged and leave the Golgi toward destinations within and outside the cell (Pantazopoulou and Glick, 2019). The Golgi processes many important proteins, but there are examples of secreted proteins that bypass the Golgi apparatus, which are altogether called unconventionally secreted proteins; but these will not be discussed in detail here. In general, the Golgi apparatus must balance biosynthetic and degradative pathways and can be characterized as a factory in the cell. The Golgi therefore must coordinate many proteins to organize the unique stacked structure and cope with dynamic bi-directional trafficking.

1.1.1 Introduction to the Golgi apparatus

The Golgi apparatus is a membrane organelle in the center of the endomembrane system. It is responsible for protein and lipid trafficking, processing, and secretion. As many as 30% of all proteins encoded by the human genome, including hormones, enzymes, and immunoglobulins, are processed by the Golgi with speed and fidelity (Pfeffer, 2010). The Golgi has a unique and recognizable shape as a stacked structure of parallel flattened cisternae (**Fig. 1.1**). It is located adjacent to the centrosome, near the center of most cell types along with the nucleus (**Fig. 1.2)**. There are on average a few dozen Golgi stacks per cell which are connected laterally to form the so-called "Golgi ribbon."

The structure of the Golgi is physically dynamic. During cell cycle progression, it is reversibly disassembled (Barr et al., 1997). During programmed cell death it is irreversibly disassembled (Mancini et al., 2000). An important aspect of Golgi biology is that its structure determines its functions (**Fig. 1.3**).

1.1.2 Golgi structure and position

The Golgi stack has essential structural features. It is polarized and it contains distinct *cis*-/*trans*-compartments. In general, incoming cargo, received from the ER, is progressively modified until the product is sorted and sent to its required destination.

In the evolutionary past, the Golgi's polarity presented cells with a problem during mitosis, a process in which the cell and each organelle must divide in half. The problem was, how to

ensure the next generation of cells would have equal proportions of the Golgi arranged in the proper way.

The cell's solution for equal proportioning of the Golgi apparatus during cell division is an elegant disassembly and reassembly process with well-defined phases. During mitosis, the Golgi ribbon becomes untethered, the stacks become unstacked, and the cisternae are shortened and become vesiculated (Tang et al., 2012). Vesiculation permits vesicles to spread evenly throughout the cytoplasm. At the end of mitosis in telophase, the entire process runs in reverse. Vesicles fuse depending on their constituent parts and membranes restack to form the Golgi ribbons again. This well-choreographed process depends on the careful coordination of many molecular machineries in the cell including kinases and phosphatases, ubiquitin ligases and deubiquitinases, vesicle fission and fusion machineries as well as many others.

In interphase, the Golgi ribbon in mammalian cells forms near the microtubule organizing center (MTOC) of the cell near the centrosome (Yadav and Linstedt, 2011). There are some exceptions, but this study observed the normal Golgi shape at the ultrastructural level is an elaborate complex of four-to-eight long membranous, stacked cisternae that connect laterally to form an articulated ribbon (**Fig. 1.3B**). This ribbon is held in place due to the persistent actions of the microtubule minus-end directed motor protein Dynein that carries Golgi membranes to a pericentriolar region along microtubule network. Microtubules are required for lateral linking of the Golgi ribbon. It was found that treatment of cells with the microtubule depolymerizing drug nocodazole disperses Golgi stacks throughout the cell (Cole et al., 1996).

1.1.3 Golgi function and significance

While the Golgi has a recognizable structure, it is not always clearly understood what it does. However, viewing the Golgi as a factory in the cell is a useful analogy. A factory receives inputs from outside sources and assembles larger, more complex, items from the basic building block components. Once the product is boxed and labeled, the item is loaded on a vehicle for delivery.

In the Golgi/factory analogy, the primary function of the Golgi involves the processes of material handling, modifications, and sorting, to produce secretory proteins and lipids. During processing there is a step-wise exposure of secretory traffic to the unique enzyme and sorting machinery containing compartments of the Golgi apparatus. As these cargos are exposed to enzymes in each Golgi cisternae, they are processed with modifications such as glycosylation and phosphorylation and grow in complexity (Capasso et al., 1989; Fleischer, 1983).

Many protein products encoded by the human genome would have no function if not for further processing by the Golgi apparatus (Miyoshi et al., 2020). A particular example takes place in professional secretory cells called goblet cells lining mucous membranes (Araujo et al., 2019). These cells produce abundant amounts of pre-glycoproteins called mucins that are received by the Golgi. There, they are modified with carbohydrate additions called O-GalNAc glycans by the activity of polypeptide O-GalNAc-transferases (GALNTs) (Brockhausen and Stanley, 2015). When ready, mature mucus molecules are secreted via secretory granules. This is the highly "sticky" substance that traps invaders in the respiratory system before they can do much harm. In this sense, the Golgi adds and refines the biological materials with more information and complexity, allowing an otherwise nonfunctional protein do a real job in the real world.

Proteins can be modified with numerous modifications in the Golgi and would not function properly otherwise; these proteins include immunoglobulins, neurotransmitters, growth factors, cell surface receptors, cell adhesion molecules, and many others needed for organism health and survival.

1.2 Golgi stress definition, types, and regulators

Golgi stress can be defined as perturbations of Golgi functions of sorting, trafficking and modifications. Because the Golgi lies in the middle of the membrane trafficking pathway and may house the majority of enzymes in the cell (Colley, 1997), disorganization of Golgi membranes often causes abrupt biological and morphological changes within the cell necessary to maintain homeostasis.

Researchers have developed numerous ways to observe Golgi structural disorganization in the cell including by using various modalities of microscopy including immunofluorescence (Thayer et al., 2013), and electron microscopy (EM) (Bekier et al., 2017). These researchers have broken down structural change into several metrics which include swelling, enlargement, compaction, disorganization, fragmentation, and so on. However, we will define Golgi structural disorganization during stress as "fragmentation" to contrast it with the "disassembly" that occurs during the cell cycle.

The Golgi is fragmented and exhibits signs of morphological and functional changes in several major human diseases including Alzheimer’s, cancer, and amyotrophic lateral sclerosis (ALS)

(**Fig. 1.4A-B**) (Mourelatos et al., 1996; Petrosyan, 2015; Sundaramoorthy et al., 2015). Some stresses including overactivation of neurons also induce a clear Golgi fragmentation phenotype (**Fig. 1.4C-F**) (Thayer et al., 2013).

Although the Golgi is directly responsible for the proper functioning of proteins essential for human health and survival, little is known about the biological processes that lead to Golgi fragmentation and Golgi functions during stress and disease. Intermediate steps could be required to transduce a change of the Golgi, such as secondary messengers like calcium or reactive oxygen species (ROS). It is also not known to what extent exogenous or endogenous stresses play in Golgi functions. How the Golgi looks during dynamic regulation to respond to multiple types of cellular stress, or damage by stress leading to functional consequences for the cell, is the topic of this research investigation.

Cellular stress is not a new field of study. Some things are known about the Golgi with respect to known stress pathways. One example of the tight coupling of secretory pathway stress responses, is the relationship between the endoplasmic reticulum unfolded protein response (UPR) and Golgi stress. This connection has been hypothesized by Oku et al. to be due to a rapid increase of substrates in the Golgi as the ER rapidly produces secretory and membrane proteins during UPR, placing increasing demands on the Golgi by cargo crowding (Oku et al., 2011). The Golgi's unique stacked structure could provide a mechanism to balance the speed by which biochemical modifications can be made, with the fidelity. For example, if there is a robust increase in demand on glycolytic processing, then it might benefit the cell to decrease Golgi stacking and increase membrane surface area. Experimental data covered in **Chapter II** showed this was the case. In

Chapter II, questions are raised concerning whether the Golgi morphological changes, that occur as a consequence to ER stress inducing drugs, actually precede the well characterized UPR. Since, the Golgi structure becomes smaller and more compact upon starvation, and fragments during apoptosis, any explanation of Golgi fragmentation must account for the occurrence during normal conditions including cell division and apoptosis.

If the Golgi is indeed not responding to ER stress but actually has the ability to enact its own changes in the cell in response to external triggers this brings up an intriguing possibility. A growing body of work, including this study, shows that there are Golgi-specific stress pathways in the cell. Many groups have reported that Golgi-associated genes, including glycosylation enzymes and vesicular trafficking components are upregulated during Golgi stress, along with Golgi fragmentation. For example, mutations that disrupt Golgi structural organization, such as those genes encoding seven of the eight conserved oligomeric Golgi complex (COG) subunits, result in malfunctions in protein processing and congenital defects of glycosylation (Smith and Lupashin, 2008). There is/are likely also one or more sensors in the Golgi that are able to recognize a need for up-regulation of Golgi genes. An example is when the function of the Golgi was disturbed in Oku et al., transcription from the cis-activating Golgi stress response element (GASE) was induced, which in turn upregulated glycosylation enzymes and post-Golgi vesicular trafficking factors (Oku et al., 2011). It will be shown, too, that other Golgi morphological changes likely take place in response to phosphorylation of Golgi matrix components such as the post-translational modification of Golgi re-assembly and stacking proteins (GRASPs) during stress.

A potentially significant consequence of the Golgi-specific stress hypothesis is that perhaps imbalanced pathways can be returned to a normal, non-diseased state by utilizing a pre-existing mechanism within the cell. A basic problem arising when considering the question of Golgi stress carefully is whether it is the Golgi detecting cellular stress and influencing other pathways, or is it reacting to existing problems within the cell producing stress responses as the influence of these problems reach some triggering level. My current understanding is that the truth lies somewhere in the middle; that the Golgi has the ability to both detect and respond to cellular stress, but this is largely based on both the type and duration of the specific insult.

Some examples of Golgi fragmentation exist during normal cellular development, such as during mitosis and apoptosis. Since these normal functions could potentially obfuscate an analysis of a Golgi-specific stress response using only fragmentation, other types of measurement and many controls are required.

1.2.1 Golgi stress in the context of the cell

There are many examples of cellular stress conditions in the literature. A list of proteins that have increased protein expression as a result of stressful stimuli was made from three published general cellular stress response screens (Alvarez-Miranda et al., 2015; Chia et al., 2012; Millarte et al., 2015). All the proteins published in these screens were upregulated by the induction of at least one of seven cellular damage response categories, i.e., DNA damage, ER stress, inflammation, osmotic pressure, oxidation, pH imbalance, and starvation (**Fig. 1.5A**). Of these stress categories, several are known to produce Golgi fragmentation in various cell types and tissues. Preliminary work for this study verified whether these stress categories caused Golgi

fragmentation in HeLa cells in cell culture. Preliminary experiments indicated many stress categories were indeed able to cause Golgi fragmentation phenotypes in HeLa cells.

1.2.2 Golgi plasticity in response to stress conditions

Golgi structure altering stresses include ER stress, inflammation, pH imbalance, and others (**Fig. 1.5A**). There are a wide array of stress-induced Golgi structural phenotypes, including compacted and diffused, but one of the most common is fragmentation (**Fig. 1.5D-E**). An exhaustive review of each stressful condition was beyond the scope of this study.

The most critical stresses that affect Golgi structure, in particular those that produce fragmentation and changes in Golgi biology, will be briefly discussed. For background, the following are short summaries of stresses recounted in literature that cause Golgi responses.

pH

The concentration of H^+ ions is believed a major factor in contributing to the organization of the Golgi (Kellokumpu, 2019). The interplay between cytosol pH and Golgi lumen pH is thought to be an important regulatory mechanism that influences trafficking. Cytosolic pH in most cells is approximately 7.2 and the Golgi pH has been reported from 6.25 – 6.58 (Schapiro and Grinstein, 2000).

The pH of the Golgi luminal compartment decreases in the direction of the plasma membrane. The pH gradient across the Golgi membrane is maintained by V-ATPases that undergo active ion transport. Many enzymes have an acidic pH requirement. For example, mannose-6-phosphate

receptors (M6PR) are transmembrane glycoproteins that undergo pH-dependent targeting of lysosomal enzymes to acidic organelles where they can carry out their function. Recycling of M6PR is important for cellular homeostasis and depends on Golgi pH (Lin et al., 2004). Treatment of cells with monensin, a drug that increases pH of the Golgi lumen to neutral levels, also prevents recycling of sorting receptors (Basu et al., 1981). Mutations of critical enzymes in the Golgi, which lead to dysregulation of pH, can also lead to protein trafficking defects and accumulation of byproducts in the lysosome or extracellular space. Therefore, the Golgi pH is important to maintain cellular homeostasis and health.

Calcium

Under stress conditions, free calcium and calcium sensitive enzymes have been shown to increase in the cytoplasm. The cytosolic Ca^{2+} level at rest is ~100 nM (Garrity et al., 2016; Zampese and Pizzo, 2012). During physiological stimulation, cytosolic free calcium can climb to 3 μM (Celsi et al., 2009). Cytosolic calcium is suppressed during mitosis (Kiehart, 1981). Dysregulation of calcium is known to accompany Golgi fragmentation (Nakagomi et al., 2008). Cytosolic calcium dysregulation appears in Alzheimer's disease. In the presence of amyloid precursor protein (APP), calpain, a calcium sensitive furin-like protease, catalyzes the conversion of p35 to p25. Then, p25 activates Cdk5, which phosphorylates GRASP65 in response to amyloid-β (Aβ) accumulation. Fragmentation of Golgi enhances trafficking of APP (Joshi et al., 2014). Therefore, it appears that changes in cytosolic or Golgi calcium during stress could cause an adaptive Golgi stress response.

The Golgi can handle cellular calcium and is important for calcium homeostasis (Dolman and Tepikin, 2006). Calcium handling depends on Golgi calcium channels and transporters to reduce cytosolic ion concentration. The Golgi has Ca^{2+} channels in common with the ER: inositol triphosphate receptors (IP_3Rs) and sarco/endoplasmic reticulum ATPase isoform 2b (SERCA2b) on its *cis*-face, and ryanodine receptors (RyRs) and secretory pathway ATPases (SPCA1) mostly on its *trans*-face. IP_3Rs are calcium efflux channels that respond to inositol triphosphatase (IP_3) and regulate the release of calcium from the ER or Golgi lumen. SERCA2b is a ubiquitously expressed ATPase that can bind two cytosolic calcium ions at once, burning ATP to move them into the Golgi lumen. SPCA1 also burns ATP to move divalent cations (Ca^{2+} and Mg^{2+}) from the cytosol into the luminal space. These pumps and transporters may be significant to cytosolic processes that are dependent on these ions. Damage to these components could occur during stress due to oxidative damage, lipid peroxidation and membrane deposition of aggregated proteins (Nakagomi et al., 2008). It may be possible that cytosolic calcium homeostasis is disrupted at critical times, like after damage to these proteins.

The Golgi is also known to store, and itself use, cellular calcium (Dolman and Tepikin, 2006). Calcium is tightly regulated within the Golgi apparatus by binding proteins. The Golgi apparatus has 4 known calcium binding proteins, Cab45, CALNUC, p54/NEFA and calumenin (Dolman and Tepikin, 2006). In addition, both Ca^{2+} and Mg^{2+} act as required biosynthetic co-factors within the Golgi lumen. The Golgi is somewhat resistant to calcium fluctuations, suggesting that changes in Golgi calcium concentration may result in disruption of Golgi processes, such as membrane trafficking, signal transduction, organelle homeostasis, and organelle acidification (Stefan et al., 2017).

There is a novel mechanism, discussed in **Chapter II**, that coordinates Golgi structure and perhaps function: Increased cytoplasmic Ca^{2+}, which activates PKCα, and subsequently phosphorylates GRASP55, impairs its function in Golgi structure organization.

Osmotic Pressure

Cellular responses to osmotic stress share much overlap with calcium handling, because excretion of solutes is not only the mechanism of reducing calcium concentration in the cell but also water movement out of the cell in a hypotonic environment. Similarly, absorption of solutes is the cellular response to hypertonic environments and allows cells to cope with stress, making the most energetically efficient means of coping with these stress pathways to overlap regulatory pathways. For example, primary astrocytes exposed to hypotonic media undergo a rapid initial swelling followed by regulatory volume decrease that depended on extracellular calcium influx (O'Connor and Kimelberg, 1993). An exhaustive review of the overlapping nature and of osmotic balance, heat shock and ion handling was outside the scope of this study.

O-Glycosylation and glucose level

Dysregulation of *O*-GlcNAc and aberrant *O*-GlcNAc modification has been implicated in pathologies of metabolic and neurodegenerative diseases as well as cancers and autoimmunity (Lefebvre et al., 2005). The Golgi has been identified as a target of *O*-GlcNAcylation during physiological growth conditions (Zhang et al., 2018). During starvation de-*O*-GlcNAcylated GRASP55 functions in linking LC3-II and LAMP2 to tether autophagosomes and lysosomes and facilitate autophagic flux.

Reactive Oxygen Species/Hypoxia

All living cells are sensitive to reactive oxygen and reactive nitrogen species (ROS/RNS) from both exogenous and endogenous sources. The process of reducing oxygen in the electron transport chain produces an endogenous source of ROS, a serious threat, predominantly in the forms of superoxide and the hydroxyl radical. The predominant exogenous source of ROS is hydrogen peroxide (H_2O_2). H_2O_2 reagent is commonly used to introduce ROS to cells, since other molecular oxygen species cannot penetrate the plasma membrane.

Several mechanisms of ROS scavenging exist within the cell to mitigate direct damage to biological tissues including glutathione, polyphosphate, vitamin C, etc. The mitochondria is typically credited as the major producer of ROS, but the Golgi apparatus is proposed to respond and play a key regulatory role in cellular responses to oxidative stress (Schieber and Chandel, 2014).

Hypoxic conditions result when mutated or damaged respiration enzymes and transporters interrupts the flow of oxygen and CO_2 to and from tissues, starving them of energy via the loss of oxygen as a terminal electron acceptor in the electron transport chain. One pathway resulting from hypoxic condition is the unfolded protein response (UPR). Oxidized proteins cannot fold properly and leads to the onset of UPR. Accumulation of misfolded proteins and proteostasis is a hallmark of age-related diseases such as Alzheimer's, Parkinson's, and Huntington’s.

It is generally believed degradation of damaged proteins and organelles is handled by the ubiquitin-proteasome or autophagy/lysosome pathways. Hypoxic conditions also interact with lipid metabolism increasing glycolysis with a decrease in gluconeogenesis, and dysregulates lipid stores (Bailey et al., 2015).

In **Chapter III** a situation in the cell will be explored, where Golgi cisternae become lost when exposed to H_2O_2. Under these conditions, H_2O_2 treatment of HeLa cells reduces the number of Golgi cisternae, leading to the loss of Golgi tethers. Of further interest (and not covered here) would be to check whether Golgi tethers are also proteolytically degraded in hypoxic conditions.

1.2.3 Key regulators of Golgi stress: GRASPs and beyond

There are several cases of Golgi fragmentation in cells and a few cases have fairly well-known mechanisms. The mechanism for Golgi fragmentation during apoptosis for example is mediated by cleavage of Golgi matrix components by caspases. Some examples of matrix components that are cleaved in this way are GRASP65, Golgin 160, and p115. Depleting a golgin often causes fragmentation.

As previously reported, during cell cycle progression, the Golgi also disassembles, releasing membranes that partition into each daughter cell (**Fig. 1.6A**). Mitotic Golgi disassembly is characterized by three stereotyped changes to the Golgi structure:

1. Ribbon unlinking
2. Cisternal unstacking
3. Vesicle release

GRASP55 and GRASP65 are peripheral membrane proteins that organize the Golgi structure through GRASP domain oligomerization, and localize to the *medial-trans* and *cis*-Golgi cisternae, respectively. The GRASP region has been predicted to contain two hydrophobic protein-protein interaction modules called PDZ domains. Unstacking of cisternae is accompanied by the phosphorylation of GRASP55 and GRASP65 at the C-terminal serine/proline rich (SPR) domain by mitotic kinase **(Fig. 1.6B**). Phosphorylation destabilizes PDZ-mediated oligomerization. During interphase, the Golgi structure is also maintained by GRASPs. Knockdown of GRASPs by RNA-interference (RNAi) is followed by complete Golgi fragmentation and unstacking of the entire Golgi stack. Knockdown also leads to disruption of protein trafficking, modification and sorting (Xiang et al., 2013).

Since GRASP55 and GRASP65 organize the Golgi structure, the dynamic Golgi regulation of GRASPs during interphase might provide a link between disruptions of Golgi structure and defects in trafficking, sorting and incomplete protein processing in disease.

1.3 Tools to study Golgi stress

There are many reagents that can be used in the lab as tools to study the effects that stress will have on cells. For example treatment of HeLa cells with Monensin hydrochloride solutions, leads to vacuolation of the Golgi apparatus, and a total block in anterograde trafficking. Disturbance of tobacco BY-2 cells with macrolide antibiotics, Concanamycin and Bafilomycin A1, which block V-ATPase, leads to a similar swelling phenotype and dysregulation of Golgi function. Upon Brefeldin A (BFA) treatment the Golgi apparatus collapses into ER. Upon washout of BFA, the exit of newly synthesized membrane proteins from the ER cisterna to the Golgi complex can

then be measured. Temperature-blocking cells (incubated at 20°C) prevents exit from the TGN, and accumulates cargo at the blocked Golgi. Reduced temperature from physiological ranges prevents transfer of a membrane glycoprotein to the cell surface but does not prevent terminal glycosylation. After returning cells to 37°C, trafficking returns to normal.

Many other tools to study the functions of the Golgi apparatus during Golgi stress will be discussed in following chapters.

1.3.1 Golgi fragmentation

Golgi stresses do not all produce the same effects on cells. However, the Golgi structure is frequently altered during cellular stresses on a temporary basis. One major alteration, called Golgi fragmentation, is the dissolution of the Golgi membranes into smaller components.

Many cellular stresses result in Golgi fragmentation in cell culture. There are a number of stress-induced Golgi structural phenotypes, including compacted and swollen, but one of the most common ones is fragmentation. Many cellular treatments result in Golgi fragmentation in cell culture including but not limited to viral infection, perturbations of cellular pH, and heat-shock.

One advantage of using the Golgi fragmentation as an indicator of Golgi stress is that it has also been observed during human disease. Since the structure of the Golgi is closely linked to cellular functions during disassembly, Golgi fragmentation might have consequences for cellular functioning during disease. Yet studies have not established a specific, mechanistic description

of the molecular changes that alter the Golgi during many stresses, or made a direct connection between drug-induced fragmentation in cell culture and disease.

Using optical approaches in tissue culture cells, this study explored the link between cellular stress and Golgi fragmentation, and investigated the mechanism and consequences of pharmacologically-induced Golgi structural changes. The hypothesis was: Golgi structure and functions are altered by Golgi stress (**Fig. 1.7**).

In order to undertake the present study, a reliable approach to quantify the Golgi fragmentation phenotype quickly and consistently was needed. In order to quantify Golgi fragmentation, an unbiased approach that could be used to define whether a Golgi is intact or fragmented was developed. Three hundred cells from each experiment was determined to be a sufficient number to get minimal variation within each experimental unit. First, cells were fixed and labeled for Golgi structural proteins of choice, and DNA. Then, slides were viewed under the microscope with a cell counter, using the following criteria:

1) If the Golgi exists as a single piece of connected membrane, it is counted as intact.
2) If a Golgi exhibits several items that are connected by visible membrane bridges, even though these bridges might be faint, the Golgi is considered intact.
3) If a Golgi exhibits ≥ 3 disconnected pieces (no visible bridges connecting them), then the Golgi is fragmented.
4) Mitotic cells, defined by the DNA pattern, and overlapping cells in which the Golgi pattern is difficult to define, are not counted. Hoechst was used to identify individual, mitotic and overlapping cells.

1.3.2 Golgi stacking and EM

Golgi stress and fragmentation was also defined using a more high resolution approach, since it was known that sometimes the Golgi became enlarged or compacted during some stress conditions, but light microscopy did provide much information about these phenotypes.

Regular fluorescence has a resolution limit of 200 nanometers. The space between Golgi cisternae is about 8 nanometers. Since routine transmission electron microscopy has the ability to resolve structures down to the 0.2 nanometers, we chose this methodology as a better choice to examine Golgi fragmentation in greater detail.

A methodology for examining Golgi ultrastructure was developed. Cells were stressed in cell culture and processed for electron microscopy (refer to methods section **Chapters II and III**). Golgi images were then captured at 11,000x magnification. Golgi morphology was quantified from at least 20 cells in each experiment for statistical robustness. A Golgi cisterna was identified as a perinuclear membrane within a Golgi stack ≥4 times longer than its width. After measurement of many different variables of Golgi stacks, the following three metrics were settled upon for providing the most information in stress conditions:

1) Stack length - the longest cisterna within a Golgi stack, using the ruler tool in Photoshop Elements 13, was measured not accounting for bends or turns.
2) Number of cisternae per stack - the number of cisternae per Golgi stack was counted. Closely associated ER-cisternae were omitted.

3) Number of vesicles per stack - round objects no greater than 80 microns in diameter within 0.5 micron distance to a Golgi stack were counted.

1.3.3 Golgi functions during stress

Many diseases and stresses affecting the Golgi apparatus are tied to impairment of Golgi functions. Familial amyotrophic lateral sclerosis or fALS transgenic mouse model of fALS (human SOD1-G93A) displayed shortened and fewer cisternae in spinal cord motor neuronal Golgi (**Fig. 1.4B**) (Mourelatos et al., 1996). Golgi fragmented several months prior to symptoms of ALS paralysis. No vesicles present around the shortened stacks suggested a loss of function. Golgi fragmentation is a result of microtubule depolymerization. A significant decrease in synaptic transmission has been reported in animals treated with microtubule depolymerizing drugs that disperse the Golgi apparatus. In neurons, many neurotransmitters are processed in the Golgi. Therefore, Golgi stress and fragmentation in ALS might cause impairment of neuronal function of axonal transport and synaptic vesicle release.

Knockdown of GRASPs by RNA-interference (RNAi) is followed by complete Golgi fragmentation and unstacking of the entire Golgi stack. Knockdown also leads to disruption of protein trafficking, modification and sorting. Since GRASP55 and GRASP65 organize the Golgi structure, the dynamic Golgi regulation of GRASPs during interphase might provide a link between disruptions of Golgi structure and defects in trafficking, sorting and incomplete protein processing in disease. The regulation of Golgi structural proteins, such as GRASP55 and GRASP65, during interphase gives a plausible explanation for Golgi fragmentation during cellular stress. The extent of a Golgi stress response during TG and H_2O_2 treatment was studied

by evaluating the Golgi structure after stimulation. The evaluation identified whether GRASP55 and GRASP65 were post-translationally modified by phosphorylation or other modifications during TG or H_2O_2 treatment, and confirmed the identity of changes that happened during stress.

1.3.4 Calcium sensors

Ca^{2+} dynamic at the Golgi as well as its role in membrane trafficking at the Golgi is still an understudied area. It's been postulated that the Golgi apparatus might sense cellular stress. If aspects of the Golgi structure are specifically regulated during stress via calcium fluctuations, these changes might significantly impact Golgi functions. Several cellular organelles, like the ER and lysosomes, have inherent mechanisms to adapt their structure to accommodate stressful conditions and help maintain their specific functions.

During ER stress, the ER-localized transmembrane protein pATF6, is transported to the Golgi where it is cleaved, at which point its cytosolic domain is translocated into the nucleus where it transcriptionally activates ER chaperone genes. There are now available reagents to detect ER stress such as antibodies that recognize the phosphorylated form of eIF2α and translational arrest that occurs during UPR. During starvation, the dephosphorylated transcription factor EB (TFEB) enters the nucleus and activates genes related to lysosomal degradation and autophagy. There are tools available to detect the activated autophagy pathway, most notably the antibody which recognizes LC3-I and LC3-II. By examining the ratio of LC3-II and LC3-I one can easily recognize if autophagy is underway.

During this study calcium, too, was discovered to play a profound role in Golgi structure regulation. Changes affecting calcium also accompany the regulation of at least one Golgi structural protein, GRASP55, during interphase. Since it is known that this mechanism depends on calcium a calcium sensing version of GRASP55 was generated that can be reliably used to detect Golgi stress. The GRASP55 calcium probe utilizes a GCaMP sensor domain that enables a researcher to observe calcium flux as a function of fluorescent output. Using this calcium sensor, careful measurement of the extent of a Golgi stress response during diverse drug or environmental treatments can aid in the evaluation of drugs that may mitigate Golgi structure changes during stress. In essence this is a tool that can be used to directly measure Golgi stress in cells.

1.4 The goal of this study

The experiments and findings, presented herein, were designed to show whether or not the Golgi may be equipped to respond to cellular stress. Having a working understanding of the regulation of the Golgi apparatus during stress might result in discovery of ways to change and improve Golgi functions and help support cellular homeostasis and organism health (**Fig. 1.7**).

1.5 Figures

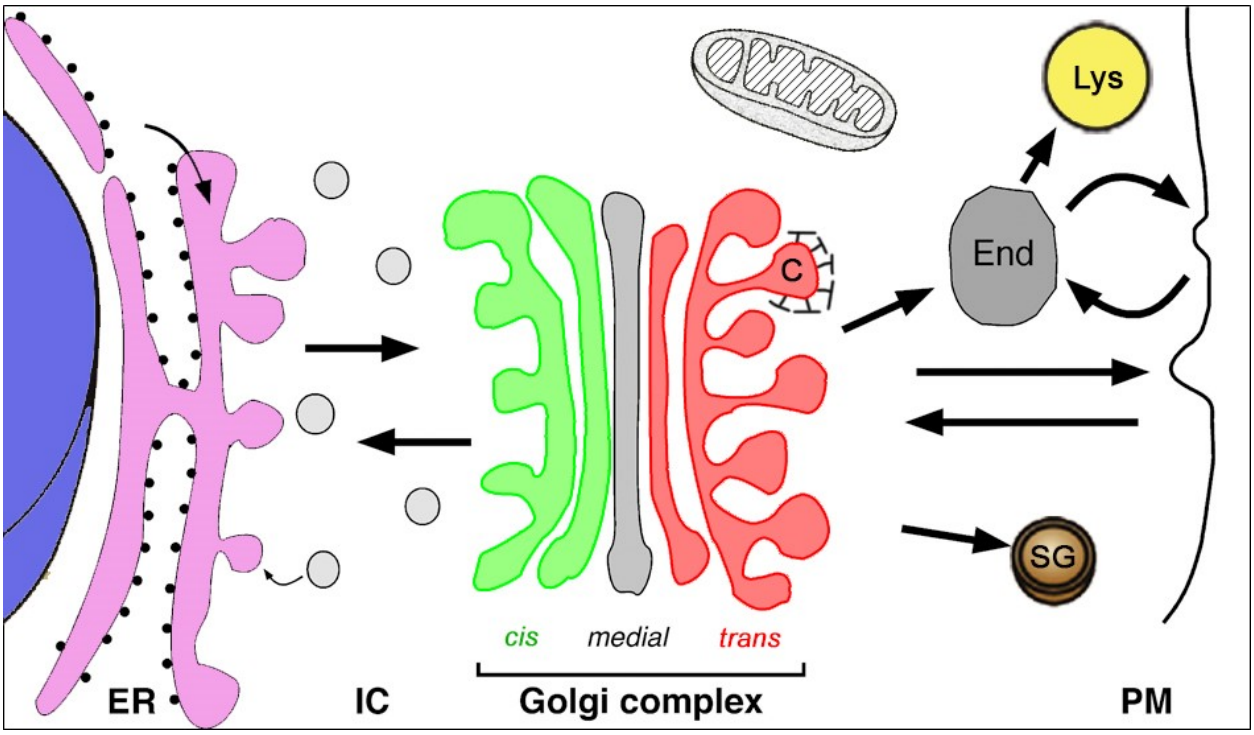

Fig. 1.1 The exocytic and endocytic trafficking network
Cargo manufactured in the ER is loaded into COPII vesicles and sent to the Golgi via the intermediate compartment (IC). Upon arrival to the Golgi, vesicles fuse, forming the *cis*-Golgi Network. Cargo then progressively moves to the trans-Golgi Network. There, it is sorted and trafficked to many destinations such as endosomes (End), lysosomes (Lys), plasma membrane (PM) or outside of the cell via secretory granules (SG).

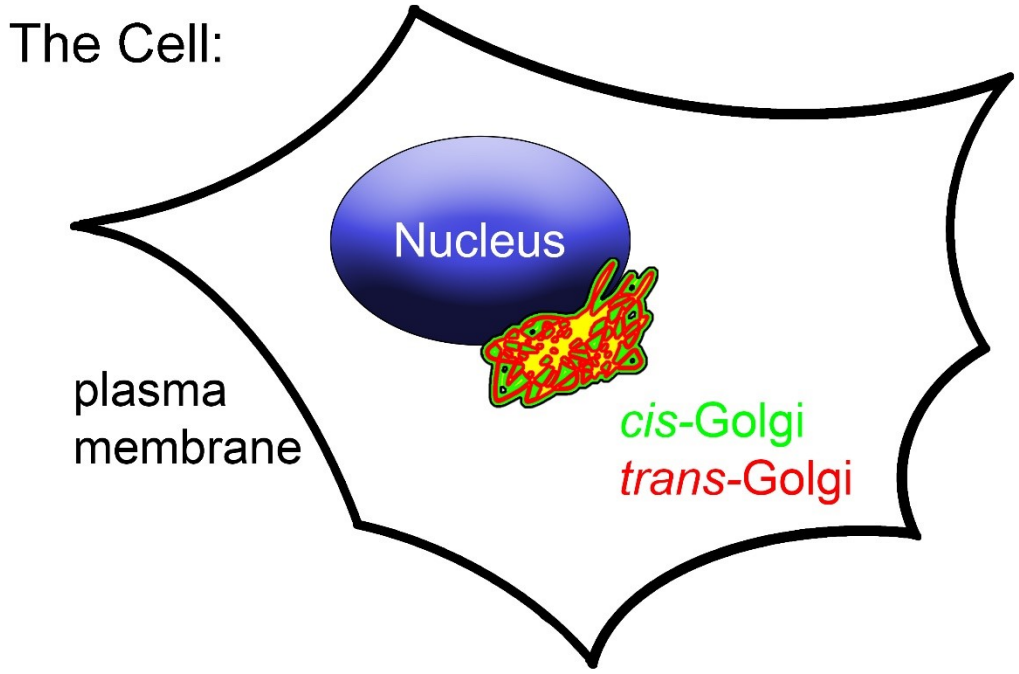

Fig. 1.2 Normal Golgi structure and position
Schematic representation of single mammalian epithelial cell indicating the Golgi apparatus in relation to the nucleus and plasma membrane structures.

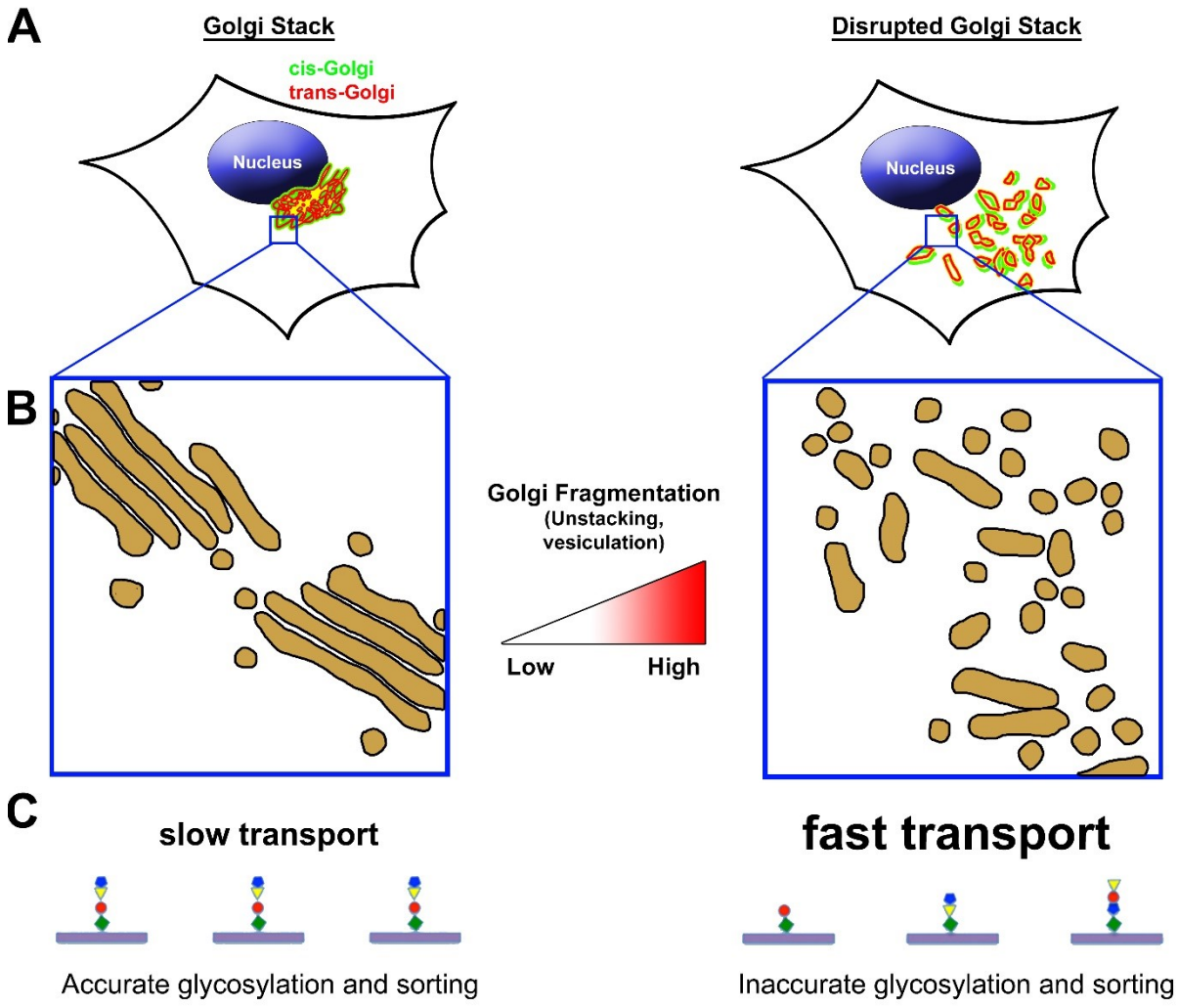

Fig. 1.3 Golgi function and significance
(A) Schematic representation of the cell indicating the Golgi apparatus in normal conditions (left side) and during a disruption of the Golgi stack (right side). **(B)** The net effect of fragmented Golgi is an increased membrane surface area for vesicle budding machinery to gain access. **(C)** The function of the cell that is altered is faster trafficking, sorting and glycosylation defects via the disruption of enzyme containing compartments.

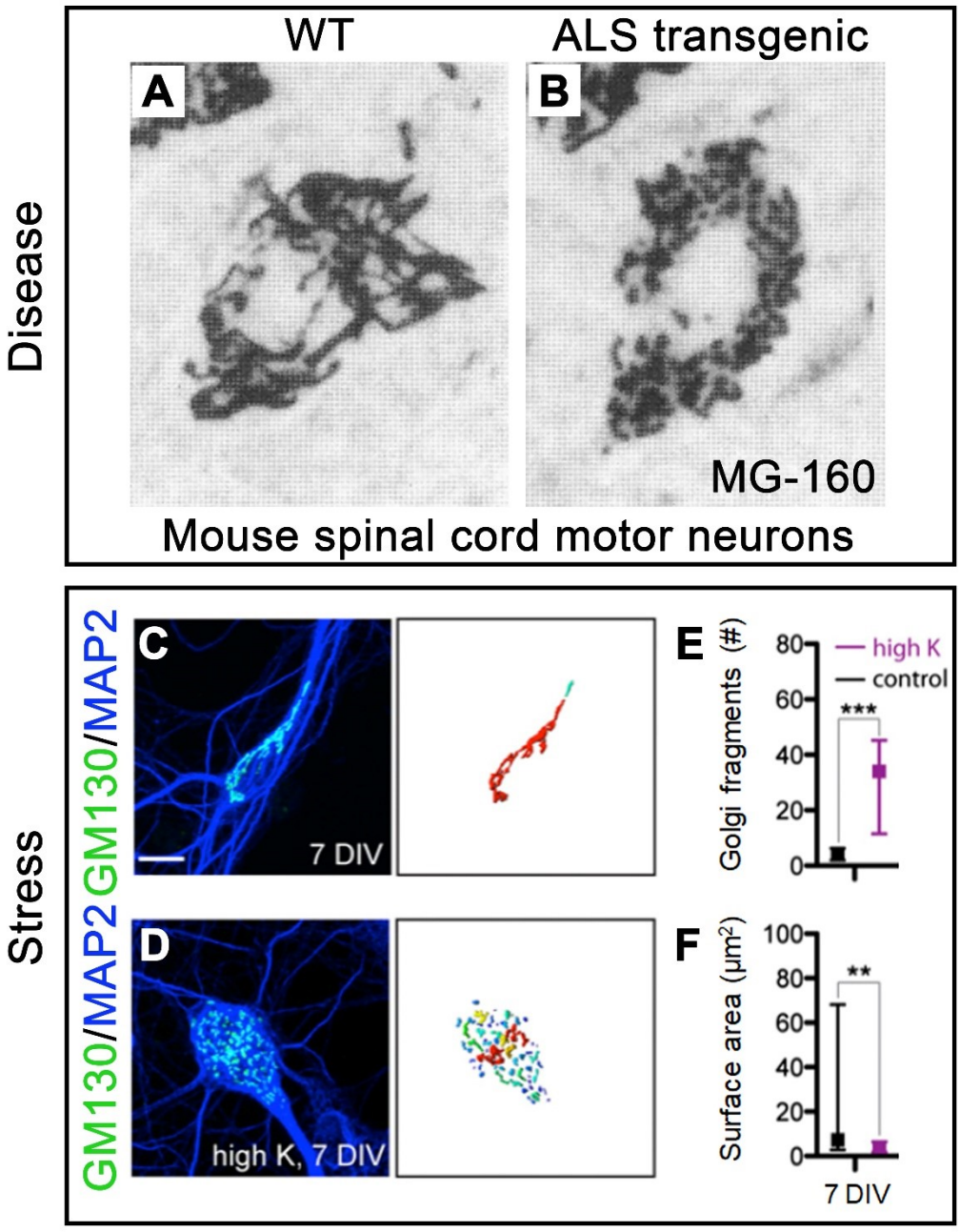

Fig. 1.4 Disease and cellular stresses disrupt Golgi structure
(A-B) Mourelatos, et al. show that ALS disease model mice having G93A mutation in the *SOD1* gene have disrupted Golgi structure (Mourelatos et al., 1996). Mouse spinal cord motor neuron Golgi apparatus showing WT Golgi in **A**, or ALS transgenic Golgi in **B**. MG-160 was the marker used. **(C-D)** Thayer et al. show that the Golgi fragments under hyper-excited conditions (Thayer et al., 2013). Neurons were cultured under normal (**C**) and overactivated (**D**) conditions (elevated potassium concentration, high potassium). Immunostaining (**left**) for GM130 (green) and MAP2 (blue) with 3D reconstruction of anti-GM130 signal (**right**). The color of the distinct Golgi fragments corresponds to the relative size of the fragment. Scale bar, 10 microns. **(E-F)**

Quantification of number (#), and surface area (μm^2) of distinct Golgi fragments from reconstructed GM130 fluorescent signal.

A

#	Stress Category	Treatment	Golgi fragmentation in HeLa cells?
1	DNA damage	staurosporine	Yes ✓
2	ER stress	thapsigargin (TG)	Yes ✓
3	inflammation	ionomycin + PMA*	Yes ✓
4	osmotic stress	sodium chloride	Yes ✓
5	oxidation	hydrogen peroxide	No ×
6	pH imbalance	monensin	Yes ✓
7	starvation	glucose free medium	No ×
	*Phorbol 12-myristate 13-acetate		

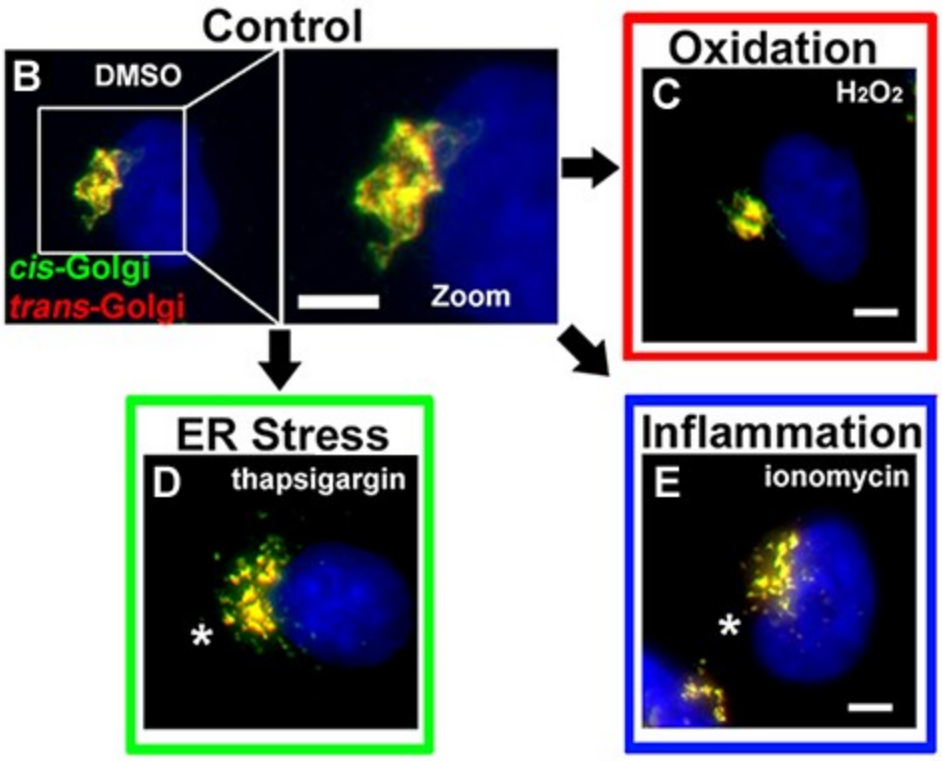

Fig. 1.5 Tools to study Golgi stress in cell culture
(A) Figure shows seven categories of cellular stress and whether they cause Golgi fragmentation in HeLa cells. **(B)** HeLa cells treated with DMSO, **(C)** 1 mM H_2O_2 for 10 minutes, **(D)** 250 nM thapsigargin for 1 hour, or **(E)** 2 μM ionomycin for 1 hour. Cells were fixed and stained for Giantin (green), TGN46 (red), and Hoechst (blue). Asterisks (*) denote fragmented Golgi. Scale bar, 5 microns.

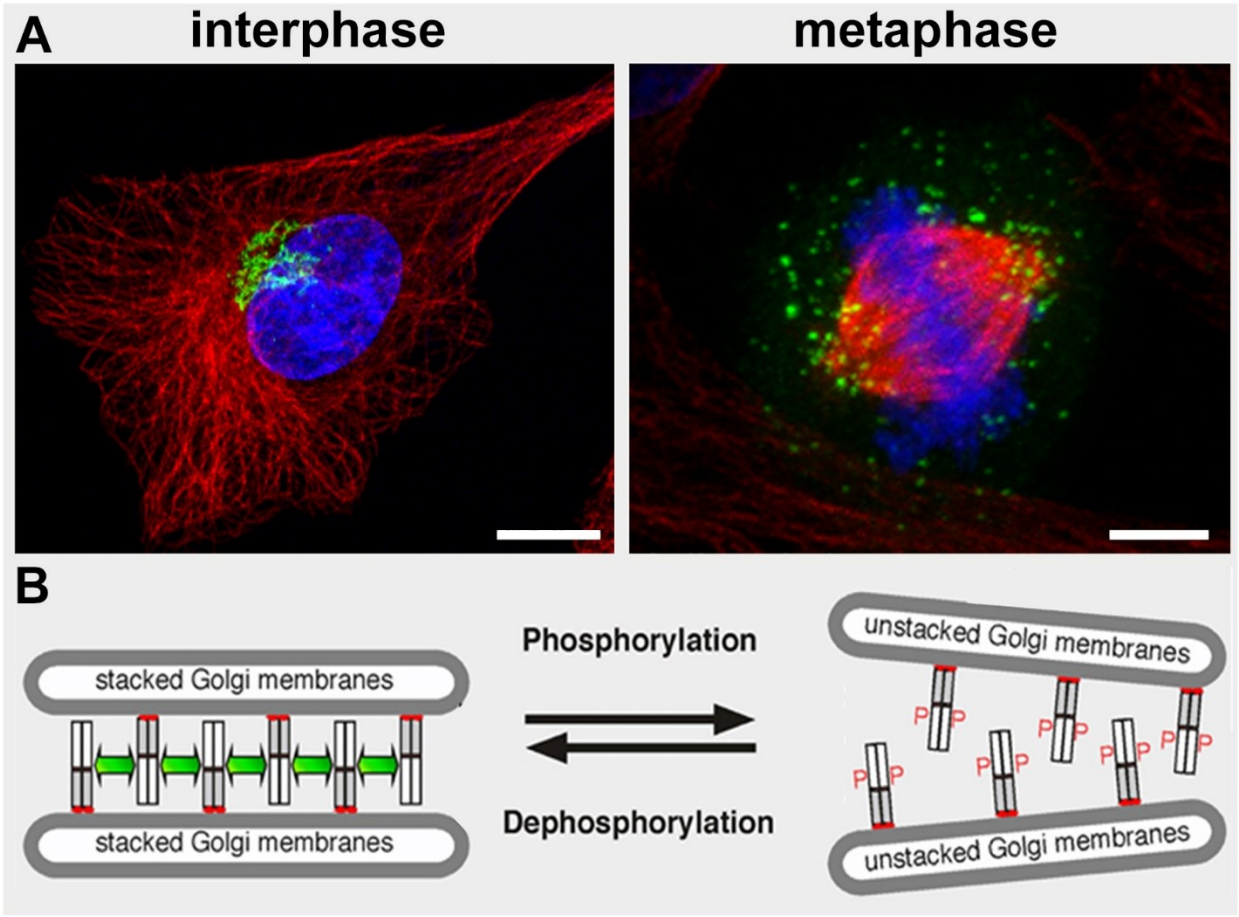

Fig. 1.6 Regulation of the Golgi stack structure
(A) Golgi structure is diffused during mitosis**.** NRK cells were fluorescently labeled for antibodies against GM130 (green), tubulin (red), and DNA (blue) . Scale bar, 10 microns. **(B)** Phosphorylation by kinases breaks the GRASP55/65 oligomers and thus unstacks the cisternae.

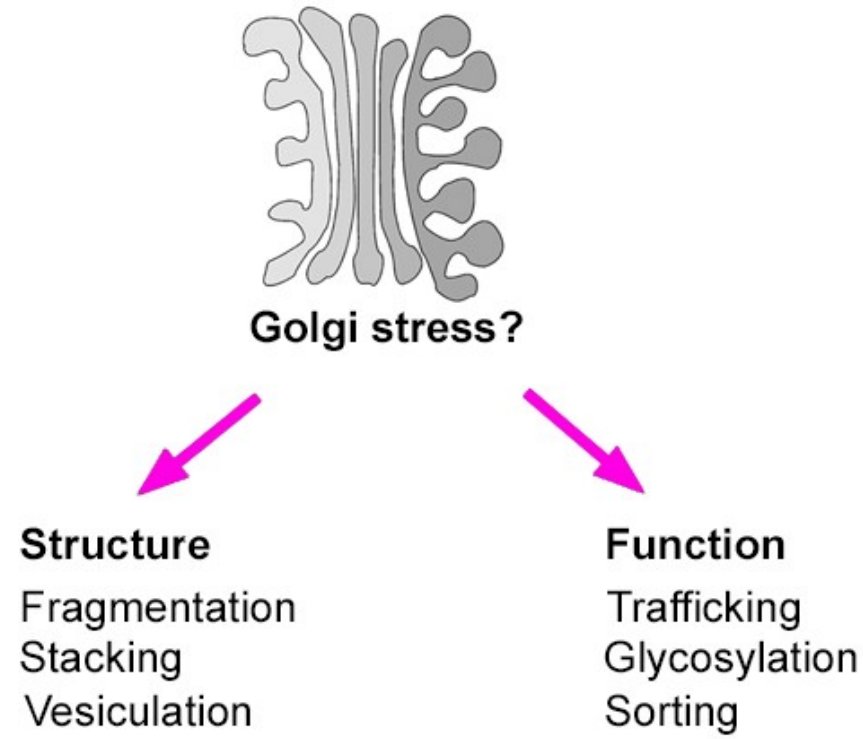

Fig. 1.7 Schematic approach for identifying mechanisms of Golgi stress response and dysfunction
How certain hallmarks of Golgi stress, including Golgi fragmentation and cisternal unstacking, regulate many aspects of membrane trafficking is unknown. It remains to be resolved how Golgi stress regulates Golgi functions including trafficking, glycosylation and sorting (pink arrows)

CHAPTER II

Cytosolic Ca^{2+} Modulates Golgi Structure Through PKCα-Mediated GRASP55 Phosphorylation[2]

2.1 Abstract

It has been well documented that the endoplasmic reticulum (ER) responds to cellular stresses through the unfolded protein response (UPR), but it is unknown how the Golgi apparatus responds to similar stresses. In this study, we treated HeLa cells with ER stress inducers, thapsigargin (TG), tunicamycin (Tm) and Dithiothreitol (DTT), and found that only TG treatment resulted in Golgi fragmentation. TG induced Golgi fragmentation at a low dose and short time when UPR was undetectable, suggesting that Golgi fragmentation occurs independently of ER stress. Further experiments demonstrated that TG induces Golgi fragmentation through elevating intracellular Ca^{2+} and protein kinase Cα (PKCα) activity, which phosphorylates the Golgi stacking protein GRASP55. Significantly, activation of PKCα with other activating or inflammatory agents, including phorbol 12-myristate 13-acetate (PMA) and

[2] This chapter was modified from a version published the journal *iScience*, with authors listed as Stephen Ireland, Saiprasad Ramnarayanan, Mingzhou Fu, Xiaoyan Zhang, Jianchao Zhang, Jie Li, Dabel Emebo and Yanzhuang Wang (see Acknowledgments section).

histamine, modulates the Golgi structure in a similar fashion. Hence, our study revealed a novel mechanism through which increased cytosolic Ca^{2+} modulates Golgi structure and function.

2.2 Introduction

In mammalian cells, the Golgi apparatus is characterized by a multilayer stacked structure of ~5-7 flattened cisternal membranes, and stacks are often laterally linked to form a ribbon located in the perinuclear region of the cell (Tang and Wang, 2013; Wang and Seemann, 2011). The exact mechanism of Golgi stack formation is not fully understood, but it has been shown that the Golgi re-assembly stacking protein of 55 kDa (GRASP55, also called GORASP2) and its homolog GRASP65 (GORASP1) play essential roles in Golgi stacking (Wang et al., 2003; Zhang and Wang, 2015). Both GRASPs are peripheral membrane proteins that share similar domain structures and overlapping functions (Wang and Seemann, 2011). GRASP65 is predominantly concentrated in the *cis* Golgi, whereas GRASP55 is localized on *medial-trans* cisternae. Both GRASPs form *trans*-oligomers through their N-terminal GRASP domains that "glue" adjacent Golgi cisternae together into stacks (Wang et al., 2003; Xiang and Wang, 2010) and ribbons (Feinstein and Linstedt, 2008; Puthenveedu et al., 2006). GRASP oligomerization is regulated by phosphorylation; mitotic phosphorylation of GRASP55 and GRASP65 at the C-terminal Serine/ Proline-Rich (SPR) domain inhibits oligomerization and results in Golgi cisternal unstacking and disassembly (Tang et al., 2012; Wang et al., 2005; Xiang and Wang, 2010).

The Golgi exhibits different morphology in different cell types and tissues as well as under different conditions. For example, in many secretory cells such as Brunner's gland of platypus, the Golgi forms large, well-formed stacks (Krause, 2000), while electron micrographs show

reorganization of Golgi membranes in prolactin cells of female rats upon cessation of a sucking stimulus (Rambourg et al., 1993). In neurons, increased neuronal activity causes dispersal of the Golgi at the resolution of light microscopy (Thayer et al., 2013). In Alzheimer's disease, the Golgi membranes are dispersed and fragmented in neurons from human brain and mouse models (Joshi et al., 2015). Golgi fragmentation is also observed in other neurodegenerative diseases, including Parkinson's (Mizuno et al., 2001) and Huntington's (Hilditch-Maguire et al., 2000) diseases and amyotrophic lateral sclerosis (ALS) (Fujita and Okamoto, 2005; Gonatas et al., 1998; Mourelatos et al., 1996). In addition, the Golgi has also been shown to be fragmented in lung, prostate and breast cancers (Petrosyan et al., 2014; Sewell et al., 2006; Tan et al., 2016). A plausible hypothesis is that the Golgi adjusts its structure and function in response to different physiological and pathological conditions; however, the molecular mechanisms that control Golgi structure and function under disease conditions are so far not well understood.

The Golgi structure can be modulated experimentally such as by molecular manipulations of GRASP55 and GRASP65. Microinjection of antibodies against GRASP55 or GRASP65 into cells inhibits post-mitotic stacking of newly formed Golgi cisternae (Wang et al., 2003; Wang et al., 2008). Knockdown (KD, by siRNA) or knockout (KO, by CRISPR/Cas9) of either GRASP reduces the number of cisternae per stack (Sutterlin et al., 2005; Tang et al., 2010b), whereas simultaneous depletion of both GRASPs causes fragmentation of the entire Golgi stack (Bekier et al., 2017; Xiang and Wang, 2010). Expression of non-phosphorylatable GRASP65 mutants enhances Golgi stacking in interphase and inhibited Golgi disassembly in mitosis (Tang et al., 2010b). Since GRASPs play critical roles in Golgi structure formation, it is reasonable to speculate that physiological and pathological cues may trigger Golgi fragmentation through

GRASP55/65 modification, such as phosphorylation (Ahat et al., 2019a; Li et al., 2019a). Using GRASPs as tools to manipulate Golgi stack formation, it has been demonstrated that Golgi cisternal unstacking accelerates protein trafficking but impairs accurate glycosylation and sorting (Bekier et al., 2017; Xiang et al., 2013). In addition, GRASP depletion also impacts other cellular activities such as cell attachment, migration, growth, and autophagy (Ahat et al., 2019b; Zhang et al., 2019; Zhang et al., 2018).

Protein kinase C (PKC) is a large family of multifunctional serine/threonine kinases that are activated by signals such as increases in the concentration of diacylglycerol (DAG) and/or intracellular calcium ions (Ca^{2+}). In cells, PKCs are mainly cytosolic, but transiently localize to membranes such as endosomes and Golgi upon activation (Chen et al., 2004; El Homasany et al., 2005). Membrane association of PKC is via a C1 domain that interacts with DAG in the membrane. Conventional PKCs (cPKCs) also contain a C2 domain that binds Ca^{2+} ions, which further enhances their membrane association and activity (Nishizuka, 1995). Knockdown of atypical PKCs (aPKCs) using siRNA causes a reduction in peripheral ERGIC-53 clusters without affecting the Golgi morphology (Farhan et al., 2010). In addition, increased PKC activity has been implicated in cancer (Cooke et al., 2017; Kim et al., 2013), but the mechanism by which PKC may contribute to invasion, inflammation, tumorigenesis, and metastasis is not fully understood (Griner and Kazanietz, 2007).

In this study, we performed high-resolution microscopy and biochemistry experiments to determine how the Golgi responds to cellular stresses such as ER stress. While not all ER stress inducers caused Golgi fragmentation, treatment of cells with the Ca^{2+}-ATPase inhibitor

thapsigargin (TG) resulted in Golgi fragmentation with a low dose and short time in which ER stress was undetectable, indicating that Golgi fragmentation occurs independently of ER stress. Further experiments demonstrated that TG-induced cytosolic Ca^{2+} spikes activate PKC that phosphorylates GRASP55. Interestingly, inflammatory factors such as histamine modulate the Golgi structure through a similar mechanism. Thus, we have uncovered a novel pathway through which cytosolic Ca^{2+} modulates the Golgi structure and function.

2.3 Results

2.3.1 TG treatment induces Golgi fragmentation and UPR

It has been hypothesized that ER stress and the unfolded protein response (UPR) cause Golgi fragmentation and dysfunction through overloading misfolded proteins into the Golgi (Oku et al., 2011). To test this hypothesis, we performed a time course treatment of HeLa cells with a well-known UPR inducer, TG, which specifically blocks the sarcoendoplasmic reticulum Ca^{2+} transport ATPase (SERCA) (Xu et al., 2004) and causes Ca^{2+} dysregulation (Ito et al., 2014). We assessed the Golgi morphology by co-staining the cells for GM130, a *cis*-Golgi marker, and TGN46, a protein in the *trans*-Golgi network. As shown in **Fig. 2.1A-B**, the Golgi became fragmented after TG treatment, and the response was linear over time (**Fig. 2.1A-B**). Although Golgi fragmentation was more obvious after a longer treatment, it became detectable in shorter treatments such as 10 min. We also performed super-resolution microscopy to examine the Golgi structure in parallel after Tm, DTT or TG treatment. Similar to that observed in control cells, the Golgi structure is intact in Tm and DTT-treated cells, with extensive overlap between *cis*- and *trans*-Golgi markers; whereas TG treatment caused not only fragmentation of the Golgi structure, but also separation of *cis*- and *trans*-Golgi markers (**Fig. 2.1C-D**). This careful

examination of the Golgi morphology by super-resolution fluorescence microscopy demonstrated that the Golgi ribbon was broken down, as the Golgi in TG treated cells appeared as disconnected puncta (**Fig. 2.1C-D**).

To correlate Golgi fragmentation with UPR, we performed Western blot of TG-treated cells to assess the levels of several UPR markers, including phosphorylated eukaryotic translation initiation factor 2A eIF2α (p-eIF2α), the ER UPR chaperone binding of immunoglobulin protein (Bip), and the CCAAT-enhancer-binding protein homologous protein (CHOP). As shown in **Fig. 2.1E-G**, longer term TG treatment, such as 2 h or longer, caused UPR, as indicated by the increase of all three markers. When the treatment was reduced to 30 min, only the p-eIF2α level increased, while Bip and CHOP did not change. This indicates that the minimal time for UPR to occur is ~30 min under our experimental conditions. Consistently, no significant increase in the level of any of these UPR markers was detected when the treatment was reduced to below 30 min. Interestingly, the Golgi in a significant proportion of cells was fragmented at this time. Golgi fragmentation was obvious with 10 min TG treatment when UPR was undetectable, and became more prevalent at 30 min treatment (**Fig. 2.1A-B**). The fact that Golgi fragmentation occurs earlier than UPR indicates that Golgi fragmentation is unlikely a downstream effect of ER stress, but rather, occurs independently of UPR.

It is worth mentioning that TG treatment did not affect the level of key Golgi structural proteins, including the Golgi stacking proteins GRASP55 and GRASP65, the Golgi tethering protein GM130, and the Golgi SNARE Gos28 (**Fig. 2.1E**), indicating that TG induces Golgi fragmentation likely through modification rather than degradation of Golgi structural proteins.

TG-induced Golgi fragmentation is reversible; when TG was washed out, the Golgi structure gradually returned to its normal shape (**Fig. 2.2A-B**). Consistently, TG-treatment did not induce apoptosis as shown by Annexin V staining. In contrast, staurosporine treatment, which is known to induce apoptosis, increased Annexin V cell surface staining (**Fig. 2.2C-D**). In addition, TG treatment did not seem to affect the organization of the actin and microtubule cytoskeleton (**Fig. 2.2E-F**).

2.3.2 Tunicamycin (Tm) or dithiothreitol (DTT) treatment induces UPR but not Golgi fragmentation

To test whether the hypothesis that Golgi fragmentation occurs independently of UPR applies only to TG treatment or also to other ER stress inducers, we repeated the same set of experiments by treating cells with tunicamycin (Tm), an antibiotic that induces ER stress by inhibiting N-glycosylation and the accumulation of misfolded proteins in the ER lumen. Tm treatment did not affect the Golgi morphology after 360 min, as indicated by the GM130 and TGN46 signals (**Fig. 2.3A-C**). Further analysis of Tm-treated cells by electron microscopy (EM) also did not reveal any significant changes in the Golgi structure (**Fig. 2.3D**). The treatment indeed induced UPR, as indicated by the robust increase in the p-eIF2α, Bip and CHOP levels, in particular after 120 min (**Fig. 2.3E-G**). 6 h Tm treatment increased the width of the ER cisternae and caused ER fragmentation (**Fig. 2.3H**). Like Tm, dithiothreitol (DTT) treatment also did not cause Golgi fragmentation, although Bip and CHOP levels increased significantly after 120 min of treatment (**Fig. 2.4**). Taken together, these results indicate that ER stress is unlikely a direct cause of Golgi fragmentation.

2.3.3 TG induces Golgi fragmentation prior to UPR through elevated cytosolic Ca^{2+}

We next sought to decouple the Golgi stress response from UPR after TG treatment. As a complimentary approach to the time-course experiment shown in **Fig. 2.1**, we titrated TG (1 - 250 nM) in the treatment. Here we treated cells for 20 min, a time point prior to UPR becoming detectable when cells were treated with 250 nM TG (**Fig. 2.5**). The results showed that Golgi fragmentation increased linearly in response to the increasing TG concentration, and importantly, TG at low doses (1 nM to 250 nM) effectively caused Golgi fragmentation (**Fig. 2.5A-B**). For comparison, we also assessed UPR in the same cells. As shown in **Fig. 2.5C-E**, treatment of cells with up to 250 nM TG for 20 minutes did not cause UPR as indicated by the p-eIF2α and Bip levels. These results indicate that TG-triggers Golgi fragmentation independent of ER stress.

We next asked how TG treatment induces Golgi fragmentation. Knowing that TG increases cytosolic Ca^{2+} (Jones and Sharpe, 1994), we employed the membrane permeable Ca^{2+} chelater BAPTA-AM to test whether TG induces Golgi fragmentation through cytosolic Ca^{2+}. We pre-treated cells with BAPTA-AM alone (60 μM) for 30 min, and then with or without TG (100 nM) for 0, 15, 30, and 60 min (**Fig. 2.5F-G**). The result showed that BAPTA-AM significantly prevented TG-induced Golgi fragmentation, while BAPTA-AM alone did not affect the Golgi morphology. Subsequent EM analysis confirmed TG-induced Golgi fragmentation and its rescue by BAPTA-AM (**Fig. 2.5H-I**). TG treatment reduced the number of cisternae per stack and the length of cisternae, but increased the number of vesicles surrounding each stack. These effects were largely abolished by the addition of 60 μM BAPTA-AM for 30 minutes. Further testing of various concentrations of BAPTA-AM for 10 minutes could inhibit 250 nm TG treatment (**Fig. 2.6A-B**). Furthermore, we carried out similar experiments in normal rat kidney (NRK) cells and

RAW 264.7 murine macrophages and obtained similar results (**Fig. 2.7**), indicating that the effect of TG treatment on the Golgi structure is not cell type specific. These results demonstrated that cytosolic Ca^{2+} is required for TG-induced Golgi fragmentation. Therefore, the driving force behind TG-induced Golgi fragmentation is the elevated cytosolic Ca^{2+}.

2.3.4 TG-induced Golgi fragmentation increases protein trafficking in the Golgi

As GRASP depletion-mediated Golgi destruction impacts Golgi functions such as protein trafficking (Ahat et al., 2019b; Xiang et al., 2013), we examined the effect of TG treatment on the trafficking of the Vesicular Stomatitis Virus Glycoprotein (VSV-G) using the well-established RUSH system (Boncompain et al., 2012). Cells were transfected with a plasmid that encodes both the invariant chain of the major histocompatibility complex (Ii, an ER protein) fused to core streptavidin and VSV-G fused to streptavidin-binding peptide (SBP). Under growth conditions without biotin, the interaction between streptavidin and SBP retains VSV-G in the ER. Upon the addition of biotin, this interaction is disrupted, resulting in synchronous release of the VSV-G reporter from the ER to the Golgi. Since VSV-G is a glycoprotein, we used endoglycosidase H (EndoH) to distinguish its core (ER and *cis* Golgi) and complex (*trans* Golgi and post-Golgi) glycosylation forms as an indicator of trafficking. As shown in **Fig. 2.8A**, TG treatment first slightly decreased VSV-G trafficking at 15 min release, but then increased VSV-G trafficking at 60 and 90 min compared to DMSO control. Our previous studies showed that VSV-G reaches the *cis* Golgi at 15-20 min and *trans* Golgi at ~90 min (Bekier et al., 2017; Li et al., 2019b). These results suggest that TG treatment may delay VSV-G release possibly by slowing down its folding; but once it reaches the *cis* Golgi, VSV-G trafficking across the Golgi stack is significantly accelerated. Monensin (Mo) is known to disrupt the Golgi structure and

blocks TGN exit (Fliesler and Basinger, 1987), and thus was used as a control. As expected, monensin treatment resulted in VSV-G accumulation in the Golgi (**Fig. 2.8A-C**).

To confirm these results using an alternative approach, we treated cells with Brefeldin A (BFA) to accumulate ManII-GFP in the ER. We then washed out BFA and analyzed ManII-GFP in ER-to-Golgi trafficking. The results showed that ManII-GFP started to accumulate in the Golgi at 60 min of BFA washout in the presence of TG, while the same observation occurred at 90 min in the control (**Fig. 2.8D**).

2.3.5 TG induces Golgi fragmentation through PKCα activation

Given that phosphorylation of Golgi structural proteins has been shown to cause Golgi fragmentation in physiological conditions such as in mitosis (Tang et al., 2010b; Wang et al., 2003; Xiang and Wang, 2010), as well as in pathological conditions such as in Alzheimer's disease (Joshi et al., 2014), we explored the possibility that phosphorylation of Golgi structural proteins may play a role in TG-induced Golgi fragmentation. We treated cells with staurosporine, a non-selective kinase inhibitor, and a number of specific inhibitors of calcium-related kinases such as protein kinase Cs (PKCs) and Ca^{2+}/calmodulin-dependent protein kinases (CAMKs). As shown in **Fig. 2.9A-B**, staurosporine significantly reduced Golgi fragmentation in TG-treated cells. In addition, Bisindolylmaleimide I (BIM1), a selective PKC inhibitor, and KN-93, an inhibitor of CAMKII, also partially reduced Golgi fragmentation in TG-treated cells (**Fig. 2.9A-B**). These results suggest that either PKC and/or CAMKII is involved in TG-induced Golgi fragmentation. Since both BIM1 and KN-93 inhibitors have pleiotropic effects, we selected two alternative drugs, Gö6976 and KN-62, to inhibit PKC and CAMKII, respectively. While Gö6976

inhibited TG-induced Golgi fragmentation effectively, KN-62 had no effect (**Fig. 2.9A-B**), suggesting a major role of PKC in TG-induced Golgi fragmentation.

To further confirm that PKC activation causes Golgi fragmentation, we treated cells with phorbol 12-myristate 13-acetate (PMA), a widely used PKC activator, and its inactive enantiomer, 4-alpha-phorbol myristate acetate (4-alpha). The results showed that 4-alpha had no effect on the Golgi structure, while PMA treatment caused Golgi fragmentation (**Fig. 2.9C-D**), although 4-alpha and PMA had no effect on the level of PKC expression (**Fig. 2.9E**). Taken together, these results indicate that TG induces Golgi fragmentation through PKC activation.

PKC has multiple isoforms including α, βI, βII, γ, δ, ε, η, ζ, and ι (Kajimoto et al., 2001). To identify the PKC isoform responsible for TG-induced Golgi fragmentation, we expressed GFP-tagged PKC isoforms, including all four known classical PKC (cPKC) isoforms (α, βI, βII, γ) that respond to Ca^{2+} stimuli, one from the non-calcium responsive novel PKC (nPKC, δ), and one from the atypical PKC (nPKC, ζ) subfamily (**Fig. 2.10A-B**). To enhance the activity of expressed PKC, we also treated cells with PMA, using 4-alpha as a control. The results showed that expression of PKCα and treatment of cells with PMA increased Golgi fragmentation (**Fig. 2.10A-B, Fig. 2.11A-C**). Interestingly, in addition to the localization to the plasma membrane as previously reported (Becker and Hannun, 2003), wild type PKCα-GFP was also concentrated on the Golgi upon PMA treatment, as indicated by the colocalization with GM130 (**Fig. 2.11A; Fig. 2.10B**); while other PKC isoforms, or the inactive PKCα K368R mutant (Baier-Bitterlich et al., 1996), did not show the same phenotype (**Fig. 2.11D-E**).

To further specify that PKCα mediates TG-induced Golgi fragmentation, we knocked down PKCα in cells with siRNA. The results showed that PKCα depletion reduces Golgi fragmentation after TG treatment (**Fig. 2.11F-H**). Taken together, these results demonstrate that PKCα activation causes Golgi fragmentation.

2.3.6 PKCα induces Golgi fragmentation through GRASP55 phosphorylation

Since activated PKCα localizes to the Golgi, we thought it might phosphorylate Golgi structural proteins. To identify potential PKCα targets on the Golgi, we performed gel mobility shift assays on a number of Golgi structural proteins, tethering factors, and SNARE proteins after TG treatment (**Fig. 2.12A**). To ensure that the band shift was caused by phosphorylation, we also applied staurosporine (2 μM for 10 min prior to TG treatment) to TG-treated cells to broadly inhibit phosphorylation. Among the proteins tested, GRASP55 and GRASP65 showed a smear above the main bands (**Fig. 2.12A**), indicating a partial phosphorylation of the proteins. To increase the resolution of phosphorylated proteins we utilized phos-tag gels, which showed GRASP55, but not GRASP65, to be significantly shifted up after TG treatment (250 nM, 1 h) (**Fig. 2.12B**). TG-induced mobility shift of GRASP55 was not seen upon Tm treatment (**Fig. 2.12C**, **lanes 2 vs. 3; Fig. 2.12D**), and was less dramatic than by nocodazole (Noc) treatment that blocks cells in mitosis when GRASP55 is fully phosphorylated (**Fig. 2.12C, lanes 3 vs. 4**) (Xiang and Wang, 2010), indicating that TG induced partial phosphorylation of GRASP55. The mobility shift of GRASP55 triggered by TG treatment was abolished by the addition of staurosporine (**Fig. 2.12B, lanes 3 vs. 2**), validating the mobility shift by phosphorylation.

To determine if PKCα could phosphorylate GRASP55 directly, recombinant GRASP55 was incubated with a small amount of active PKCα *in vitro* and products were run on phos-tag gel and Coomassie stained (**Fig. 2.12E**). The Coomassie stained band pattern revealed two p-GRASP55 bands. We next increased the amount of PKCα in the reaction and incubated it with recombinant GRASP55. When Western blot was performed GRASP55 phosphorylation bands were confirmed showing that PKCα can directly phosphorylate GRASP55 (**Fig. 2.12F, upper panel**). In this experiment, PKCα was also auto-phosphorylated (**Fig. 2.12F, lower panel**). To identify the specific phosphorylation sites on GRASP55, a series of point mutants were constructed based on likely PKC consensus sites within the GRASP55 protein sequence: S255A, S260A, S262A/S263A, S269A, S273A/T274A, T278A, S289A, and S292A. These sites were assayed but none seemed to strongly abolish the GRASP55 mobility shift induced by PKC (data not shown).

GRASP55 contains an N-terminal GRASP domain that forms dimers and oligomers, and a C-terminal serine/proline-rich (SPR) domain with multiple phosphorylation sites (Xiang and Wang, 2010; Zhang and Wang, 2015). To map the PKCα phosphorylation site on GRASP55, we expressed GFP-tagged GRASP55 truncation mutants (Zhang et al., 2018), treated the cells with TG, and determine their phosphorylation. A visible mobility shift of the GRASP55 variants was observed on the mutants possessing amino acids (aa)251-300, but not the truncated forms shorter than aa250 (**Fig. 2.13A-B**). To further determine the functional consequence of GRASP55 phosphorylation, we expressed these constructs and treated cells with or without TG. The exogenously expressed GRASP55 truncation mutants were targeted to the Golgi as indicated by giantin as a Golgi marker, but had no impact on the Golgi structure (**Fig. 2.13C**). However, when

cells were treated with TG, expression of the N-terminal aa250 or shorter reduced TG-induced Golgi fragmentation; while expression of N-terminal aa300 or longer had no significant effect (**Fig. 2.13C-D**). These results demonstrated that phosphorylation of GRASP55 within aa251-300 is important for TG-induced Golgi fragmentation. Taken together, these results demonstrate that TG treatment activates PKCα, which localizes to the Golgi membrane and subsequently phosphorylates GRASP55.

2.3.7 Histamine modulates the Golgi structure

It is known that histamine activates Ca^{2+}-dependent PKC isoforms and up-regulates cytokine secretion via the release of calcium from the ER into the cytosol (Matsubara et al., 2005). It has also been shown that histamine triggers protein secretion and Golgi fragmentation (Saini et al., 2010), but the underlying mechanism has not been revealed. Therefore, we treated HeLa cells with histamine and determined the effect on Golgi morphology. EM analysis confirmed that histamine treatment induced alterations in the Golgi structure at a concentration and time often used in previous studies (Sahoo et al., 2017; Xie et al., 2018) (**Fig. 2.14**). As shown in **Fig. 2.15A-B**, histamine treatment induced Golgi fragmentation in a dose and time dependent manner. More than 40% of cells possessed fragmented Golgi after 100 μM histamine treatment for 1 h (**Fig. 2.15B**). Subsequent EM analysis confirmed that histamine treatment induced alterations in the Golgi structure including fewer cisternae per stack, shorter cisternae, and an increased number of Golgi-associated vesicles **(Fig. 2.15C-D; Fig. 2.14)**

It has been previously shown that histamine activates Gβγ, which causes TGN fragmentation (Saini et al., 2010). Since HeLa cells do not express Gβγ, and histamine treatment triggers

fragmentation of the entire Golgi stack (**Fig. 2.15C-D**), the Golgi fragmentation observed in our study may occur through a different mechanism. Indeed, like TG, histamine-induced Golgi fragmentation also depended on PKC, as the addition of the PKC inhibitor Gö6976 reduced histamine-induced Golgi fragmentation (**Fig. 2.15E-F**). These results demonstrate that histamine treatment impacts Golgi structure through a similar mechanism as TG.

While it has been well documented that TG or histamine treatment elevates Ca^{2+} level in the cytosol, whether this is also true for the Ca^{2+} level in the Golgi region has not been reported. To test the effect of TG or histamine treatment on the Ca^{2+} level in the Golgi region in real-time, we fused the Ca^{2+} probe GCaMP (Muto et al., 2013) to GRASP55, expressed the GRASP55-GCaMP construct in cells (**Fig. 2.15G**), and performed live cell imaging. Treatment of cells with 100 μM histamine caused a robust calcium spike (**Fig. 2.15H**). Subsequent experiments using this novel Golgi-localized Ca^{2+} probe demonstrated that treatment of cells with TG and Io also significantly elevated the Ca^{2+} level in the Golgi (**Fig. 2.15I**). Taken together, our results demonstrated that histamine or TG treatment elevates the Ca^{2+} level in the Golgi region, which subsequently activates PKCα, leading to GRASP55 phosphorylation and Golgi fragmentation (**Fig. 2.16**). Thus, this study revealed a novel mechanism of how histamine, and perhaps other drugs, modulates Golgi structure and function.

2.4 Discussion

In this study, by comparing Golgi fragmentation with ER stress in response to TG, Tm and DTT treatments, we uncovered a novel signaling pathway through which increased cytosolic Ca^{2+} triggers Golgi fragmentation through PKCα activation and GRASP55 phosphorylation.

Significantly, we also demonstrated that histamine modulates the Golgi structure via a similar mechanism, which opens a new window through which we can better understand the effect of histamine on cell physiology.

One possible model of Golgi stress is that the expanding capacity of the ER during cellular stress leads to the failure of the Golgi as it is over-burdened with misfolded or improperly folded proteins, affecting its functions like glycosylation (Oku et al., 2011). However, our results do not support this hypothesis for two reasons: First, although three ER stress inducers, TG, Tm and DTT, all induce ER stress, only TG treatment causes Golgi fragmentation. Second, TG induces Golgi fragmentation at a low dose and time when UPR is undetectable. These results demonstrate that Golgi fragmentation occurs independently of ER stress; instead, the Golgi may possess its own mechanism to sense and respond to stress. Furthermore, our study revealed a novel mechanism that coordinates Golgi structure and perhaps function: TG treatment increases cytoplasmic Ca^{2+}, which activates PKCα, that subsequently phosphorylates GRASP55, impairing its function in Golgi structure formation. GRASP55 therefore provides the conceptual link between an extracellular cue and Golgi morphological change during stress.

GRASP55 is comprised of an N-terminal GRASP domain (aa1-212) that forms dimers and oligomers and functions as a membrane tether to maintain an intact Golgi structure, and an SPR domain (aa212-454) that undergoes post-translational modifications and functions as the regulatory domain of the protein (Xiang and Wang, 2010; Zhang and Wang, 2015). Originally, GRASP55 was found to be phosphorylated by ERK2 at T225 and T222 (Jesch et al., 2001). Subsequently, additional sites, such as S245 and T249, were identified to be phosphorylated in

mitosis, which is required for mitotic Golgi disassembly (Xiang and Wang, 2010). Recently, GRASP55 was discovered to be de-O-GlcNAcylated upon energy or nutrient deprivation and regulates autophagosome maturation (Zhang et al., 2019; Zhang et al., 2018). These results indicate that GRASP55 is an excellent candidate to function as both a sensor and effector of cellular stresses. Thus, GRASP55 is likely a master regulator of Golgi structure formation, function, and stress responses.

Our *in vitro* phosphorylation assay demonstrated that PKCα can directly phosphorylate GRASP55 likely on more than one site. Previously, it has been shown by mass spectrometry that GRASP55 is phosphorylated on S441 after TG treatment, but the kinase mediating this phosphorylation is unknown (Gee et al., 2011). Although our results are consistent with this previous study, the exact phosphorylation site(s) need further investigation.

Histamine is a neuroendocrine hormone involved in the regulation of stomach acid secretion, brain function and immune response; many of these functions involve secretion (Karpati et al., 2018; Sahoo et al., 2017; Xie et al., 2018). The role of histamine in immune response is often through the activation of the downstream kinase PKCα. For example, histamine enhances the secretion of granulocyte-macrophage colony stimulation factor (GM-CSF) and nerve growth factor (NGF) in different cell types, both through a PKCα-dependent mechanism (Sohen et al., 2001). Interestingly, histamine promotes HeLa cell proliferation and growth, and has been shown to be elevated in cancers where Golgi is fragmented and secretion is enhanced. Histamine does not induce ER stress (Deniaud et al., 2008). In our experiments, histamine induced a clear Golgi fragmentation phenotype, confirming a link between histamine and Golgi fragmentation.

Additionally, expression of PKCα, but not other PKC isoforms, along with a stimulation with PMA, exhibited an additive Golgi fragmentation effect. Interpreting results of drug treatments used in this study present problems, and this was mitigated by using minimum doses consistent with those found in literature, or even less in the case of thapsigargin. Consistent with prior work showing that disassembly of Golgi stacks accelerates protein trafficking (Xiang et al., 2013), our findings therefore offer a mechanism for how histamine increases secretion of inflammatory factors.

How Ca^{2+} controls membrane trafficking at the plasma membrane has been well documented in regulated secretion in specific cell types such as neurons, neuroendocrine cells and mast cells; while its role in other cell types is less well known. Ca^{2+} dynamic at the Golgi as well as its role in membrane trafficking at the Golgi is still an understudied area. There are EF-hand Ca^{2+} binding proteins associated in the Golgi. For example, Cab45 is located in the Golgi lumen, while Calnuc is found in both cell cytosol and membrane fractions (Lin et al., 1998). At the *cis*-Golgi, Calnuc binds Gαi and Gαs, which is thought to be important for vesicular trafficking (Lin et al., 2000). There are also P-Type ATPases (SPCAs) such as SPCA1 located in the Golgi that regulate Ca^{2+} homeostasis in the Golgi and control neural polarity (Sepulveda et al., 2009; Vanoevelen et al., 2007). Our study provided a novel link between thapsigargin and histamine treatment, elevation of Ca^{2+} concentration in the Golgi region, activation of PKC and phosphorylation of Golgi GRASP55, and modification of Golgi structure and function.

Our study revealed that TG induces Golgi fragmentation through increasing cytosolic Ca^{2+} and GRASP55 phosphorylation. A similar case has been described previously in Alzheimer's disease,

where cytosolic calcium increases by Aβ treatment triggers activation of a cytosolic protease, calpain, which cleaves p35 to generate p25 and activate Cdk5, a cytoplasmic kinase that is highly expressed in neurons (Lew et al., 1994). Subsequently, activated Cdk5 phosphorylates GRASP65 and perhaps other Golgi structural proteins, leading to Golgi fragmentation (Joshi et al., 2015; Joshi et al., 2014). Although PKC and GRASP55 were not the focus in this study, expression of a phosphorylation deficient mutant of GRASP55 significantly reduced Golgi fragmentation as well as Aβ production. Taken together, our studies indicate that the Golgi is sensitive to cellular stimuli and stresses as in disease conditions, and responds to signaling cues to adjust its structure and function through increasing cytosolic Ca^{2+} and GRASP55 modification. Future studies defining the detailed mechanisms may help understand disease pathologies with Golgi and trafficking defects.

2.5 Materials and Methods

Reagents, Plasmids and siRNA

All reagents used were from Sigma-Aldrich (St. Louis, MO), Roche (Basel, Switzerland) or Calbiochem (EMD Millipore, Burlington, MA), unless otherwise stated. The Annexin V apoptosis detection kit was from BioVision Inc. (San Francisco, CA). PKCα-GFP and GFP-PKCβII plasmids were provided by Dr. Yusuf Hannun (Stony Brook Cancer Center). GFP-PKCβI, GFP-PKCδ, and GFP-PKCζ plasmids were provided by Dr. Hesham El-Shewy (Medical University of South Carolina). The CAMKIIβ plasmid was provided by Dr. Mohammed Akaaboune (University of Michigan). The Str-li_VSVGwt-SBP-EGFP plasmid was provided by Dr. Franck Perez (Institut Curie). PKCγ-GFP cDNA construct was purchased from Addgene

(Cambridge, MA). The ManII-GFP HeLa cell line was made in house by transfecting HeLa cells with α-mannosidase II covalently linked to GFP.

Control siRNA (Silencer Select Negative Control #1 siRNA) was purchased from Applied Biosystems (ThermoFisher). PKC-specific custom siRNA targeting to endogenous human PKCα (5'-CAGAAGAACTGTATGCAAT-3') was purchased from Ambien (ThermoFisher). To perform knockdowns, 200 nM of each oligo was used to transfect cells for 48 hours.

Antibodies

The following antibodies were used: monoclonal antibodies against β-actin and GFP (Sigma-Aldrich), Gos28 and GM130 (BD Biosciences, Franklin Lanes, NJ), PKCα (Santa Cruz Biotechnology, Dallas, TX), and α-tubulin (Developmental Studies Hybridoma Bank, University of Iowa); polyclonal antibodies against CHOP, p-eIF2α, eIF2α and p115 (Cell Signaling, Danvers, MA), Giantin, GRASP55 and GRASP65 (Proteintech), Bip (Santa Cruz), GM130 ("N73" from Dr. J. Seemann), and TGN46 (Bio-Rad). Secondary antibodies were purchased from Jackson Laboratory (Bar Harbor, ME). Secondary antibodies used for fluorescence microscopy include fluorescence-labelled goat anti-mouse, goat anti-rabbit and goat anti-sheep (for TGN46) antibodies, all used in 1:200 dilution. Secondary antibodies used for Western blot include HRP-conjugated goat anti-mouse and goat anti-rabbit antibodies, all used in 1:5000 dilution.

Cell Culture and Drug Treatments

For all experiments, mycoplasma-free HeLa were obtained from ATCC (Manassas, VA) and passaged ≤20 times prior to use in experiments. NRK cells were a gift from Dr. Peter Arvan (University of Michigan). HeLa and NRK cells were cultured in Dulbecco's modified Eagle's medium (DMEM; ThermoFisher, Waltham, MA) supplemented with 10% fetal bovine serum (FBS; Gemini Bio-Products, Sacramento, CA) and 100 units/ml penicillin-streptomycin at 37°C with 5% CO_2. RAW 264.7 murine macrophages were kindly provided by Dr. Kezhong Zhang (Wayne State University) and cultured in RPMI 1640 medium supplemented with 10% fetal bovine serum and 100 units/ml penicillin-streptomycin at 37°C with 5% CO_2. Cells were grown on glass coverslips according to standard tissue culture methods (Tang et al., 2012). Coverslips were pre-coated with poly-lysine (Gibco) to aid in cell attachment. For mitotic synchronization, cells were treated with 100 ng/ml nocodazole for 18 h and "shake-off" cells (Xiang et al., 2007) were collected and lysed for Western blot analysis. All drugs, except cAMP-dependent protein kinase inhibitor (PKI) that is a peptide and dissolved in water, were made in DMSO, aliquoted, and stored at -20ºC. Stocks were diluted into working solutions of DMEM at the time of the experiment as described in the text or figure legend. Upon the addition of the drug, cells were incubated at 5% CO_2 and 37°C for the indicated times. Cells were washed 3 times with ice cold phosphate buffered saline (PBS) and collected with a cell scraper.

Immunofluorescence Microscopy

For fluorescence microscopy, cells were rinsed 3 times in ice cold PBS, fixed with 4% (w/v) paraformaldehyde, quenched with 50 mM NH_4Cl, permeabilized in 0.2% v/v Triton X-100 in PBS, and blocked for 1 h with PBS with 1% w/v bovine serum albumin (BSA) Fraction V (ThermoFisher, Waltham, MA) (Tang et al., 2016). Cells were incubated with a primary

antibody diluted in 1% BSA in PBS (PBSB) at room temperature for 1.5 h, washed with PBS, and incubated with an FITC- or TRITC-labeled secondary antibody (1:200 dilution) in PBSB for 45 min at room temperature. Cells were washed 3 times with PBS and stained with 1:5,000 Hoechst dye for 5 min, mounted on glass slides with Moviol, and images were captured with a Zeiss (Oberkochen, Germany) Observer fluorescent microscope with a 63x oil objective lens with a numerical aperture of 1.4 and an Axiocam Mrm camera. TIF files were exported with AxioVision software (Zeiss).

For super-resolution microscopy, Alexa Fluor 647, and Alexa Fluor 488-labeled secondary antibodies (ThermoFisher) were used. After washing, coverslips were mounted to slides using ProLong Diamond antifade super-resolution imaging mountant (ThermoFisher). Super-resolution images were imaged using Leica (Wetzlar, Germany) TCS SP8 STED super-resolution microscope. Images were quantified using the NIH ImageJ software and assembled into figures with Photoshop Elements (Adobe, San Jose, CA). To clearly show the Golgi structure, brightness or contrast was adjusted linearly across all samples within each experiment.

For calcium imaging, GRASP55-GCaMP7 transfected cells were plated onto glass bottomed dishes and imaged by a Nikon C2-plus Laser Scanning Confocal Microscope System configured with a Ti2-E inverted microscope. Images were captured at 488 nm and 561 nm in sequential scanning mode. Z-stacks of 5 slices at 1 μm interval were acquired every 30 seconds for a total period of 10 min. The NIS-Elements C software was used for acquisition, analysis and visualization. The "+Histamine" symbol in Movie S1 was added in Adobe Premiere Pro 2020.

For quantification, fluorescence intensity was measured every minute for 60 min. 20 cells were measured for each drug treatment.

To quantify Golgi fragmentation, cells were evaluated by eye under a microscope according to predefined fragmentation criteria, at least 300 cells were counted in each reaction. The following criteria are used to define whether a Golgi is intact or fragmented: 1) If the Golgi exists as a single piece of connected membrane, it is intact. 2) If a Golgi exhibits several items that are connected by visible membrane bridges, even though these bridges might be faint, the Golgi is considered intact. 3) If a Golgi exhibits ≥ 3 disconnected pieces (no visible bridges connecting them), then the Golgi is fragmented. 4) Mitotic cells, defined by the DNA pattern, and overlapping cells in which the Golgi pattern is difficult to define, are not counted. Hoechst was used to identify individual, mitotic and overlapping cells. In experiments where transfected proteins were employed, only transfected cells were counted, and 100 cells were counted per replicate. In experiments where an inhibitor screen was performed, an unbiased image thresholding method was used to extract fragmentation data from ≥40 cells per replicate.

Protein Biochemistry

For immunoblotting, cells from a culture dish were pelleted and lysed with 30 µl lysis buffer (40 mM Hepes, pH 7.4, 200 mM KCl, 5 mM $MgCl_2$, 1% Triton X-100 (Bio-Rad, Hercules, CA), 50 mM beta-glycerol phosphate, protease inhibitor cocktail (Roche), and phosphatase inhibitors NaF and NaVan pH 8.0). Samples were mixed with 6X SDS-PAGE sample buffer (400 mM Tris-Cl pH 6.8, 15% SDS, 10 mM DTT, 50% glycerol, 0.05% bromophenol blue), denatured at 95°C for 4 min and then run on PAGE gels. For **Fig. 2.12, subpanels C and D** 8% gels were run

at 4°C for 8 h. Protein was transferred to nitrocellulose membranes using semi-dry transfer (Bio-Rad, Hercules, CA) at constant 16 V. Membranes were blocked for 10 min with 3% milk in 0.2% Tween-20 in phosphate buffered saline (PBST) and immunoblotted. Western blots were captured with Enhanced Chemiluminescence (ECL) dye reagent (ThermoFisher), in a FluorChem M chemi-luminescent imager (ProteinSimple, San Jose, CA).

Electron Microscopy (EM)

For EM, cells were fixed in pre-warmed serum-free DMEM, 20 mM Hepes, pH 7.4, 2% glutaraldehyde at room temperature for 30 min or 4°C overnight as previously described (Tang et al., 2010a). Cells were washed 2 times with 0.1 M Sodium cacodylate (Electron Microscopy Sciences, Hatfield, PA), and post-fixed on ice in 1% v/v reduced Osmium tetroxide, 0.1 M Sodium cacodylate (w/v) and 1.5% cyanoferrate (w/v) in water. Cells were rinsed 3 times with 50 mM maleate buffer, pH 5.2, 3 times with water, scraped, and pelleted in microcentrifuge tubes for embedding. The EMBED 812 (EMD) protocol was used to embed cells and resin blocks were sectioned to 60 nm with a diamond knife and mounted on Formvar-coated copper grids. Samples were double contrasted with 2% uranyl acetate then with lead citrate and rinsed with copious amounts of water. Grids were imaged using a Philips (Amsterdam, Netherlands) transmission electron microscope. Golgi images were captured at 11,000x magnification. Golgi stacks were identified using morphological criteria and quantified using standard stereological techniques. A Golgi cisterna was identified as a perinuclear membrane within a Golgi stack ≥4 times longer than its width. Stack length was measured for the longest cisterna within a Golgi stack using the ruler tool in Photoshop Elements 13. For the number of cisternae per stack, the number of cisternae was counted. For the number of vesicles per stack, round objects no greater

than 80 μm in diameter within 0.5 μm of a Golgi stack were counted. At least 20 cells were quantified in each experiment, and the EM results represent two independent experiments.

VSV-G Trafficking using RUSH system

VSV-G trafficking was performed as previously described (Li et al., 2019b). Briefly, HeLa cells were transfected with the Str-li_VSVG wt-SBP-EGFP plasmid (Boncompain et al., 2012) and cultured at 37°C for 16 h. Cells were then incubated with 250 nM TG or 10 μM monensin in fresh medium for 0.5 h at 37°C before 40 μM D-biotin (VWR Life Science, Radnor, PA) was added. Cells were then lysed at indicated time points (chase), treated with or without EndoH, and analyzed by Western blotting for VSV-G-GFP using a GFP antibody. The percentage of EndoH resistant VSV-G was quantified using the ImageJ software.

Molecular Cloning

Catalytically inactive PKCα, PKCα-GFP (K368R), was made in-house using site-directed mutagenesis. Constructs for GRASP55 truncation mutants, aa1-212, aa1-250, aa1-300, aa1-400, aa1-430 were constructed in pEGFP-N1 vector using BamHI and HindIII sites (Zhang et al., 2018). GRASP55 phosphorylation deficient mutants, S255A, S260A, S262A/S263A, S269A, S273A/T274A, T278A, S289A and S292A were constructed by site-directed mutagenesis. The genetically encoded calcium indicator GRASP55-GCaMP7 was made in-house by inserting the GCaMP7a gene (kind gift from Dr. Haoxing Xu) into a pmCherry-N1-GRASP55 WT vector (Zhang et al., 2018) using BamH1 and NotI restriction sites. All cDNAs generated in this study were confirmed by DNA sequencing.

In vitro Kinase Assay

In the presence or absence of 2 mM ATP, twenty μg/ml recombinant GRASP55 protein (Xiang and Wang, 2010) was incubated with 10 μg/ml (for WB) or 20 μg/ml (for Coomassie blue staining) recombinant PKCα (SignalChem, British Columbia, Canada), respectively. Reactions were performed in kinase buffer (20 mM HEPES-NaOH, pH 7.4, 1 mM $CaCl_2$, 1 mM DTT, 10 mM $MgCl_2$, 200 μg/ml phosphatidylserine, 20 μg/ml diacylglycerol) at 30°C for 3 h. Reactions were terminated by adding SDS sample buffer and boiling. GRASP55 proteins were separated by Phos-tag SDS-PAGE and visualized by Coomassie blue staining or immunoblotting. In brief, 50 μM Phos-tag acrylamide and 100 μM $MnCl_2$ were included in the gel recipe according to the manufacturer's instructions. Phos-tag gels were washed twice in water and stained by Coomassie blue or three times in transfer buffer supplemented with 10 mM EDTA and twice in transfer buffer without EDTA before transferring to membranes.

Quantitation and Statistics

All data represent the mean ± SEM (standard error of the mean) of at least three independent experiments unless noted. A statistical analysis was conducted with two-tailed Student's t-test in the Excel program (Microsoft, Redmond, WA). Differences in means were considered statistically significant at $p \leq 0.05$. Significance levels are: *, $p<0.05$; **, $p<0.01$; ***, $p<0.001$. Figures were assembled with Photoshop (Adobe, San Jose, CA). Pearson's colocalization coefficient values were computed using the "Coloc 2" function in ImageJ software.

2.6 Figures

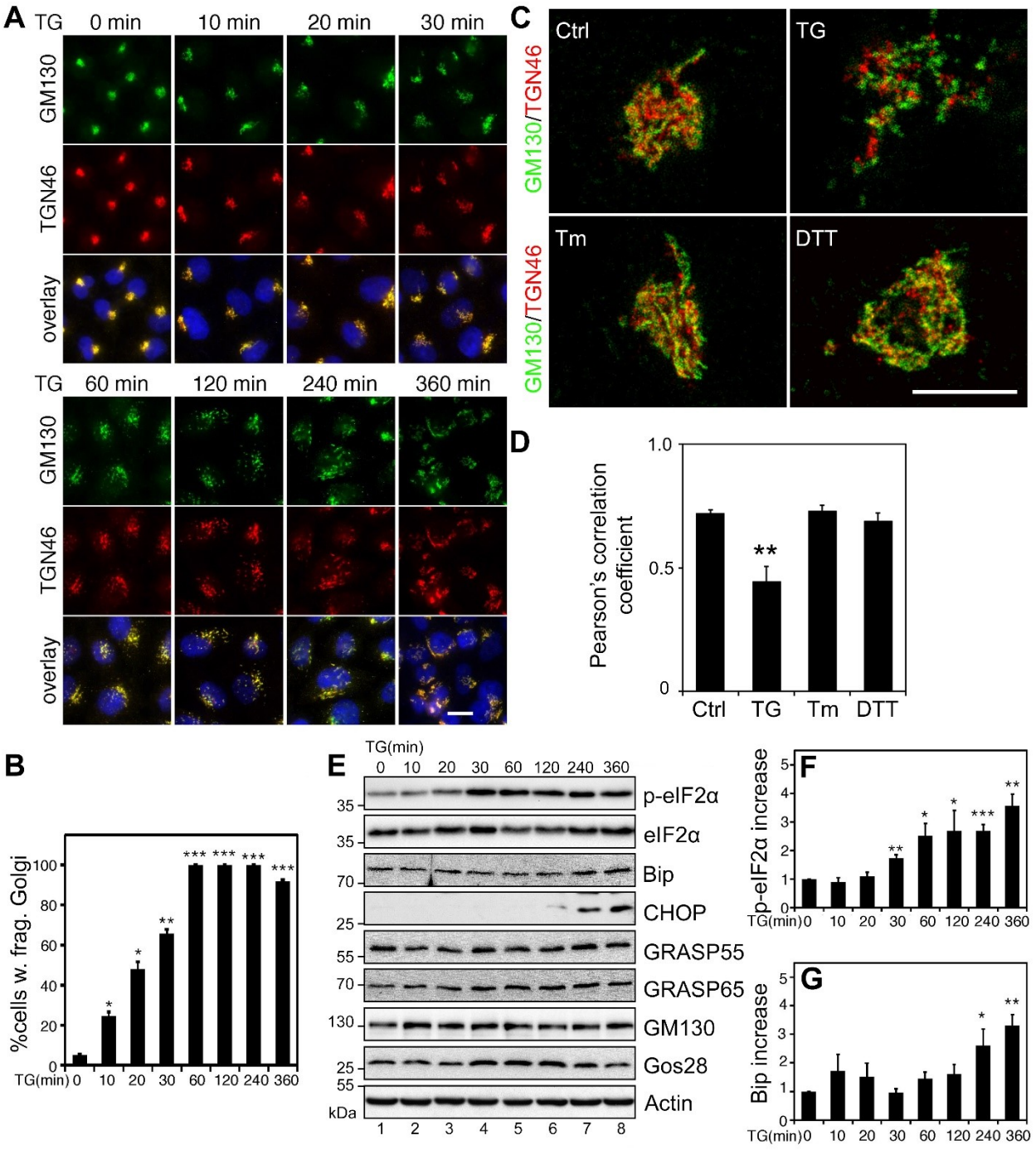

Fig. 2.1 TG treatment induces Golgi fragmentation and UPR
(A) Short term TG treatment causes Golgi fragmentation. HeLa cells were treated with 250 nM TG, fixed at the indicated time points, and stained for GM130 (*cis*-Golgi) and TGN46 (*trans*-Golgi). Scale bar, 20 μm. **(B)** Quantitation of **A** for cells with fragmented Golgi using GM130 as

the Golgi marker. **(C)** HeLa cells were treated with DMSO, 250 nM TG for 20 min, 5 μM Tm for 6 h, or 10 mM DTT for 2 h. Cells were stained for GM130 (green) and TGN46 (red) and analyzed by super-resolution microscopy. **(D)** Pearson's correlation coefficients of GM130 and TGN46 signals in **C**. Two-tailed Student's *t*-tests were used to calculate statistical significance (**, $p \leq 0.01$). **(E)** Longer term TG treatment results in ER stress. Cells treated as in **A** were analyzed by Western blot of indicated proteins. Note that TG treatment increases the levels of p-eIF2α, Bip and CHOP. **(F-G)** Quantitation of the ratio of p-eIF2α/eIF2α and the Bip levels from (E), with the no-treatment control normalized to 1. All quantitation results are shown as Mean ± SEM from at least 3 independent experiments; statistical analyses were performed using two-tailed Student's *t*-tests (*, $p \leq 0.05$; **, $p \leq 0.01$; ***, $p \leq 0.001$).

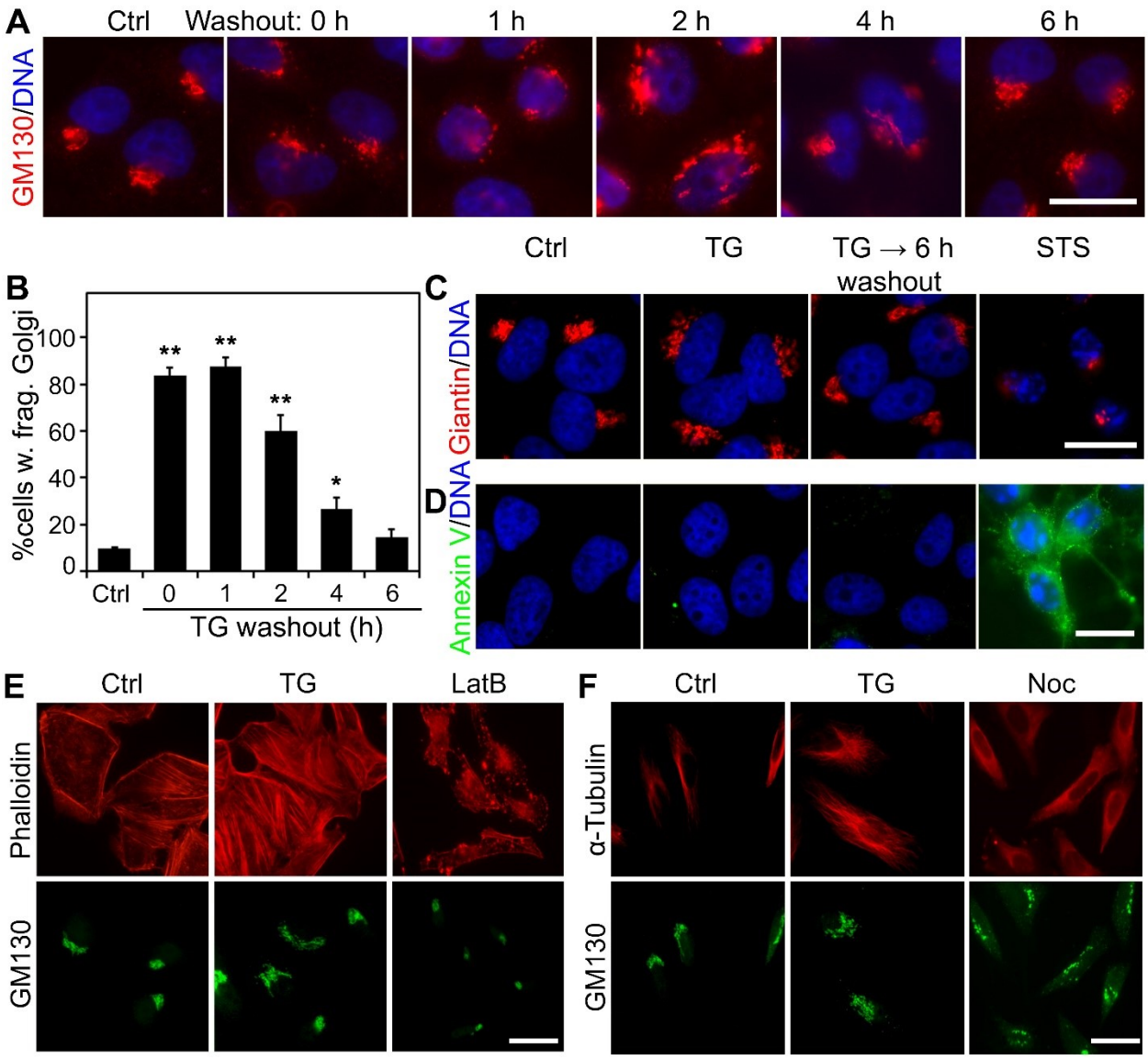

Fig. 2.2 TG-induced Golgi fragmentation is reversible

(A) TG-induced Golgi fragmentation is reversible. Cells were treated with either DMSO or 100 nM TG for 1 h. After washing out TG, TG-treated cells were incubated in fresh growth medium for the indicated times and stained for GM130 (red) and DNA (blue). **(B)** Quantitation of **A** for cells with fragmented Golgi. For statistical analyses, treated cells were compared to the DMSO control (Ctrl). *, $p \leq 0.05$; **, $p \leq 0.01$. **(C)** Acute TG treatment does not cause apoptosis. Cells were treated with either DMSO or 100 nM TG for 20 min without or with 6 h washout, or with 2 µM staurosporine (STS) for 4 h, and stained for GM130 and DNA. **(D)** Cells in **C** were surface stained with Annexin V-EGFP. Scale bars in all fluorescent images, 20 µm. **(E)** Cells were treated with 0.5 µM latrunculin B for 2 h and 250 nM TG was added for the last 20 min. Cells were stained for F-actin with phalloidin (red) and GM130 (green). Scale bar, 20 µm. **(F)** Cells were treated with 1 µM Noc for 2 h and 250 nM TG was added for the last 20 min. Cells were stained for α-tubulin (red) and GM130 (green). Scale bar, 20 µm.

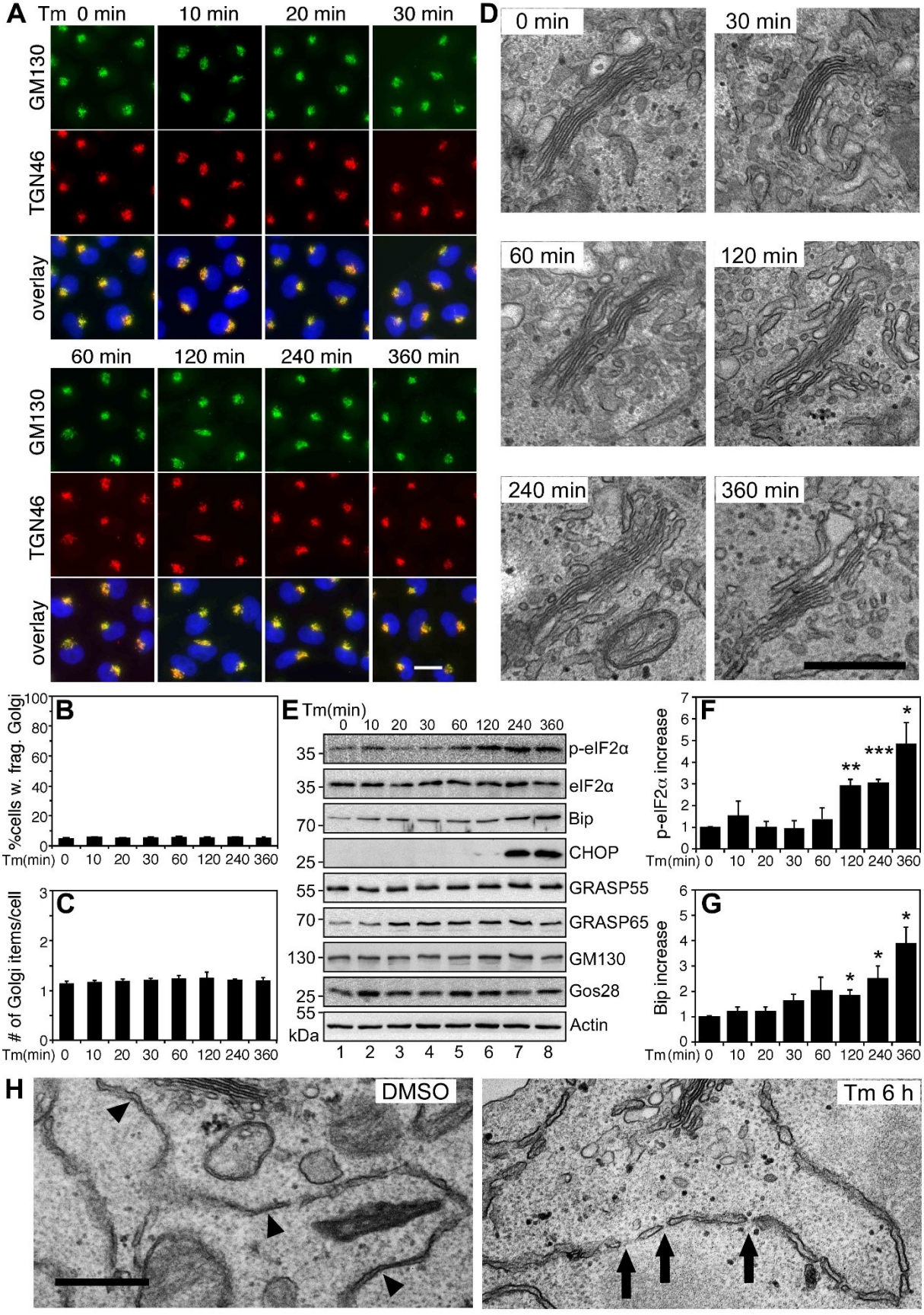
A
Tm 0 min
10 min
20 min
30 min
GM130
TGN46
overlay
60 min
120 min
240 min
360 min
D
0 min
30 min
60 min
120 min
240 min
360 min
B
%cells w. frag. Golgi
Tm(min) 0 10 20 30 60 120 240 360
C
# of Golgi items/cell
E
Tm(min)
0 10 20 30 60 120 240 360
p-eIF2α
eIF2α
Bip
CHOP
GRASP55
GRASP65
GM130
Gos28
Actin
kDa
1 2 3 4 5 6 7 8
F
p-eIF2α increase
G
Bip increase
H
DMSO
Tm 6 h

Fig. 2.3 Tm treatment induces UPR but not Golgi fragmentation
(A) Tm treatment has no effect on the Golgi morphology. HeLa cells were treated with 5 μg/ml Tm for indicated times and stained for GM130 (green) and TGN46 (red). Scale bar, 20 μm. **(B-C)** Quantitation of Golgi fragmentation in Tm-treated cells in **A**. **(D)** EM micrographs of the Golgi region in Tm-treated cells. Scale bar, 0.5 μm. **(E)** Tm-treated cells as in **A** were analyzed by Western blots. Note the increased levels of p-eIF2α, Bip and CHOP over time. **(F-G)** Quantitation of p-eIF2α/eIF2α and Bip in **E**. Results are shown as Mean ± SEM from at least 3 independent experiments; statistical analyses were performed using two-tailed Student's *t*-tests (*, $p \leq 0.05$; **, $p \leq 0.01$; ***, $p \leq 0.001$). **(H)** Representative EM images of ER cisternae in cells treated with DMSO (Ctrl) or tunicamycin (Tm, 5 μg/ml) for 6 h. ER cisternae in Ctrl cells, indicated by arrowheads (►), appear to have a narrow, intact structure; where in Tm treated cells, the ER cisternae appear to be swollen and fragmented, as indicated by arrows (→). Scale bar, 0.5 μm.

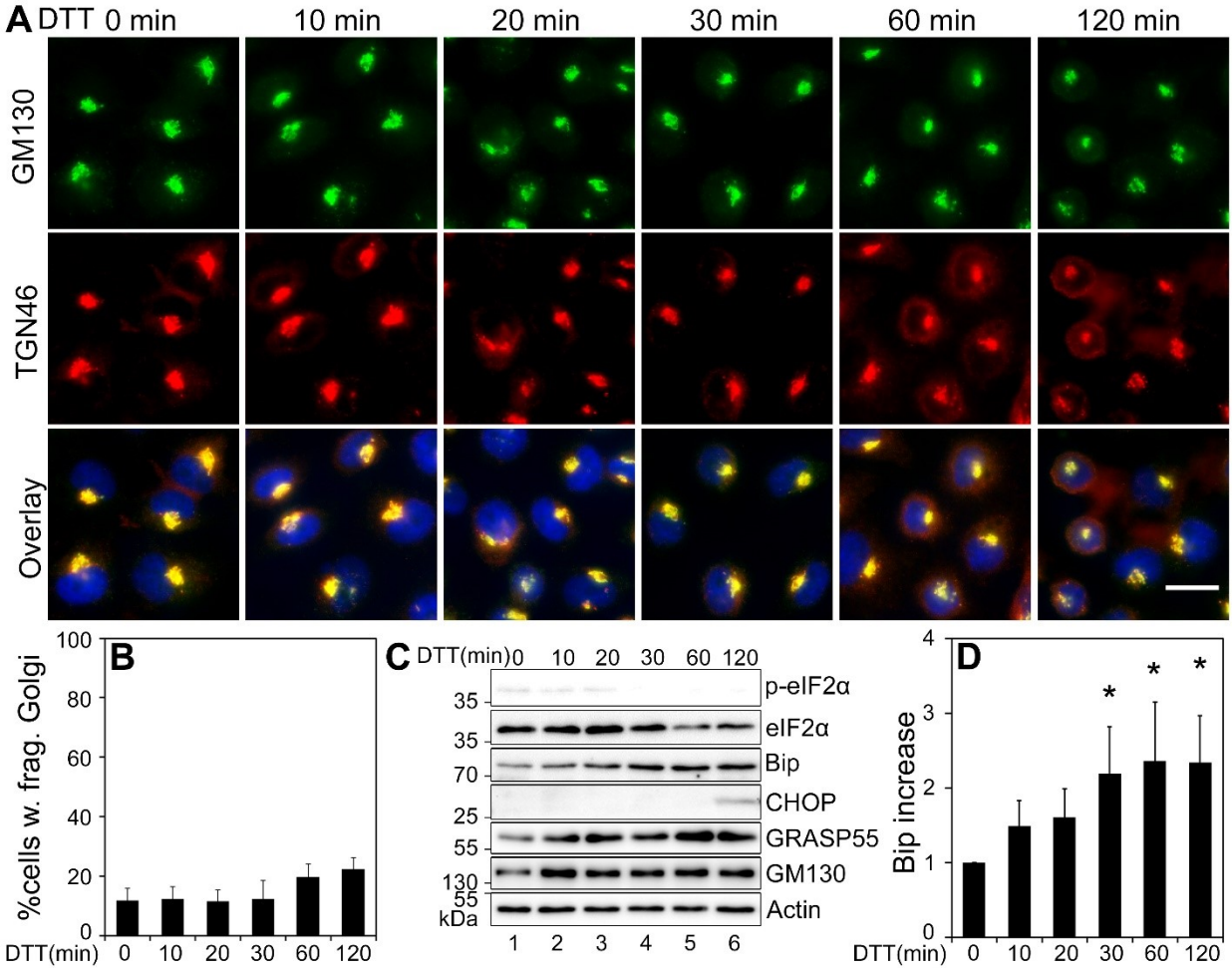

Fig. 2.4 DTT treatment induces UPR but not Golgi fragmentation
(A) HeLa cells were treated with DMSO or 10 mM DTT for indicated times and stained for GM130 (green), and TGN46 (red). Scale bar, 20 µm. **(B)** Quantitation of **A** for cells with fragmented Golgi. **(C)** Western blots of ER stress and Golgi proteins showing UPR induction upon DTT treatment. **(D)** Quantitation of Bip levels from four independent experiments. Two-tailed Student's *t*-tests were used to calculate statistical significance (*, $p \leq 0.05$).

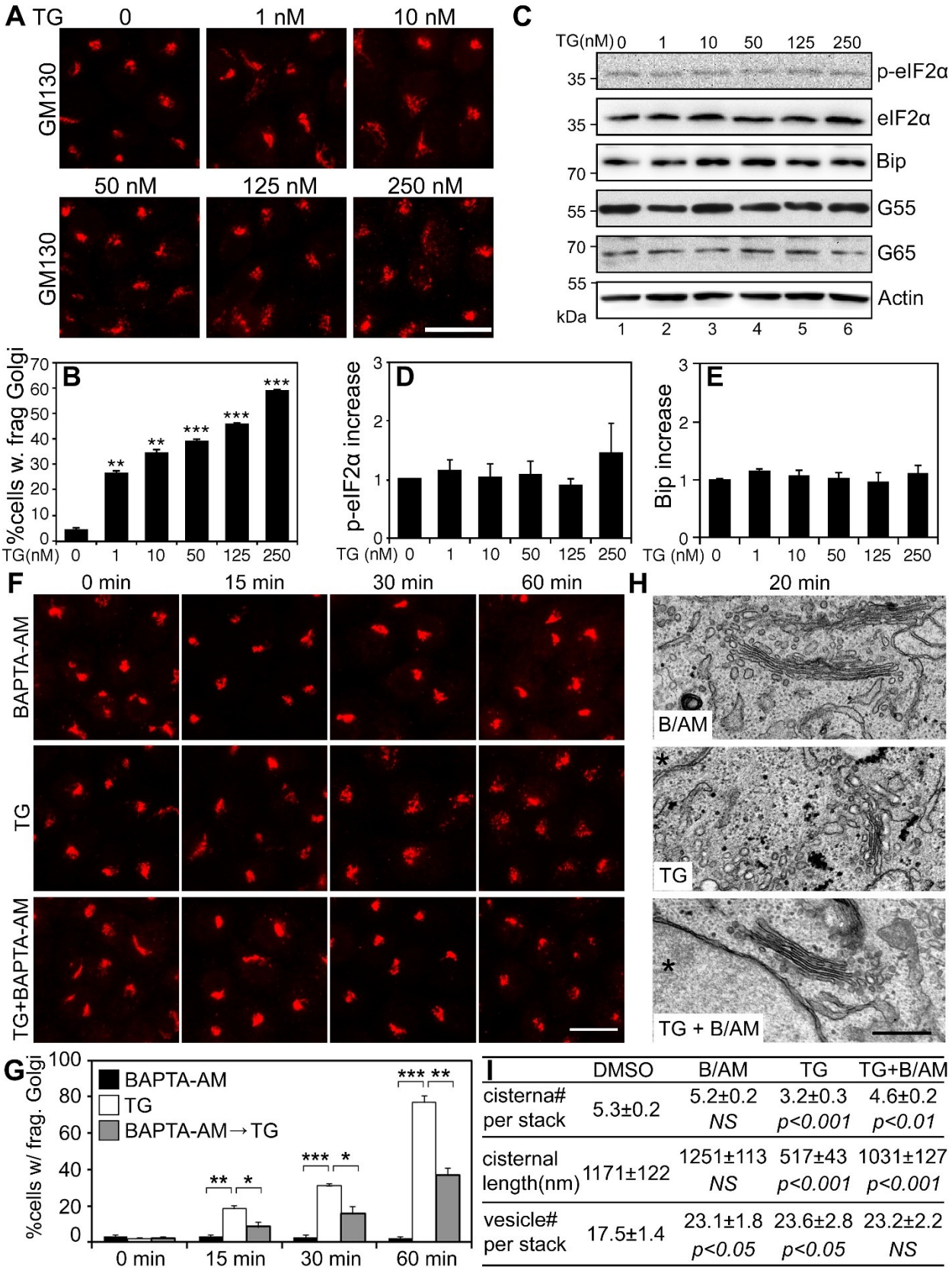

I	DMSO	B/AM	TG	TG+B/AM
cisterna# per stack	5.3±0.2	5.2±0.2 *NS*	3.2±0.3 *p<0.001*	4.6±0.2 *p<0.01*
cisternal length(nm)	1171±122	1251±113 *NS*	517±43 *p<0.001*	1031±127 *p<0.001*
vesicle# per stack	17.5±1.4	23.1±1.8 *p<0.05*	23.6±2.8 *p<0.05*	23.2±2.2 *NS*

Fig. 2.5 TG induces Golgi fragmentation prior to UPR through elevated cytosolic Ca^{2+}

(A) HeLa cells were treated with the indicated concentrations of TG for 20 min and stained for GM130. Scale bar, 20 μm. **(B)** Quantitation of cells with fragmented Golgi in **A**. **(C)** Cells treated with TG as in **A** were analyzed by Western blots. **(D-E)** Quantitation of p-eIF2α/eIF2α and Bip in **C** from five independent experiments. **(F)** BAPTA-AM inhibits TG-induced Golgi fragmentation. HeLa cells treated with 100 nM TG for indicated times with or without 60 μM BAPTA-AM (B/AM) 30 minute pre-treatment, and stained for GM130. Scale bar, 20 μm. **(G)** Quantitation of **F** from three independent experiments. **(H)** Electron micrographs of Golgi profiles in HeLa cells treated with 250 nM TG and B/AM for 20 min. Note that the Golgi is comprised of bulbous saccules in the TG-treatment, whereas in the B/AM pretreated cells the cisternae appear straight and well-stacked. Asterisks (*) indicate nuclei. Scale bar, 0.5 μm. **(I)** Quantitation of the morphological features of Golgi stacks on the EM images in **H**. For statistics, B/AM and TG were compared to DMSO treatment, while TG+B/AM was compared to TG treatment.

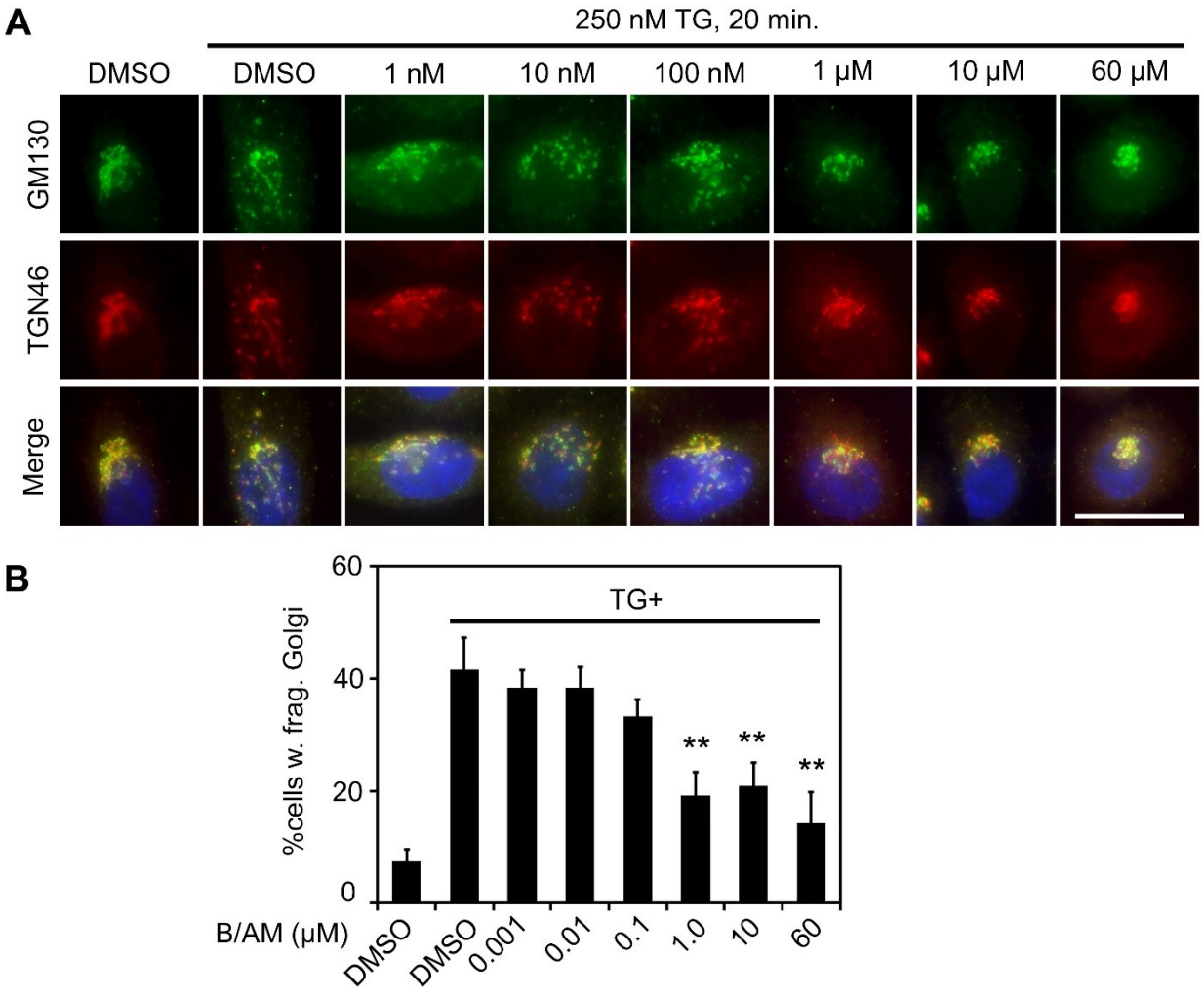

Fig. 2.6 BAPTA-AM inhibits TG-induced Golgi fragmentation
(A) HeLa cells were pretreated with BAPTA-AM for 10 minutes in the amounts shown and then treated with 250 nM TG for 20 minutes, and then with 250 nM TG for 20 min followed by immunostaining of GM130 and TGN46. Scale bar, 20 μm. **(B)** Quantitation of cells in (A) with fragmented Golgi based on the GM130 pattern in the cell. Quantitation of %cells w. Golgi frag. in **B** from 3 independent experiments. Two-tailed Student's *t*-tests were used to calculate statistical significance (**, $p \leq 0.01$).

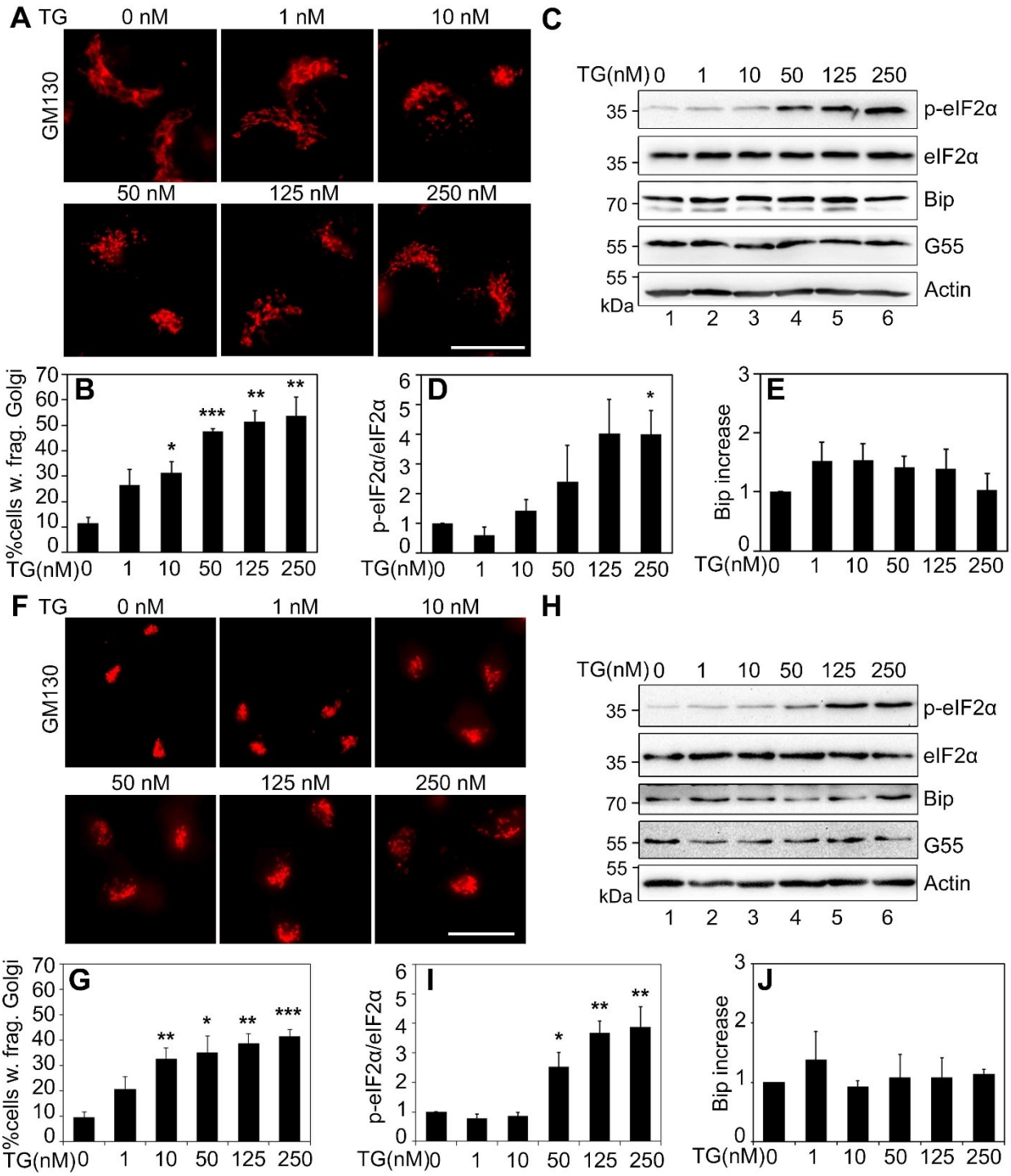

Fig. 2.7 Low concentration of TG induces Golgi fragmentation in NRK cells and RAW 264.7 macrophages

(A) NRK cells were treated with the indicated concentrations of TG for 20 min and stained for GM130. Scale bar, 20 μm. **(B)** Quantitation of cells with fragmented Golgi in **A**. **(C)** Cells treated with TG as in **A** were analyzed by Western blots. **(D-E)** Quantitation of p-eIF2α/eIF2α

and Bip in **C** from 3 independent experiments. **(F)** RAW 264.7 murine macrophage cells were treated with the indicated concentrations of TG for 20 min and stained for GM130. Scale bar, 10 μm. **(G)** Quantitation of cells with fragmented Golgi in **F**. **(H)** Cells treated with TG as in **F** were analyzed by Western blots. **(I-J)** Quantitation of p-eIF2α/eIF2α and Bip in **H** from 3 independent experiments. Two-tailed Student's *t*-tests were used to calculate statistical significance (*, $p \leq 0.05$; **, $p \leq 0.01$; ***, $p \leq 0.001$).

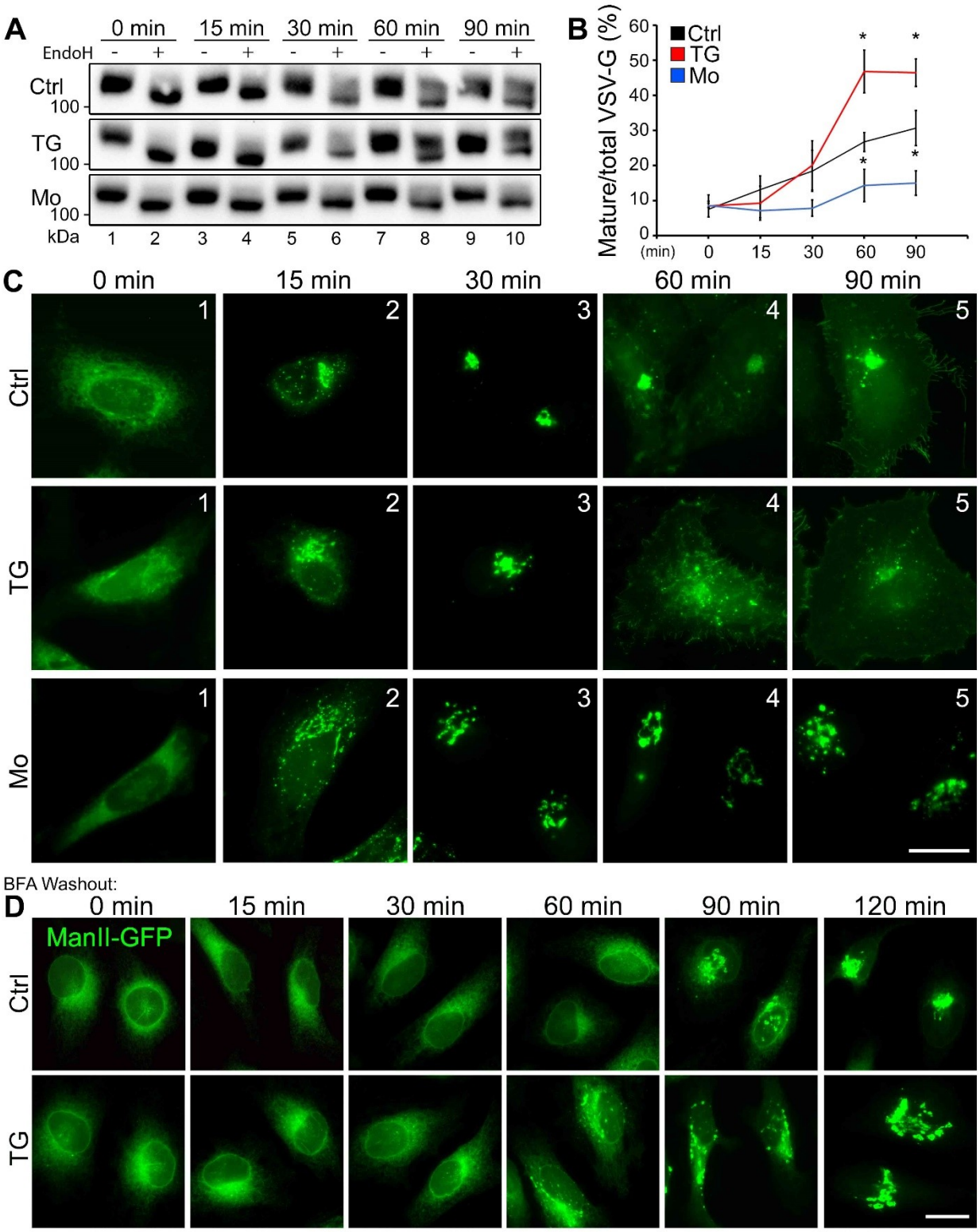

Fig. 2.8 TG-induced Golgi fragmentation increases protein trafficking in the Golgi

(A) Cells were transfected with the Str-li_VSVG wt-SBP-EGFP plasmid for 16 h followed by a 30 min treatment with DMSO, 250 nM TG, or 10 µM monensin (Mo) at 37°C. Cells were then incubated with complete medium containing 40 µM biotin (chase) for the indicated times, lysed and treated with (+) or without (-) EndoH, and analyzed by Western blot for GFP. **(B)** Quantification of **A** for the percentage of EndoH resistant VSV-G from three independent experiments. Quantitation results are shown as Mean ± SEM. Statistical analyses were performed using two-tailed Student's *t*-tests by comparing to the control (*, $p \leq 0.05$). **(C)** Representative images of **A** showing the subcellular localization of VSVG-EGFP at indicated time points after biotin chase. Scale bar, 20 µm. **(D)** Fluorescent images showing the subcellular localization of ManII-GFP in cells treated with DMSO (Ctrl) or 250 nM TG at the indicated time points of BFA washout. ManII-GFP appears in the Golgi area beginning at 60 min, whereas this takes longer in control cells. Scale bar, 20 µm.

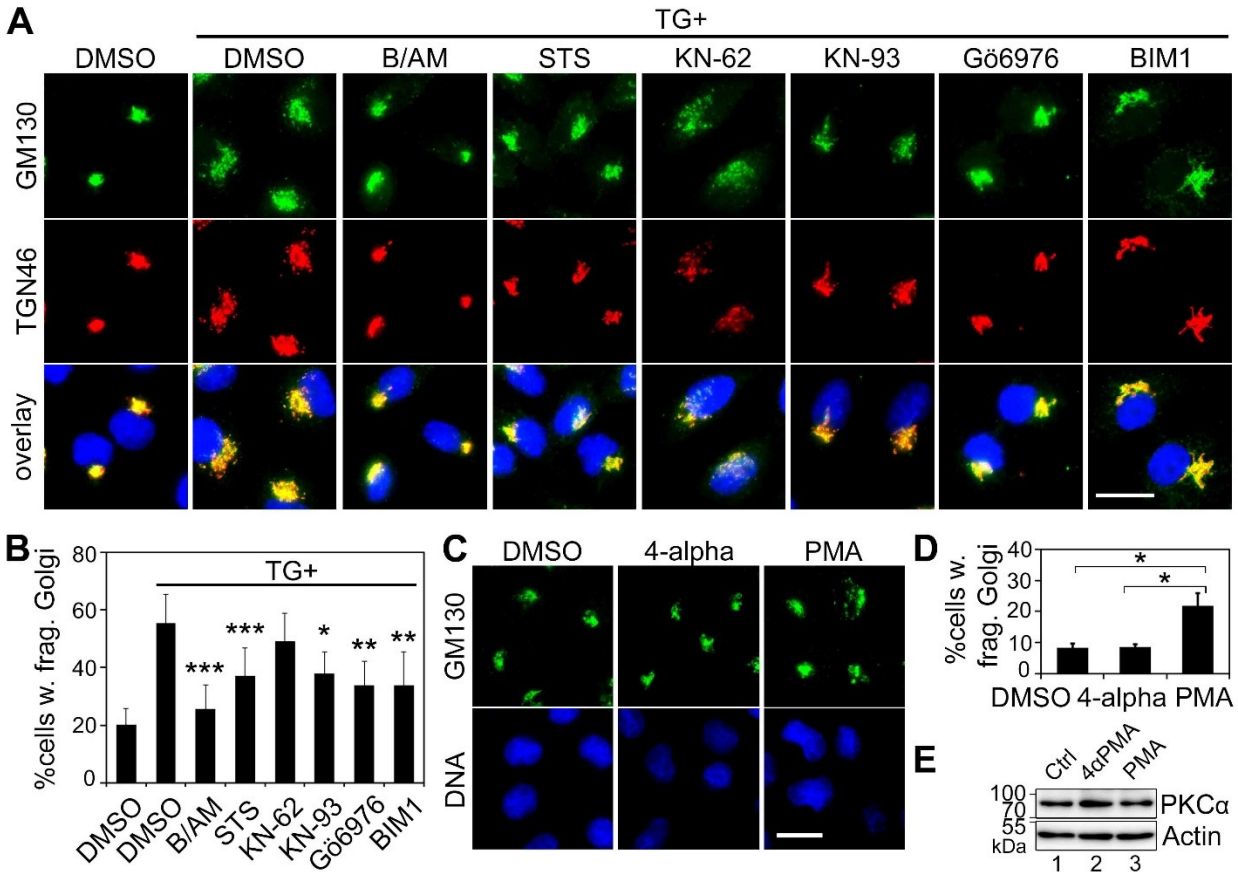

Fig. 2.9 TG induces Golgi fragmentation through PKCα activation
(A) Inhibition of PKC reduces TG-induced Golgi fragmentation. HeLa cells were pre-treated with DMSO, BAPTA-AM (B/AM, 60 μM for 10 min), staurosporine (STS, general kinase inhibitor, 2 μM for 10 min), KN-62 or KN-93 (CAMKII inhibitors, 10 μM and 5 μM, respectively, 10 min), or BIM1 or Gö6976 (PKC inhibitors, 2 μM and 4 μM, respectively, 10 min), and then with 250 nM TG for 20 min followed by immunostaining of GM130 and TGN46. Scale bar, 20 μm. **(B)** Quantitation of cells in (A) with fragmented Golgi based on the GM130 pattern in the cell. **(C)** HeLa cells were treated with 100 nM PMA for 1 h; 4-alpha-PMA of the same concentration was used as a control. **(D)** Quantitation of cells with fragmented Golgi in **C**. **(E)** Cells treated as in **C** were analyzed by Western blot to show that PMA treatment does not change the PKCα expression level.

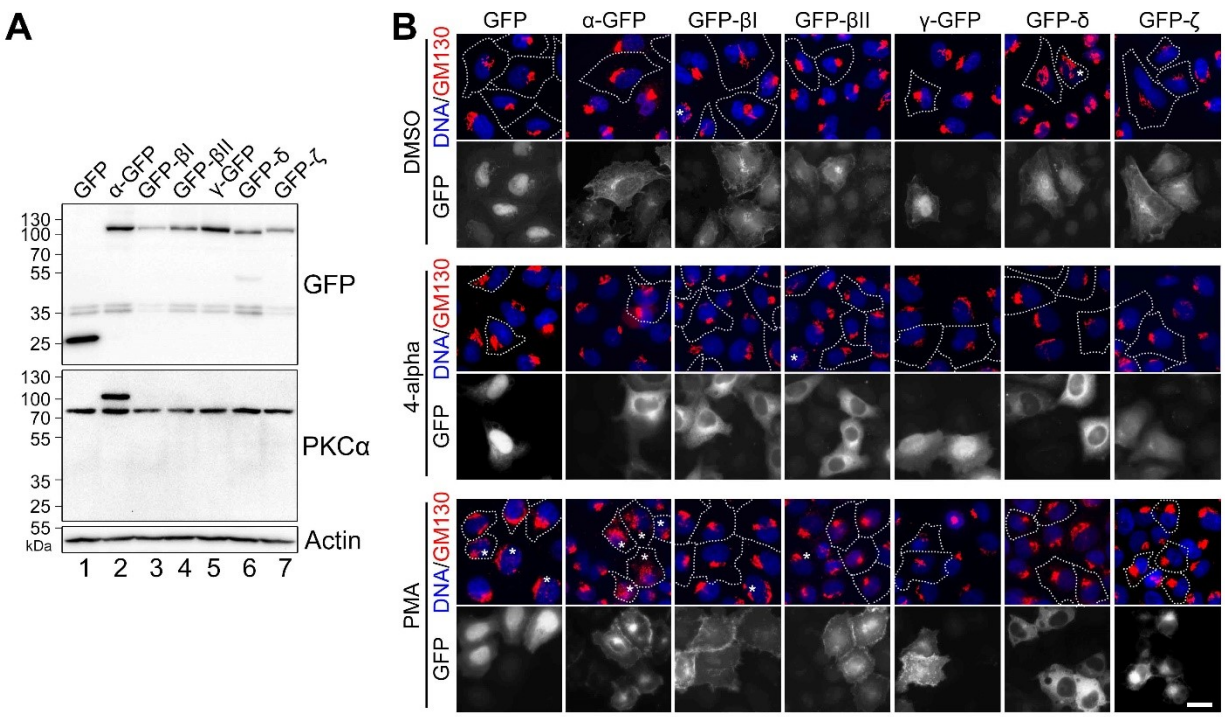

Fig. 2.10 PKCα localizes to the Golgi upon activation
(A) Expression of PKC isoforms. HeLa cells were transfected with indicated PKC isoforms and analyzed by Western blot for GFP or PKCα. **(B)** Fluorescent images showing the localization of expressed PKC isoforms after treatment with DMSO, 4-alpha, or PMA. PMA induces PKCα (α-GFP) localization to the Golgi area, a similar but less dramatic effect was observed for PKCβII (GFP-βII). Scale bar, 20 μm.

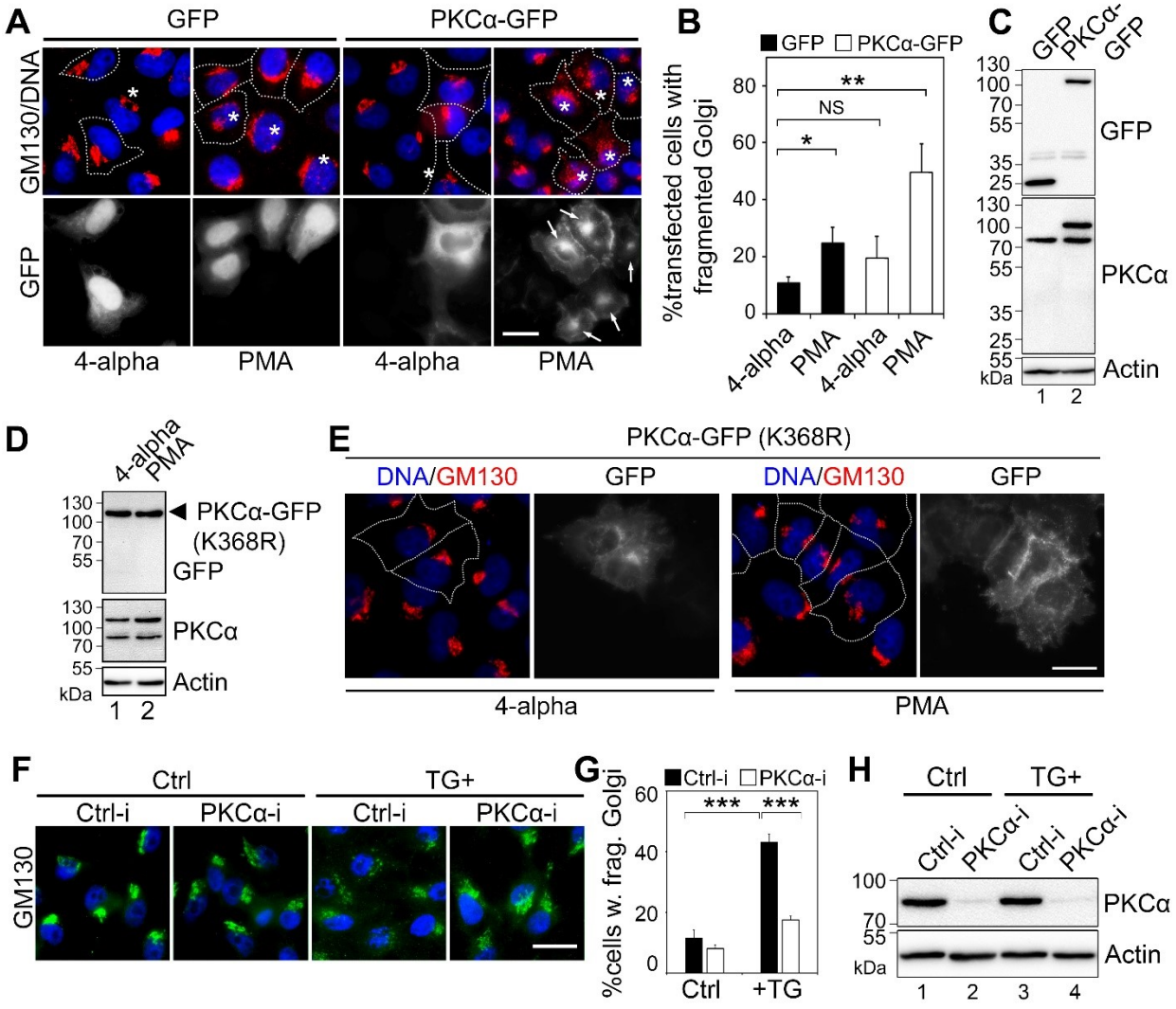

Fig. 2.11 PKCα is required for Golgi fragmentation during PKCα activation
(A) Activation of ectopically expressed PKCα triggers its Golgi localization (indicated by "→") and Golgi fragmentation (*). Cells transfected with GFP or PKCα-GFP were treated with 100 nM PMA or 4-alpha for 1 h. Note the fragmented Golgi in these cells upon PMA treatment. Scale bar, 20 μm. **(B)** Quantitation of cells in **A** with fragmented Golgi. **(C)** Western blot of cells from **A** showing that ectopic PKC expression does not alter the endogenous PKCα expression level. **(D)** PKCα-GFP (K368R) expressed in HeLa cells and treated with either 4-alpha or PMA and visualized by Western blotting. **(E)** Cells in **D** were probed for GM130 (red) and DNA (blue). **(F)** HeLa cells were transfected with control (Ctrl-i) or PKC-specific siRNA for 48 h and then treated with 250 nM TG for 20 min. Cells were fixed and stained for GM130 (green) to show the Golgi structure. Scale bar, 20 μm. **(G)** Quantitation of Golgi fragmentation of cells in **F**. **(H)** Cells in **F** were blotted for endogenous PKCα to evaluate the siRNA knockdown efficiency. All quantitation results are shown as Mean ± SEM from three independent experiments. Statistical analyses were performed using two-tailed Student's *t*-tests (*, $p \leq 0.05$; **, $p \leq 0.01$; ***, $p \leq 0.001$; NS, non-significant).

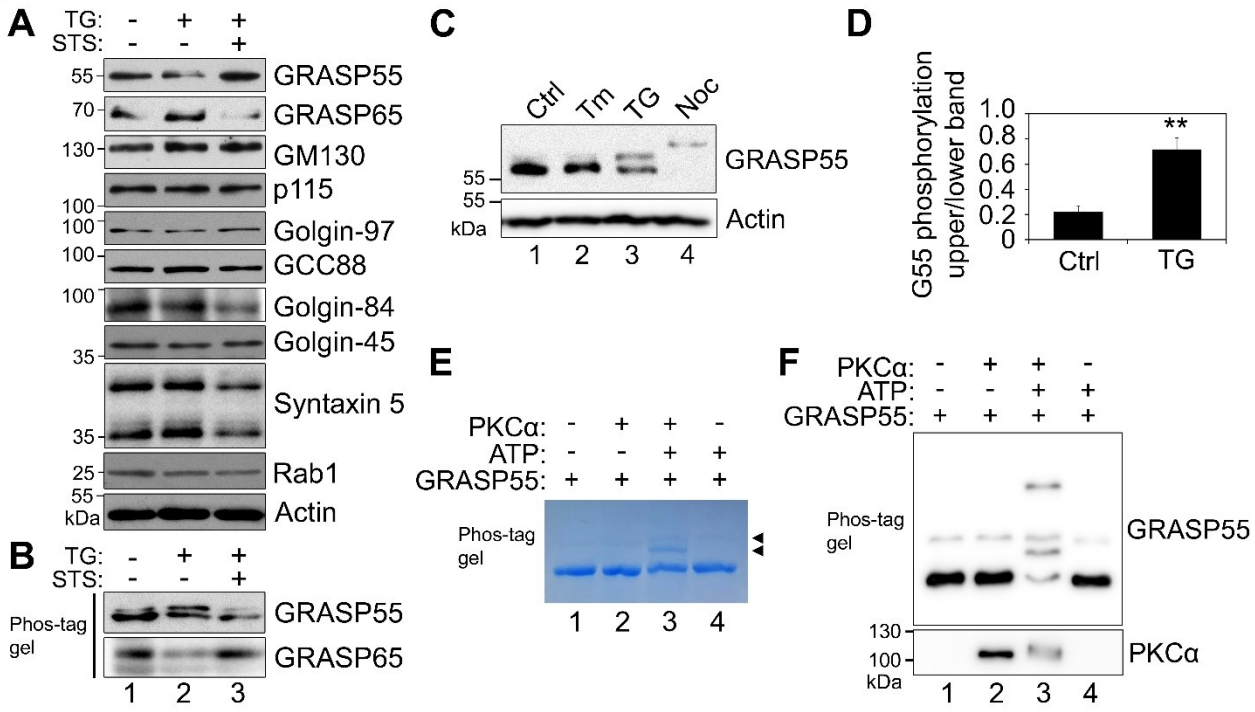

Fig. 2.12 PKCα induces Golgi fragmentation through GRASP55 phosphorylation
(A) TG treatment results in the phosphorylation of GRASP55 but not other Golgi proteins. HeLa cells were treated with 250 nM TG for 1 h, with or without 2 μM staurosporine (STS) pre-treatment for 10 min, and analyzed by Western blot. **(B)** Cell lysates in **A** were analyzed by phos-tag gels and Western blot. **(C)** GRASP55 is phosphorylated upon TG treatment. HeLa cells treated with Tm, TG or nocodazole (Noc) were analyzed by phos-tag gels and Western blot. Note the mobility shift of GRASP55 upon TG treatment compared to control (Ctrl). Nocodazole-arrested mitotic cells were used as a positive control for GRASP55 phosphorylation. **(D)** Quantitation of GRASP55 phosphorylation in TG treated cells. The intensity of the phosphorylated (upper) band was quantified by densitometry analysis, and plotted relative to the intensities of the full length (lower) band. Shown are the results of relative phosphorylation of GRASP55 from 3 independent experiments. **(E)** PKCα phosphorylates GRASP55 *in vitro*. Phosphorylated GRASP55 (►) was analyzed by phos-tag gels and visualized using Coomassie blue staining. **(F)** PKCα phosphorylates GRASP55 *in vitro*. Purified PKCα and GRASP55 were incubated in a kinase buffer with or without ATP as indicated, and analyzed by phos-tag gels and Western blot for GRASP55 and PKCα.

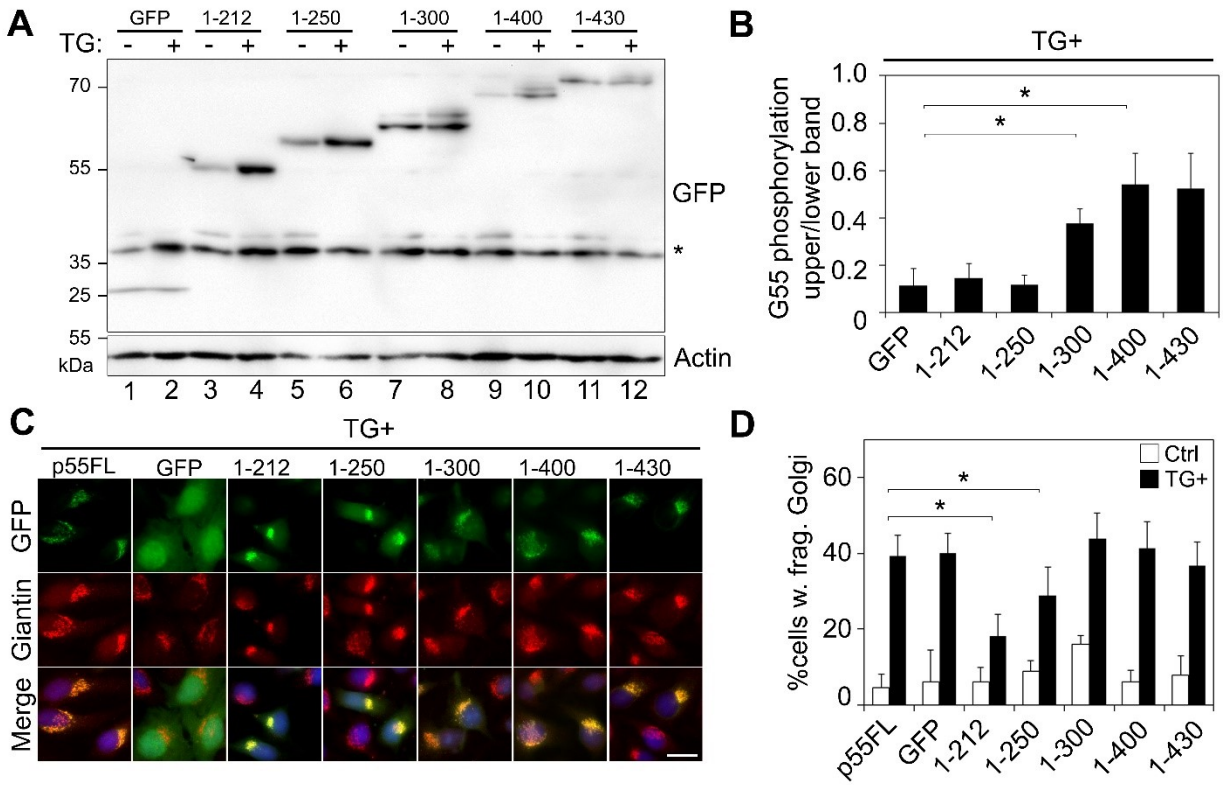

Fig. 2.13 Phosphorylation of GRASP55 within aa251-300 is important for TG-induced Golgi fragmentation

(A) Mapping the phosphorylation site on GRASP55 by expressing GRASP55 truncation mutants. Indicated GFP-tagged GRASP55 constructs were expressed in HeLa cells. After TG treatment, GRASP55 was analyzed by mobility shift. Note the mobility shift in lanes 8, 10, and 12. **(B)** Quantitation of GRASP55 phosphorylation in TG treated cells from **A**. **(C)** TG-induced Golgi fragmentation is rescued by the expression of non-phosphorylatable GRASP55 proteins. Cells expressing the indicated GRASP55 constructs were stained for giantin. **(D)** Quantitation of cells in **C** with fragmented Golgi. Results are shown as Mean ± SEM. Statistical analyses were performed using two-tailed Student's *t*-tests (*, $p \leq 0.05$; **, $p \leq 0.01$).

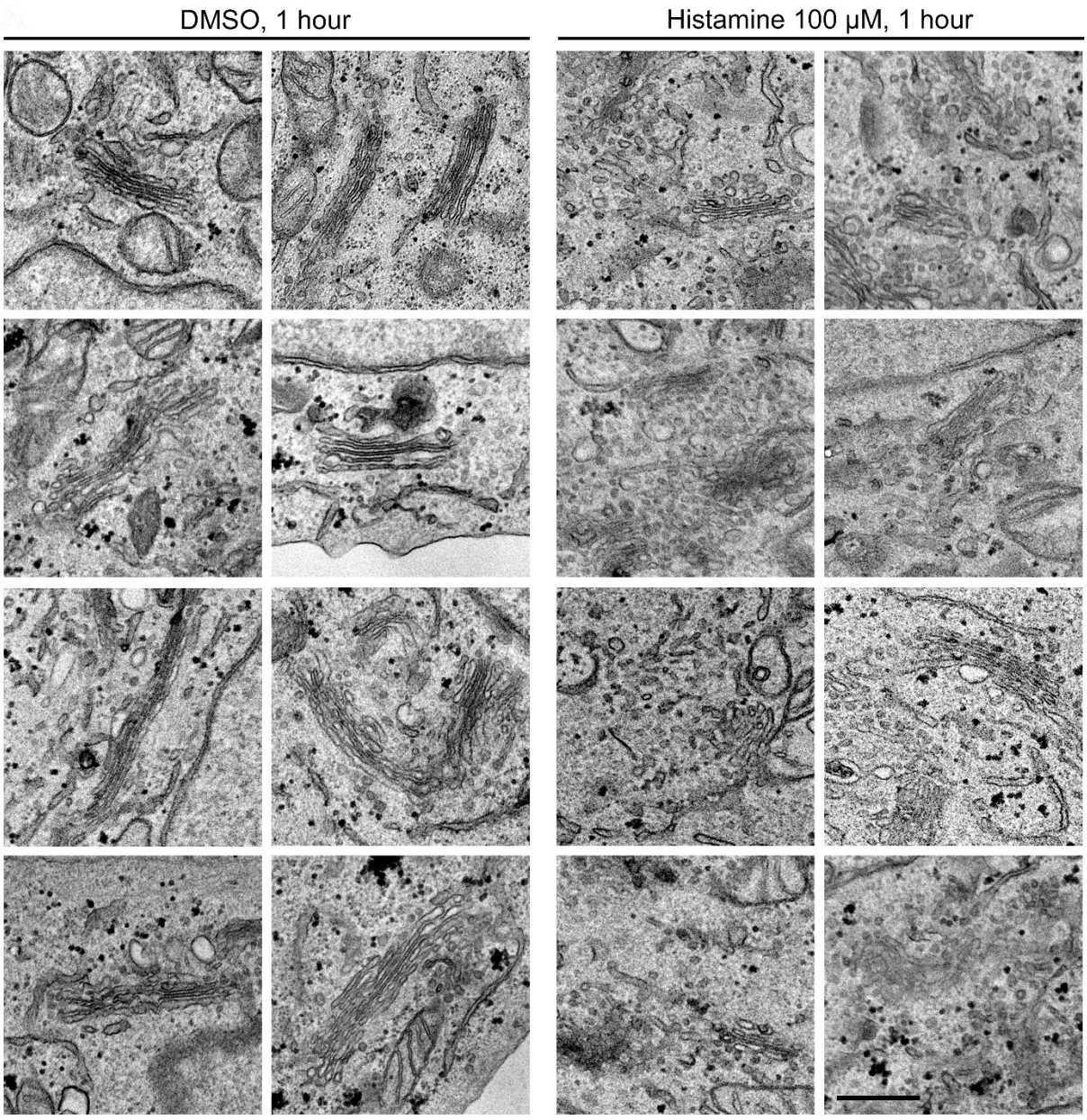

Fig. 2.14 Histamine treatment alters the Golgi structure

HeLa cells treated with either DMSO (control, 1 h) or histamine (100 µM, 1 h) were analyzed by EM. Shown are collections of electron micrographs representing the two treatments. Consistent aberrations in Golgi shape were frequently seen in histamine-treated cells, including reduced cisternae number and stack length, and increased number of vesicles. Scale bar, 0.5 µm.

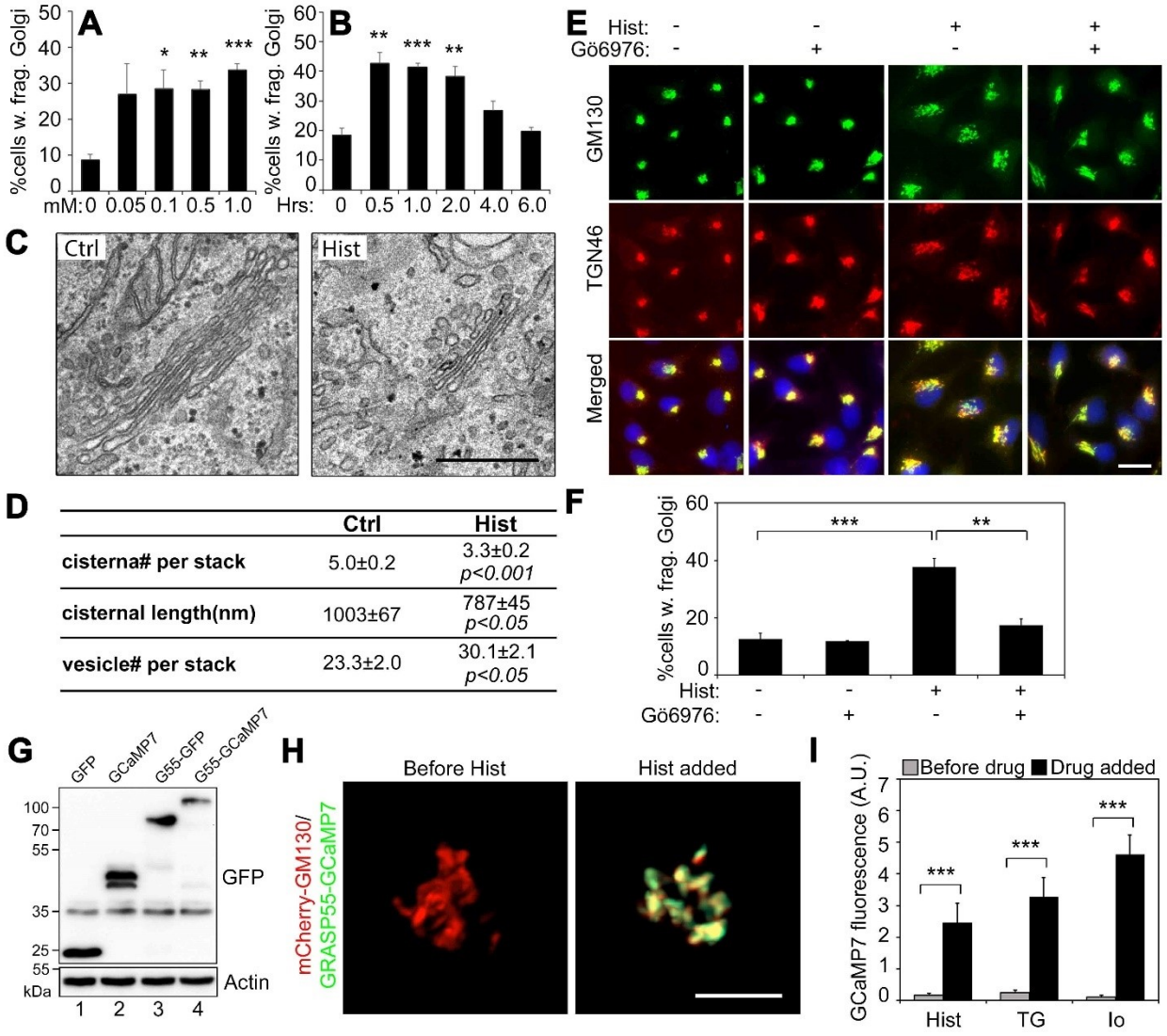

Fig. 2.15 Histamine induces Golgi fragmentation through PKC activation
(A) HeLa cells were treated with indicated concentrations of histamine for 1 h, stained for GM130, and quantified for the percentage of cells with fragmented Golgi. Shown are the quantitation results. **(B)** HeLa cells were treated with 100 μM histamine for the indicated times and analyzed as in **A**. Note that histamine induced Golgi fragmentation within 2 h. **(C)** Electron micrographs of Golgi profiles in HeLa cells treated with DMSO control (Ctrl, left panel) or 100 μM histamine for 1 h (right panel). Note the reduced size of the Golgi in histamine-treated cells. Scale bar, 0.5 μm. **(G)** Expression of the GRASP55-GCaMP7 Golgi Ca^{2+} sensor. HeLa cells transfected with indicated proteins were analyzed by Western blot for GFP. **(H)** Histamine treatment increases the GRASP55-GCaMP7 signal. HeLa cells were co-transfected with mCherry-GM130 (red) and GRASP55-GCAMP7 (green). Shown are still frames before (left panel) or after (right) histamine was added. **(I)** TG and ionomycin treatments increase the GRASP55-GCaMP7 signal. HeLa cells expressing GRASP55-GCaMP7 were treated with 100 μM histamine (Hist), 250 nM TG, or 1 μM ionomycin (Io) for 1 h. Shown are the quantitation of the fluorescence intensity before and after the drug was added. All quantitation results are shown

as Mean ± SEM. Statistical analyses were performed using two-tailed Student's *t*-tests (*, $p \leq 0.05$; **, $p \leq 0.01$; ***, $p \leq 0.001$).

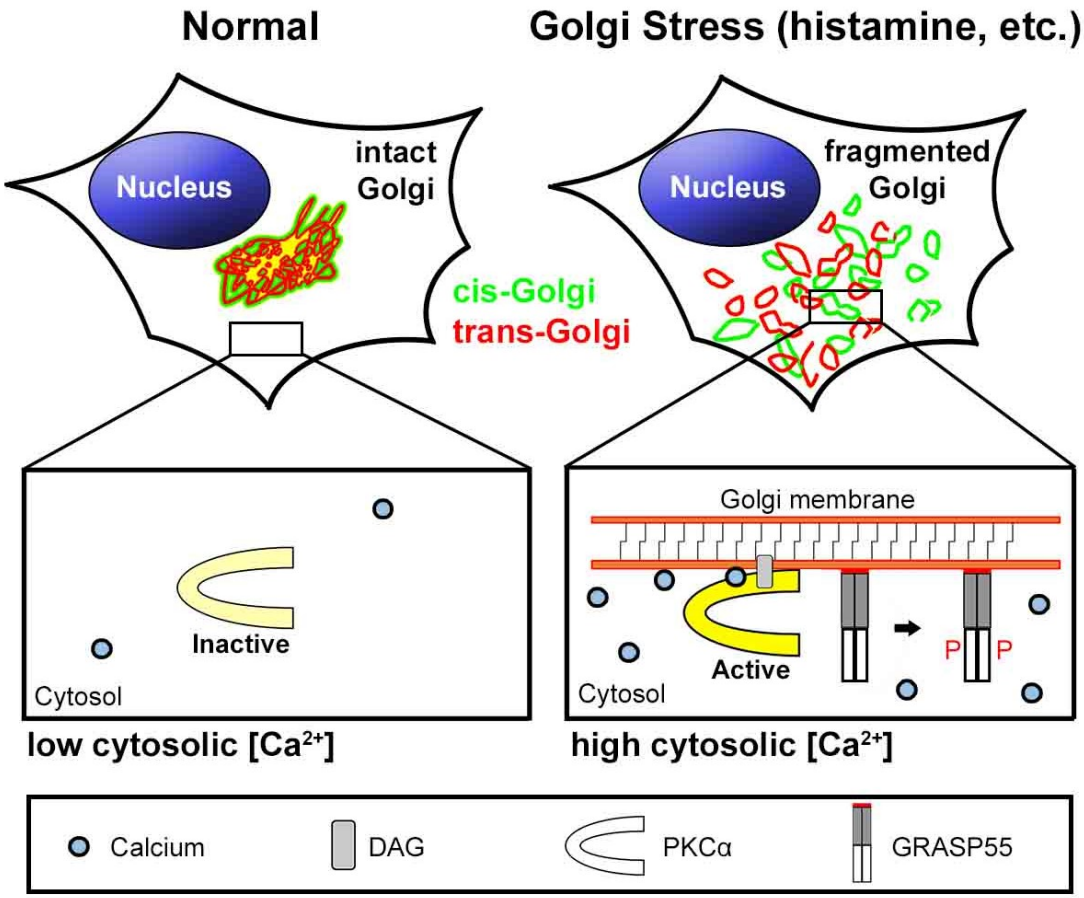

Fig. 2.16 Proposed model of PKCα during stress
Under normal conditions (upper left), cells contain intact Golgi and low cytosolic calcium. Under certain types of calcium stress, such as during histamine or thapsigargin treatment, the Golgi becomes fragmented and unstacked (upper right). This morphology is accompanied by an increase in cytosolic calcium and activation of PKCα which localizes to the Golgi membrane and phosphorylates GRASP55.

CHAPTER III

Hydrogen Peroxide Induces Arl1 Degradation and Impairs Golgi-Mediated Trafficking[3]

3.1 Abstract

Reactive oxygen species (ROS)-induced oxidative stress has been associated with diseases such as amyotrophic lateral sclerosis (ALS), stroke and cancer. While the effect of ROS on mitochondria and endoplasmic reticulum (ER) has been well documented, its consequence on the Golgi apparatus is less well understood. In this study, we characterized the Golgi structure and function in HeLa cells after exposure to hydrogen peroxide (H_2O_2), a reagent commonly used to introduce ROS to cells. Treatment of cells with H_2O_2 resulted in the degradation of Arl1 and dissociation of GRIP-domain containing proteins Golgin-97 and Golgin-245 from the *trans*-Golgi. This effect could be rescued by treatment of cells with protease inhibitors. Structurally, H_2O_2 treatment reduced the number of cisternal membranes per Golgi stack, suggesting a loss of *trans*-Golgi cisternae. Functionally, H_2O_2 treatment inhibited both anterograde and retrograde

[3] This chapter is modified from a version that has been submitted to the journal *Molecular Biology of the Cell* with authors listed as Stephen C. Ireland, Haoran Huang and Yanzhuang Wang (see Acknowledgements section).

protein transport, consistent with the loss of membrane tethers on the *trans*-Golgi cisternae. This study revealed membrane tethers at the *trans*-Golgi as novel specific targets of ROS in cells.

3.2 Introduction

In eukaryotic cells the reduction of O_2 to H_2O during ATP generation in the mitochondria necessarily leads to the production of reactive oxygen species (ROS). ROS can damage various cellular components such as lipids, proteins and nucleic acids. Oxidative stress of cells occurs when damage to cellular components is high enough to lead to a constellation of system failures. For example, treatment of hemoglobin and rat globular basement membrane with hydrogen peroxide (H_2O_2) makes them more susceptible to proteolytic cleavage (Davies, 2016; Fligiel et al., 1984). In addition, oxygen free radicals such as superoxide anion, singlet oxygen, hydroxyl, and perhydroxyl, either generated by the cell or from an external source, can cause the death of multiple cell types *in vitro* and are thought to contribute to many inflammatory conditions (Ahsan et al., 2003; Singh et al., 2007). High levels of oxidative stress are often associated with diseases such as cancer, diabetes, atherosclerosis, stroke, and neurodegenerative disorders such as amyotrophic lateral sclerosis (ALS), in which there is a failure in the cells to reduce ROS (Manoharan et al., 2016; Nindl et al., 2004).

ROS can damage membrane organelles. For example, oxidation and thereby inactivation of protein tyrosine phosphatases (PTPs) can increase steady-state protein phosphorylation of eIF2α and endoplasmic reticulum (ER) stress through redox inhibition of protein phosphatase 1 (Santos et al., 2016). H_2O_2 treatment inactivates catalase and disrupts mitochondria in Hs27 human fibroblasts, and increases the secretion of matrix metalloproteases (Koepke et al., 2008). H_2O_2

can also damage the fluidity and function of the plasma membrane in vascular endothelial cells (Block, 1991). So far, how ROS affects the structure and function of the Golgi apparatus has not been well documented.

The Golgi is a membrane organelle with a stacked structure that functions as a trafficking hub in the cell for the delivery of proteins and lipids to their final destinations. In anterograde trafficking, the *cis* Golgi cisternae receive proteins synthesized by the ER in COPII vesicles and sends them to the endosomal/lysosomal system, the plasma membrane, or outside of the cell. In retrograde trafficking, the *trans* face of the Golgi receives vesicles from the plasma membrane and endosomes for subsequent delivery to the ER (Huang and Wang, 2017). These functions rely on a group of long coiled-coil proteins called golgins, which act as membrane tethers to capture vesicles and facilitate their fusion with the Golgi membranes (Lupashin and Sztul, 2005; Muschalik and Munro, 2018; Witkos and Lowe, 2015; Xiang and Wang, 2011). These include GM130 in the *cis*-Golgi that functions in ER-to-Golgi trafficking, and a group of four GRIP ("Golgin-97, ranBP2alpha, imh1p and p230/golgin-245")-domain containing proteins, Golgin-97, Golgin-245, GCC88 and GCC185, in the *trans*-Golgi (Jackson, 2003; Lu and Hong, 2003; Luke et al., 2003).

The GRIP-domain containing golgins are important for both anterograde and retrograde trafficking at the *trans*-Golgi (Munro, 2011). GCC88 and GCC185 have been shown to differ in their membrane binding properties and localize to distinct subdomains of the *trans*-Golgi, and facilitate the sorting and delivery of distinct cargo sets to and from the *trans*-Golgi network (TGN) (Derby et al., 2004). Golgin-97 and Golgin-245 localize to overlapping but non-identical

subdomains of the TGN and mediate endosome-to-Golgi trafficking (Lu et al., 2004; Wong and Munro, 2014), but only Golgin-97 has been implicated in the anterograde trafficking of E-Cadherin to the cell surface (Lock et al., 2005). Therefore, the GRIP domain tethers regulate the transport of diverse cargo molecules. The GRIP domain of Golgin-97 and Golgin-245 anchors these golgins to the *trans*-Golgi by the interaction with Arl1 (ADP-ribosylation factor-like protein 1), a member of the ARF/Arl family of small GTPases that is localized on *trans*-Golgi membranes. Depletion of Arl1 by RNAi causes dissociation of Golgin-97 and Golgin-245 from the *trans*-Golgi membranes and impairs both anterograde and retrograde trafficking at the TGN (Nishimoto-Morita et al., 2009).

In this study we determined the effect of ROS on Golgi structure and function by acute treatment of cells with H_2O_2. We found that H_2O_2 treatment resulted in a reduction of the number of Golgi cisternae in the stacks, a rapid loss of Arl1, and dissociation of Golgin-97 and Golgin-245 from the *trans*-Golgi, which impaired both anterograde and retrograde trafficking. This study revealed the *trans*-Golgi and trafficking at the *trans*-Golgi as novel targets of ROS in cells, which may help understand the toxicity of ROS in human diseases.

3.3 Results

3.3.1 H_2O_2 treatment causes specific degradation of Arl1 and its binding partners Golgin-97 and Golgin-245

Oxidative stress is most frequently studied using hydrogen peroxide (H_2O_2), a membrane-permeable source of the peroxide ion (O_2^{2-}) that is relatively stable in aqueous solutions (Stone and Yang, 2006). To investigate the effect of ROS on the Golgi, we applied H_2O_2 to HeLa cells

in culture for 10 min with increasing concentrations consistent with physiological levels present in cells (Schroder and Eaton, 2008). Since it has been previously shown that ROS triggers protein degradation (Pajares et al., 2015), we first examined the effect of H_2O_2 treatment on the level of Golgi structural proteins by Western blotting. As shown in **Fig. 3.1A**, H_2O_2 treatment at 1.4 mM, the highest concentration we tested, had no significant effects on most Golgi structural proteins, including GCC88, GCC185, GM130, GRASP65, GRASP55, Golgin-160, cation independent mannose-6-phosphate receptor (CI-M6PR), and syntaxin 6. However, Arl1, Golgin-97 and Golgin-245 were significantly reduced. In this experiment we also tested α-tubulin, a microtubule protein that has previously been shown to be degraded upon 200 μM H_2O_2 treatment for 1 or 4 h (Hu and Lu, 2014). However, total α-tubulin level was unaffected in our experiments, possibly because we used a shorter time for the treatment, indicating that our experimental condition is milder than that of previous studies. Syntaxin 6 is an important SNARE protein in TGN trafficking (Bock et al., 1997), but the level of syntaxin 6 remained unchanged after H_2O_2 treatment at all concentrations. Based on these results, we chose to use 1 mM H_2O_2 and 10 min for the treatment in most of our following experiments; at this condition Arl1, Golgin-97 and Golgin-245 are degraded whereas GM130 and other Golgi structural proteins did not change.

As an alternative approach, we performed high-speed centrifugation to separate cytosolic proteins from cellular membranes. This approach allowed us to examine not only the protein level, but also the membrane association of Arl1 and other proteins (**Fig. 3.1B**). As controls we used GS28 and actin as markers for membranes and cytosol, respectively. As shown in **Fig. 3.1B**, Arl1, Golgin-97 Golgin-245, GCC88, and GCC185 were all enriched in the membrane

fraction of control cells. After H_2O_2 treatment, Arl1, Golgin-97 and Golgin-245 were reduced in the membrane fractions, while GCC88 was relatively stable, consistent with the results shown above.

3.3.2 H_2O_2 treatment reduces membrane association of GRIP domain-containing golgins in *trans*-Golgi

Our results showed that H_2O_2 treatment reduced the protein level of Arl1, Golgin-97 and Golgin-245 but not the other two GRIP domain-containing golgins, GCC88 and GCC185 (**Fig. 3.1**). To further confirm that H_2O_2 treatment reduces the level of GRIP domain-containing golgins in the Golgi by an alternative method, we analyzed their subcellular localization by immunofluorescence microscopy. As shown in **Fig. 3.2A-B**, H_2O_2 treatment reduced the level of Arl1 and Golgin-97 in the Golgi region indicated by GM130 in a dose dependent manner. Similarly, Golgin-245 also reduced its level in the Golgi region (**Fig. 3.3**). Unlike Golgin-97 and Golgin-245, GCC88 and GCC185 signals reduced in the Golgi region but increased in the cytosol after H_2O_2 treatment (**Fig. 3.3**), indicating that GCC88 and GCC185 were dissociated from the Golgi, although they were not degraded (**Figure 3.1A**). Taken together, our results indicate that H_2O_2 treatment reduces the level of membrane tethers in the *trans*-Golgi membranes.

3.3.3 Short term H_2O_2 treatment does not cause Golgi fragmentation but reduces the number of cisternae per Golgi stack

Because no significant change was observed in the Golgi morphology by immunofluorescence microscopy using GM130 and TGN46 as markers (**Fig. 3.4A-B**), we next performed electron

microscopy (EM) to analyze the ultrastructure of the Golgi stacks in more detail. As shown in **Fig. 3.5**, the average number of Golgi cisternae per stack was reduced by H_2O_2 treatment (3.5 ± 0.3) compared to that of control cells (4.8 ± 0.3), indicating a loss of Golgi cisternae. Previously, we have observed that depletion of GRASP65 and/or GRASP55 reduces the number of cisternae in the Golgi stack and the length of the Golgi cisternae, resulting in vesiculation of Golgi membranes (Bekier et al., 2017; Xiang and Wang, 2010). However, unlike GRASP depletion, the number of vesicles surrounding each Golgi stack did not significantly change after H_2O_2 treatment, nor did the average length of the stacks (**Fig. 3.5; Fig. 3.6**). The shape of the Golgi cisternae appeared to be normal, with flat, well aligned cisternae within the stacks, and with narrow and uniform gaps between them. The reduction in cisterna number in the stacks and the loss of *trans*-Golgi membrane tethers suggest a possibility that *trans*-Golgi cisternae were removed or reduced after H_2O_2 treatment.

3.3.4 H_2O_2 treatment reduces anterograde and retrograde trafficking

Arl1 and the GRIP domain-containing golgins are best known for their roles in tethering vesicles from the endosomes to facilitate their fusion with Golgi membranes. To determine the effect of H_2O_2 treatment on retrograde trafficking, we first looked at the subcellular localization of CI-M6PR, which is constantly recycled between the TGN and late endosomes. While treatment of cells with 1 mM H_2O_2 had no effect on the protein level of CI-M6PR at various time points (**Fig. 3.7A**), the CI-M6PR signal in the Golgi region reduced over time (**Fig. 3.7B-C**). The reduction of the CI-M6PR signal in the Golgi region indicates an inhibition of CI-M6PR trafficking from the endosomes to the Golgi in H_2O_2-treated cells. As a complimentary approach, we used Shiga toxin 1 B subunit (StxB) as a tool to measure retrograde trafficking (Selyunin and

Mukhopadhyay, 2015a). Cells were first incubated with StxB at 4ºC to allow it to bind to the cell surface, and then warmed up to 37ºC to allow StxB trafficking toward the Golgi (chase). After 60 min chase, StxB was accumulated in the Golgi region in control cells; in contrast, it existed mostly as cytoplasmic puncta in H_2O_2-treated cells (**Fig. 3.7D**). Consistent with the loss of Arl1 tethering complexes, our results demonstrate that H_2O_2-treatment impairs the function of the *trans*-Golgi in retrograde trafficking.

Since TGN also play essential roles in anterograde trafficking, we determined the effect of H_2O_2 treatment on Vesicular Stomatitis Virus-Glycoprotein (VSV-G) trafficking using the RUSH system (Boncompain et al., 2012). Cells were transfected with a plasmid that encodes both the invariant chain of the major histocompatibility complex (Ii, an ER protein) fused to core streptavidin and VSV-G fused to streptavidin-binding peptide (SBP). Under normal conditions the interaction between streptavidin and SBP retains VSV-G in the ER. Upon the addition of biotin, this interaction is displaced by the strong binding of biotin with SBP, resulting in the release of the VSV-G reporter from the ER for trafficking to the plasma membrane. Since VSV-G is a glycoprotein, we used endoglycosidase H (EndoH) to distinguish its core (ER and *cis*-Golgi) and complex (post-Golgi) glycosylation forms as an indicator of trafficking. As shown in **Fig. 3.7F**, H_2O_2 treatment decreased the EndoH resistant post-Golgi forms of VSV-G at 30 and 60 min time points after release compared to that in the control, demonstrating that H_2O_2 treatment decreased VSV-G trafficking through the Golgi. Using the same experimental scheme, we also labelled cell surface VSV-G with an antibody that recognizes its extracellular domain in unpermeabilized cells at different time points to determine its arrival to the plasma membrane after release. In the control treatment, VSV-G started to appear at the cell surface after 30 min

release; whereas in H_2O_2 treated cells VSV-G was still undetectable after 60 min release (**Fig. 3.7G**). Taken together, degradation of membrane tethers in the *trans*-Golgi upon H_2O_2 treatment impairs both anterograde and retrograde trafficking.

3.3.5 H_2O_2 treatment causes golgin-97 degradation by cytoplasmic proteases

As demonstrated above, Arl1, Golgin-97 and Golgin-245 are degraded upon H_2O_2 treatment; therefore, we determined whether this degradation was mediated by proteasomes or lysosomes, two major protein degradation pathways in the cell. Because it has been previously shown that oxidative stress triggers autophagy, a cellular process that delivers cargo molecules to lysosomes for degradation, we first inhibited autophagy and lysosomal degradation with Bafilomycin A1 (BafA1) and determined the effect on H_2O_2-induced Golgi protein degradation. As shown in **Fig. 3.8A**, BafA1 treatment resulted in the accumulation of p62, a cargo protein for autophagosomal degradation (**lane 2 vs. 1**), but had no effect on H_2O_2-induced Arl1 or Golgin-97 degradation (**Fig. 3.8A, lane 4 vs. 3**), indicating that H_2O_2-induced Arl1 or Golgin-97 degradation is not through autophagy or lysosomes. We also confirmed that the addition of BafA1 had no effect on H_2O_2-induced Golgin-97 reduction in the Golgi region by immunofluorescence microscopy (**Fig. 3.8C**).

Proteasomal degradation is a process in which cells target ubiquitinated proteins for degradation by the proteasome (Eisenberg-Lerner et al., 2020). By examining our Western blots, we did not detect ubiquitinated forms of Arl1 and Golgin-97. In addition, inhibition of proteasomal degradation by MG132 had no effect on H_2O_2-induced Arl1 and Golgin-97 degradation as examined by Western blotting or fluorescence microscopy (**Fig. 3.8D-F**). These results

demonstrated that ROS-induced Arl1 and Golgin-97 degradation is not via lysosomes or proteasomes.

In addition to proteasomal and lysosomal degradation pathways, cytosolic proteases are known to degrade Golgi proteins such as Golgin-160 (Mancini et al., 2000). Therefore, we added a protease inhibitor cocktail (Roche) into the treatment to determine if it could rescue H_2O_2-induced Arl1 degradation. This cocktail contains a set of chemicals that can effectively inhibit a broad spectrum of serine and cysteine proteases. As shown in **Fig. 3.8G-H**, the addition of the protease inhibitors blocked H_2O_2-induced Arl1 and Golgin-97 degradation. Furthermore, immunofluorescence microscopy confirmed that adding protease inhibitors effectively inhibited H_2O_2-induced Golgin-97 reduction in the Golgi region (**Fig. 3.8I**). Taken together, these results indicate that the degradation of Arl1 and Golgin-97 upon H_2O_2 treatment is by cytoplasmic proteases.

3.4 Discussion

In this study, we revealed that H_2O_2 treatment induces a rapid degradation of Golgi tethering proteins on the *trans*-Golgi, including Arl1, Golgin-97 and Golgin-245, which could be rescued by protease inhibitors, indicating that H_2O_2-induced ROS activates a cytoplasmic protease to selectively degrade Arl1, Golgin-97 and Golgin-245 on the *trans*-Golgi. This results in a reduction of the cisternal number per Golgi stack and impairs both anterograde and retrograde trafficking. Our results revealed a novel mechanism by which oxidative stress within physiological levels induces rapid and selective degradation of Arl1 and its associated golgins on

the *trans*-Golgi, which impairs both anterograde and retrograde trafficking. This study has identified the Golgi as a novel site of ROS to exert its toxicity in cells.

It is interesting to see that the degradation of Arl1 and its associated golgins is not by proteasomes or lysosomes, but rather by cytoplasmic proteases. How proteins in the Golgi are degraded is so far not well understood. Theoretically, Golgi proteins can be degraded by the following pathways: 1) by lysosome-mediated protein degradation, which requires delivery of Golgi proteins to the lysosomes either by direct trafficking or by autophagy; 2) by ER-associated degradation (ERAD), in which particular Golgi proteins traffic back to the ER for degradation by proteasomes; 3) by direct ubiquitination at the Golgi and degradation by the proteasomes on site; and 4) by cytoplasmic proteases. We originally speculated lysosomal degradation as the most likely mechanism for Arl1 degradation as it has previously been shown that oxidative stress triggers autophagy (Zhang et al., 2016) and that there is a link between Golgi function and autophagy (Zhang et al., 2019; Zhang et al., 2018). However, this possibility was ruled out by BafA1 treatment, which inhibits lysosomal degradation. Similarly, inhibition of proteasomes by MG132 also had no effect on Arl1 degradation. It is possible that a cytoplasmic protease may be more readily accessible than proteasomes or lysosomes for Arl1, Golgin-97 and Golgin-245.

The identity of this cytoplasmic protease is as yet unknown and remains a subject for future investigation. One possible candidate is calpain, which is non-lysosomal and is known to be activated by ROS in intermittent hypoxia (Bailey et al., 2015). Calpain has two isoforms that are both calcium-activated neutral protease that function in the cytoplasm (Croall and DeMartino, 1991). Convincing evidence for a role of these proteases is lacking for most of the described

functions, however calpain may proteolytically regulate PKC suggesting a possible explanation for why the Golgi is not fragmented during H_2O_2 treatment in **Fig. 3.4**. Calpain cleavage specificity is likely mediated by substrate tertiary structure and not primary protein sequence, which increases the difficulty to predict the precise cleavage sites on its target proteins.

In contrast to some other Golgi stresses such as thapsigargin treatment that triggers Golgi fragmentation (Ireland et al., 2019), H_2O_2 does not cause obvious Golgi fragmentation, nor apoptosis. The loss of Arl1 and its associated golgins, together with the lack of Golgi fragmentation and the impairment of anterograde and retrograde trafficking in H_2O_2 treated cells, indicates that Arl1 and its associated golgins play critical roles in membrane trafficking, but may not be essential for Golgi structure formation. Alternatively, Golgi fragmentation may take longer than 10 min at which our assays were performed. Indeed, H_2O_2 treatment reduced the number of cisternae in the Golgi stack and Golgi-mediated trafficking, indicating that trafficking defects occur prior to Golgi fragmentation. The identity of the lost cisternae remains unknown; but given that Arl1 and its associated golgins reside in the *trans*-Golgi, it is more likely that some *trans* cisternae are lost upon H_2O_2 treatment, which requires further investigation.

Our study revealed that the *trans*-Golgi is uniquely sensitive to oxidative stress in cells, which may help understand the toxicity of ROS in human diseases. ROS has been found to occur in several human diseases such as ALS, cancer and diabetes (Manoharan et al., 2016; Nindl et al., 2004), and Golgi structural and functional defects have been observed in Parkinson's (Mizuno et al., 2001), Huntington's (Hilditch-Maguire et al., 2000) and Alzheimer's (Joshi et al., 2015; Joshi et al., 2014; Joshi and Wang, 2015) diseases and ALS (Fujita and Okamoto, 2005; Gonatas et al.,

1998; Mourelatos et al., 1996). It would be interesting to test whether Arl1 and its associated golgins are degraded in these diseases in future studies.

3.5 Materials and Methods

Reagents and Plasmids

All reagents used in this study were purchased from Sigma-Aldrich (St. Louis, MO), Roche (Basel, Switzerland), EMD Millipore (Burlington, MA), or ThermoFisher (Waltham, MA), unless otherwise stated. H_2O_2 (30% in water) was from Fisher Chemical. Trypan blue was from Gibco (Dublin, Ireland). N-acetyl cysteine (NAC) was from Sigma. The cOmplete, EDTA-free protease inhibitor (PI) tablets were from Roche. Shiga toxin 1 Subunit B (StxB) was from BEI Resources (Manassas, VA). D-Biotin was from VWR Life Science (Radnor, PA). Bafilomycin A1 (BafA1) was from Fisher Scientific. MG132 was from EMD Millipore. The Str-li_VSVGwt-SBP-EGFP plasmid was provided by Dr. Franck Perez (Institut Curie).

Antibodies

The following primary antibodies were used. Monoclonal antibodies against β-actin and GFP (Sigma-Aldrich); Shiga Toxin B (Fisher); GM130, Gos28, Golgin-245 and syntaxin 6 (BD Biosciences, Franklin Lanes, NJ); α-tubulin (Developmental Studies Hybridoma Bank, University of Iowa); Arl1 (Abcam); VSV-G extracellular domain (David Sheff). Polyclonal antibodies against GCC88, Golgin-160, CI-M6PR, GRASP55 and GRASP65 (Proteintech); GCC185 (Abcam); GM130 ("N73" from J. Seemann); TGN46 (Bio-Rad). Secondary antibodies were purchased from Jackson Laboratory (Bar Harbor, ME). Secondary antibodies used for fluorescence microscopy include fluorescence-labelled goat anti-mouse, goat anti-rabbit and goat

anti-sheep antibodies. Secondary antibodies used for Western blot include HRP-conjugated goat anti-mouse and goat anti-rabbit antibodies.

Cell Culture and Drug Treatments

HeLa were obtained from ATCC (Manassas, VA), cultured in Dulbecco's modified Eagle's medium (DMEM; ThermoFisher) supplemented with 10% fetal bovine serum (FBS; Gemini Bio-Products, Sacramento, CA) and 100 units/ml penicillin-streptomycin at 37°C with 5% CO_2, and routinely screened for mycoplasma contamination. Cells were grown on glass coverslips according to standard tissue culture methods (Tang et al., 2011). Coverslips were pre-coated with poly-lysine (Gibco) to aid in cell attachment. H_2O_2, NAC and PI solutions were made fresh in Milli-Q water. All other drugs were dissolved in DMSO and stock solution aliquoted and stored at -20°C until use. Stock solutions were diluted into working solutions of DMEM or water at the time of the experiment. Depending on the chemical, H_2O or DMSO was used as control in the experiments.

Protein Biochemistry

For immunoblotting, cells from a 6 cm dish were washed 3 times with ice cold PBS and collected with a cell scraper. Cells were pelleted and lysed with 100 µl lysis buffer (20 mM Tris-HCl, 150 mM NaCl, 1% Triton X-100 (Bio-Rad, Hercules, CA), 20 mM glycerolphosphate and protease inhibitor cocktail). Samples, excluding GCC185 samples (see below), were mixed with 6X SDS PAGE buffer with fresh DTT, denatured at 95°C for 4 min and then analyzed by SDS-PAGE. Protein was transferred to nitrocellulose membranes using semi-dry transfer at a constant 16 V. Membranes were blocked for 10 min with 3% milk in 0.2% Tween-20 in phosphate

buffered saline (PBST) and immunoblotted. GCC185 and Golgin-245 samples were denatured at 50°C for 5 min before loading onto a SDS-PAGE and transferred to nitrocellulose membranes by a wet-transfer at 50 V for 2 h. Western blots were captured with enhanced chemiluminescence (ECL) dye reagent (ThermoFisher) in the FluorChem M chemi-luminescent imager (ProteinSimple).

Subcellular Fractionation

Fractionation of membranes was performed as described (Xiang et al., 2013). Briefly, control (Ctrl) HeLa cells and cells treated with 1 mM H_2O_2 for 10 min (H_2O_2) were washed with PBS, collected in HBS buffer (0.25 M sucrose, 10 mM HEPES, pH7.2, 1 mM $Mg(OAc)_2$, 1 mM EDTA, 0.5 mM PMSF, and protease inhibitor cocktail) with a cell scraper, and homogenized using 349 a ball-bearing (Ø=8.008) homogenizer (HGM Lab Equipment) to ~80% cell breakage (Tang et al., 2011; Tang et al., 2010a). Plasma membrane disruption efficiency was examined by a trypan blue exclusion method. Homogenate was centrifuged at low speed for 10 min at 1000 g at 4°C. Post-nuclear supernatant (PNS) was then subjected to ultracentrifugation for 1 h in a TLA55 rotor at 100,000 g at 4°C to separate membranes (M) from cytosol (C). An equal amount of PNS, C and M were loaded onto SDS-PAGE and analyzed by Western blot using the indicated antibodies (Xiang et al., 2013).

Immunofluorescence Microscopy

For fluorescence microscopy, cells were rinsed 3 times in ice cold phosphate buffered saline (PBS), fixed with 4% (w/v) paraformaldehyde, quenched with 50 mM NH_4Cl in PBS, permeabilized in 0.2% (v/v) Triton X-100 in PBS, and blocked for 1 h with PBSB - PBS

supplemented with 1% (w/v) bovine serum albumin (BSA) Fraction V (ThermoFisher, Waltham, MA) (Tang et al., 2016). Cells were incubated with a primary antibody diluted in PBSB at overnight gently rocking at 4°C, thoroughly washed with PBS, and incubated with an FITC-, TRITC- or CY5-labeled secondary antibody (1:200 dilution in PBSB) at room temperature for 30 min. Cells were then washed 3 times with PBS and stained with 1:10,000 Hoechst dye for 3 min, and then mounted on glass slides with Moviol plus fluorescence brightener (DABCO; Acros Organics). Images were captured with a Zeiss Observer fluorescent microscope with a 63x oil objective lens and Axiocam Mrm camera. TIF files were exported with AxioVision software (Zeiss). For the data in **Fig. 3.7B and C**, images were collected at random locations on the coverslip with the autofocus function of ZEN software at 20x magnification.

Electron Microscopy

All EM related reagents were from Electron Microscopy Sciences (EMS; Hatfield, PA). Cells were fixed in pre-warmed serum-free DMEM, 20 mM HEPES, pH 7.4, 2% glutaraldehyde at room temperature for 30 min or 4°C overnight as previously described (Tang et al., 2010a; Wang et al., 2005). Cells were washed 2 times with 0.1 M Sodium cacodylate, and post-fixed on ice in 1% (v/v) reduced Osmium tetroxide, 0.1 M Sodium cacodylate (w/v) and 1.5% cyanoferrate (w/v) in water. Cells were rinsed 3 times with 50 mM maleate buffer, pH 5.2, 3 times with water, scraped, and pelleted in microcentrifuge tubes for embedding. The EMBED 812 protocol was used to embed cells and resin blocks were sectioned to 60 nm with a diamond knife and mounted on Formvar-coated copper grids (Tang et al., 2010a). Samples were double contrasted with 2% uranyl acetate then with lead citrate and rinsed with copious amounts of water. Grids were imaged using a Philips (Amsterdam, Netherlands) transmission electron microscope. Golgi

images were captured at 11,000x magnification. Golgi stacks were identified using morphological criteria and quantified using standard stereological techniques. A Golgi cisterna was identified as a perinuclear membrane within a Golgi stack ≥4 times longer than its width. Stack length was measured for the longest cisterna within a Golgi stack using the ruler tool in Photoshop Elements 13. For the number of cisternae per stack, the number of cisternae was counted. For the number of vesicles per stack, round objects no greater than 80 microns in diameter within 0.5 micron distance to a Golgi stack were counted. Golgi morphology was quantified from at least 20 cells in each experiment.

Shiga toxin 1B subunit (StxB) transport assay

Shiga toxin assay was performed as previously described (Selyunin and Mukhopadhyay, 2015b). In short, cells were plated onto poly-lysine coated coverslips and cultured overnight, incubated with 4 μg/mL purified Shiga toxin 1B subunit (StxB) DMEM at 4°C for 30 min, and then washed thoroughly with cold PBS. Cells were then incubated with H_2O_2 in growth medium for 10 minutes at 37ºC, washed with growth medium, and further incubated in growth medium without H_2O_2 for an additional 50 min at 37ºC. After treatment, cells were fixed and permeabilized as described above, stained with indicated primary and secondary antibodies for 1.5 h each at room temperature, and analyzed by fluorescence microscopy.

VSV-G protein trafficking and exofacial labelling

For EndoH treatment and Western blotting, cells in a dish were transfected with the Str-li_VSVG wt-SBP-EGFP plasmid for 16 h followed by a 10 min treatment with 1 mM H_2O_2. Cells were then incubated with fresh growth medium containing 40 μM biotin (chase) for the indicated

times. Cells were lysed with denaturing buffer (0.5% SDS, 40 mM DTT), boiled at 90°C for 10 minutes, and treated with (+) or without (-) EndoH in G5 buffer (50 mM Sodium Citrate, pH 5.5) at 37°C for 1 h. Reaction was mixed with SDS buffer and analyzed by Western blot for GFP. Bands on Western blots were quantified using densitometry analysis. The intensity of the upper EndoH resistant band was divided by that of the total of the upper and lower bands to calculate the mature/total ratio.

For immunofluorescence analysis of cell surface VSV-G, HeLa cells grown on poly-lysine coated coverslips were transfected with the Str-li_VSVG wt-SBP-EGFP plasmid for 16 h. Cells were then fixed in 4% paraformaldehyde without permeabilization, blocked with 1% BSA in PBS, and incubated with an anti-VSV-G antibody overnight at 4°C. After washing 3 times with PBS, the cells were briefly permeabilized with 0.3% Triton X-100 and processed for immunofluorescence.

Quantitation and Statistics

All data represent the mean ± SEM (standard error of the mean) of at least three independent experiments unless noted. A statistical analysis was conducted with two-tailed Student's t-test in the Excel program (Microsoft, Redmond, WA). Differences in means were considered statistically significant if $p \leq 0.05$. Significance levels are: *, $p \leq 0.05$; **, $p \leq 0.01$; ***, $p \leq 0.001$. Figures were assembled with Photoshop (Adobe, San Jose, CA). For **Fig. 3.7C**, automatic thresholding was performed in ImageJ, and the Golgi-localized M6PR signal was plotted. Over 300 cells were evaluated for each timepoint.

3.6 Figures

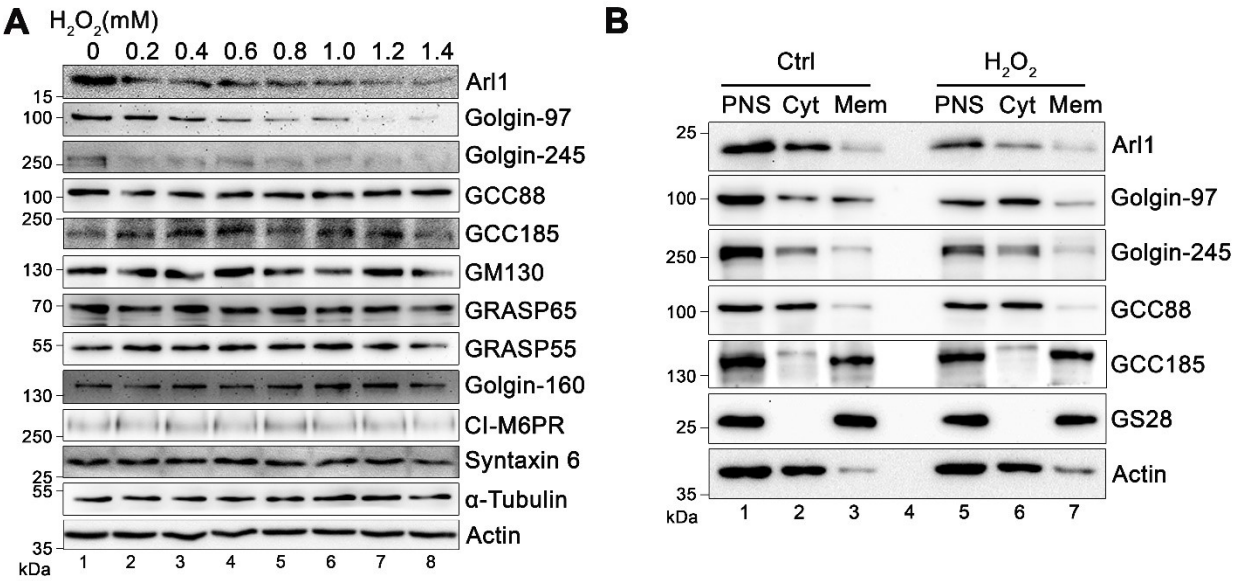

Fig. 3.1 H_2O_2 treatment causes specific degradation of Arl1 and its binding partners
(A) Effect of H_2O_2 treatment on indicated proteins. HeLa cells were treated with the indicated concentrations of H_2O_2 for 10 min, collected, and blotted for the indicated proteins. **(B)** Distribution of indicated proteins in membrane and cytosolic fractionations. Control (Ctrl) cells and cells treated with 1 mM H_2O_2 for 10 min were homogenized with a ball-bearing homogenizer followed by a low speed centrifugation to prepare post nuclear supernatant (PNS). The PNS was then subjected to ultracentrifugation to separate membranes (Mem) from the cytosol (Cyt). GS28 and Actin were used to denote Mem and Cyt fractions, respectively.

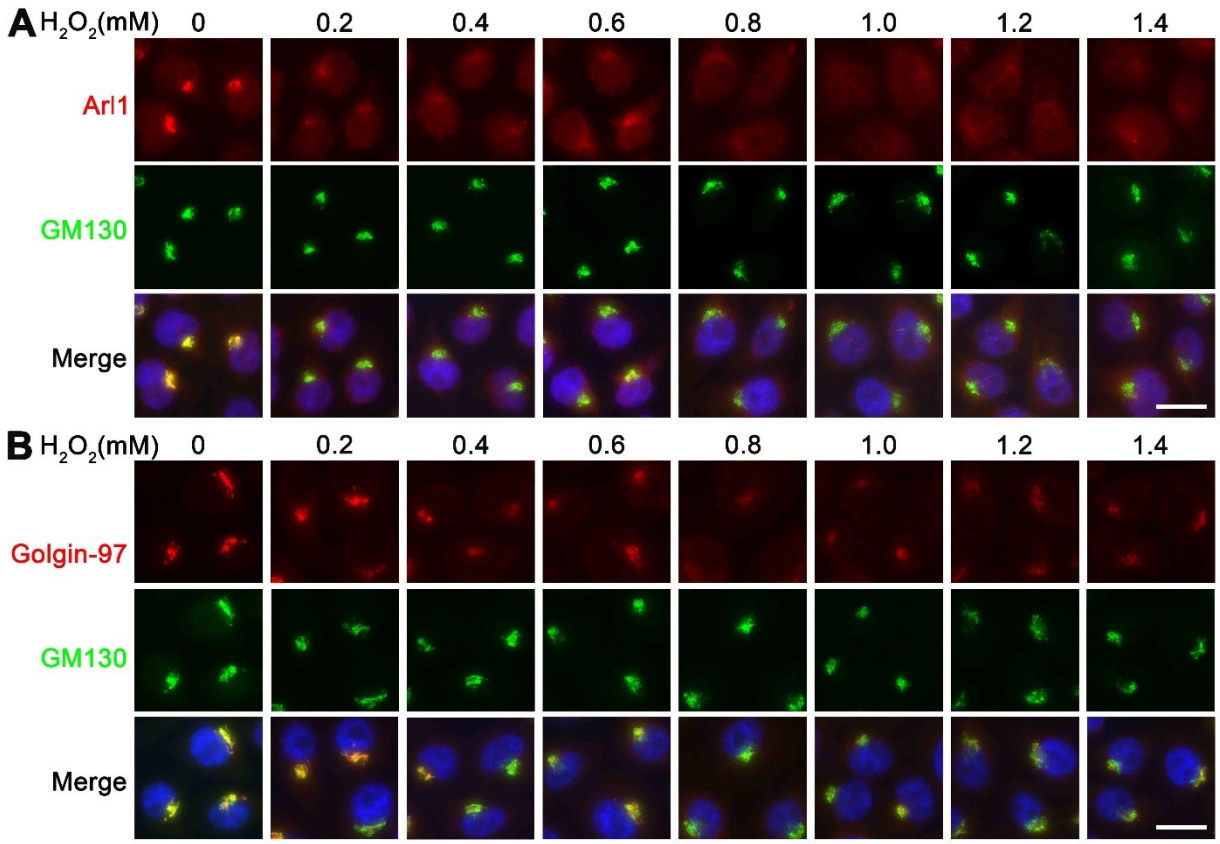

Fig. 3.2 H_2O_2 treatment causes specific degradation of Arl1 and Golgin-97 by IF
(A) H_2O_2 treatment reduces the Golgi localization of Arl1. HeLa cells were treated with the indicated concentrations of H_2O_2 for 10 min, fixed, and stained for Arl1 (red), GM130 (green) and DNA (blue). **(B)** H_2O_2 treatment reduces the Golgi localization of Golgin-97. HeLa cells were treated as above and stained for Golgin-97, GM130 and DNA.

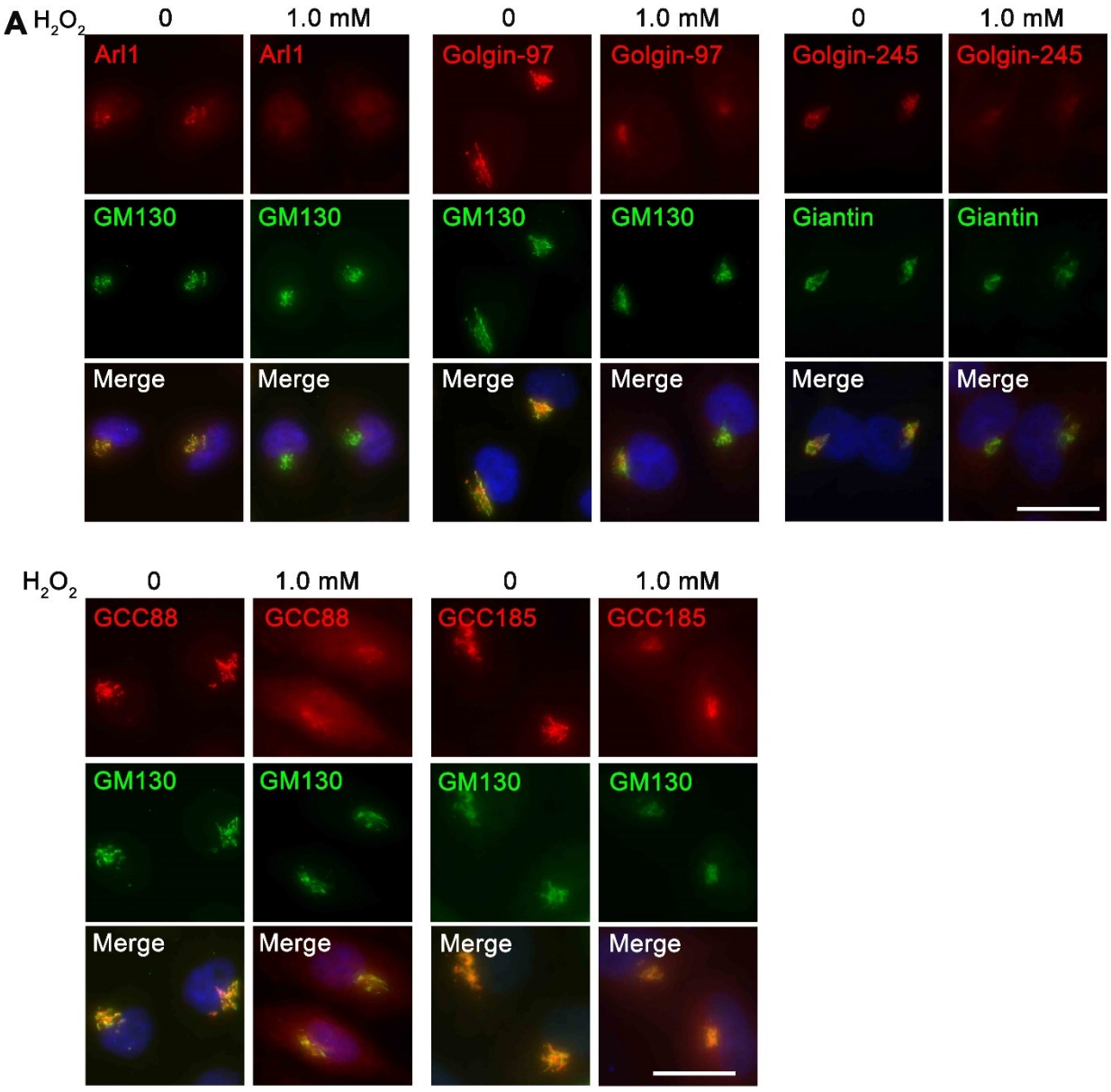

Fig. 3.3 H_2O_2 treatment reduces membrane association of golgins in the trans-Golgi
(A) HeLa cells treated with 1 mM H_2O_2 for 10 min were stained for GCC88 (left panels), EGFP-GCC185 expressing HeLa cells with the same treatment were analyzed for GCC185 (right panels). Note that GCC88 and GCC185 have reduced signals in the Golgi but diffused signals in the cytosol after H_2O_2 treatment. Scale bar, 20 μm.

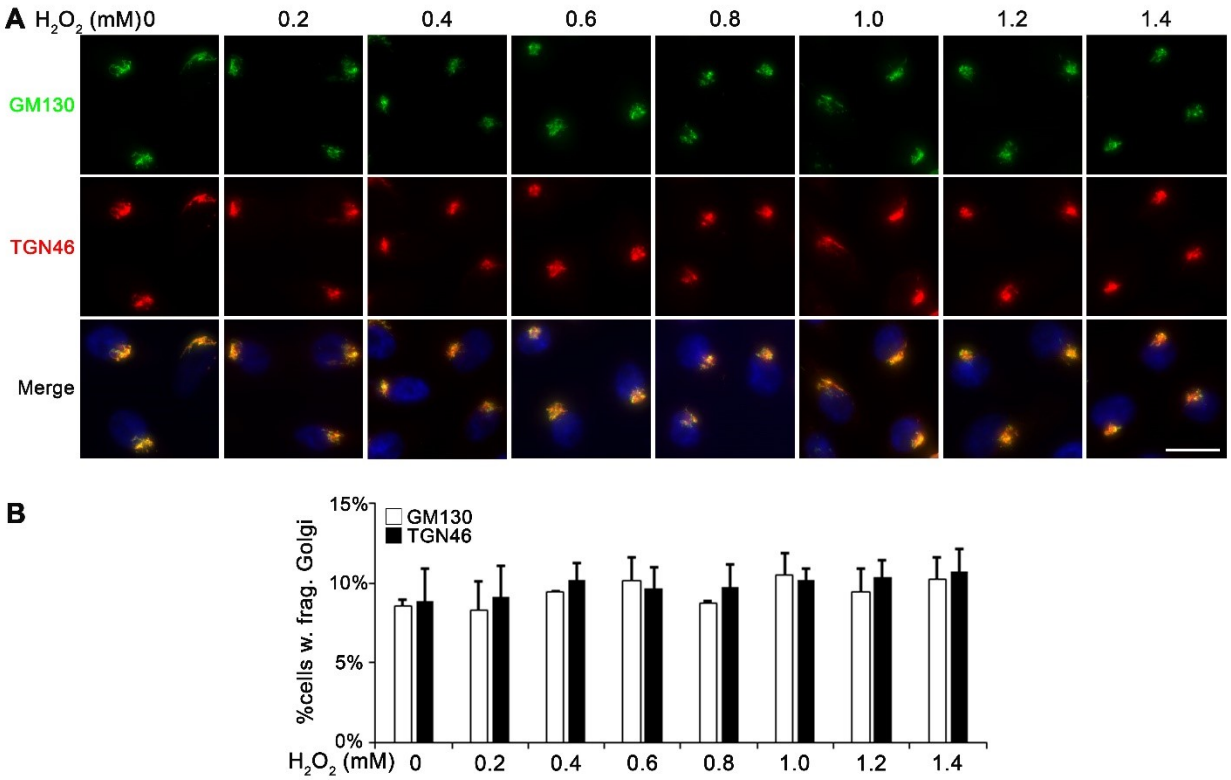

Fig. 3.4 H_2O_2 treatment does not cause Golgi fragmentation

(A) H_2O_2 treatment does not induce significant Golgi fragmentation. HeLa cells were treated with indicated concentrations of H_2O_2 for 10 min and stained for GM130 and TGN46. Scale bar, 20 µm. **(B)** Quantitation of Golgi fragmentation in H_2O_2-treated cells in A. Results are shown as Mean ± SEM from three independent experiments. No significant changes were detected by two-tailed Student's *t*-tests.

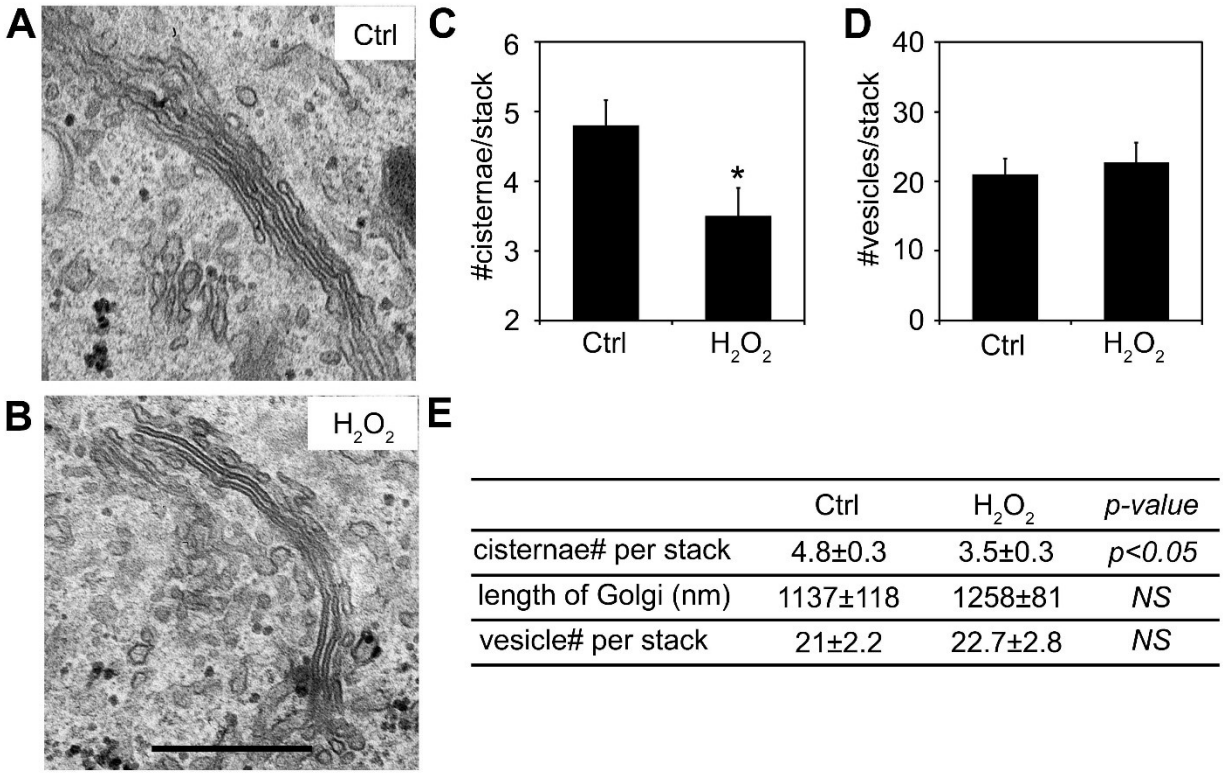

	Ctrl	H_2O_2	*p-value*
cisternae# per stack	4.8±0.3	3.5±0.3	*p<0.05*
length of Golgi (nm)	1137±118	1258±81	*NS*
vesicle# per stack	21±2.2	22.7±2.8	*NS*

Fig. 3.5 Short term H_2O_2 treatment reduces the number of cisternae per Golgi stack
(A-B) Representative electron micrographs of Golgi profiles in HeLa cells either untreated (Ctrl; **A**) or treated with 1 mM H_2O_2 for 10 min (H_2O_2; **B**). Note that the Golgi stacks contain fewer cisternae in the H_2O_2-treatment compared to Ctrl cells. Scale bar, 0.5 µm. **(C-D)** Quantitation of Golgi stack morphological features of cells in **A** and **B**. **(E)** Summary of quantitation of the morphological features of Golgi stacks on the EM images represented in **A** and **B**. Results are shown as Mean ± SEM; statistical analyses were performed using two-tailed Student's *t*-tests (*, $p \leq 0.05$; NS, not significant).

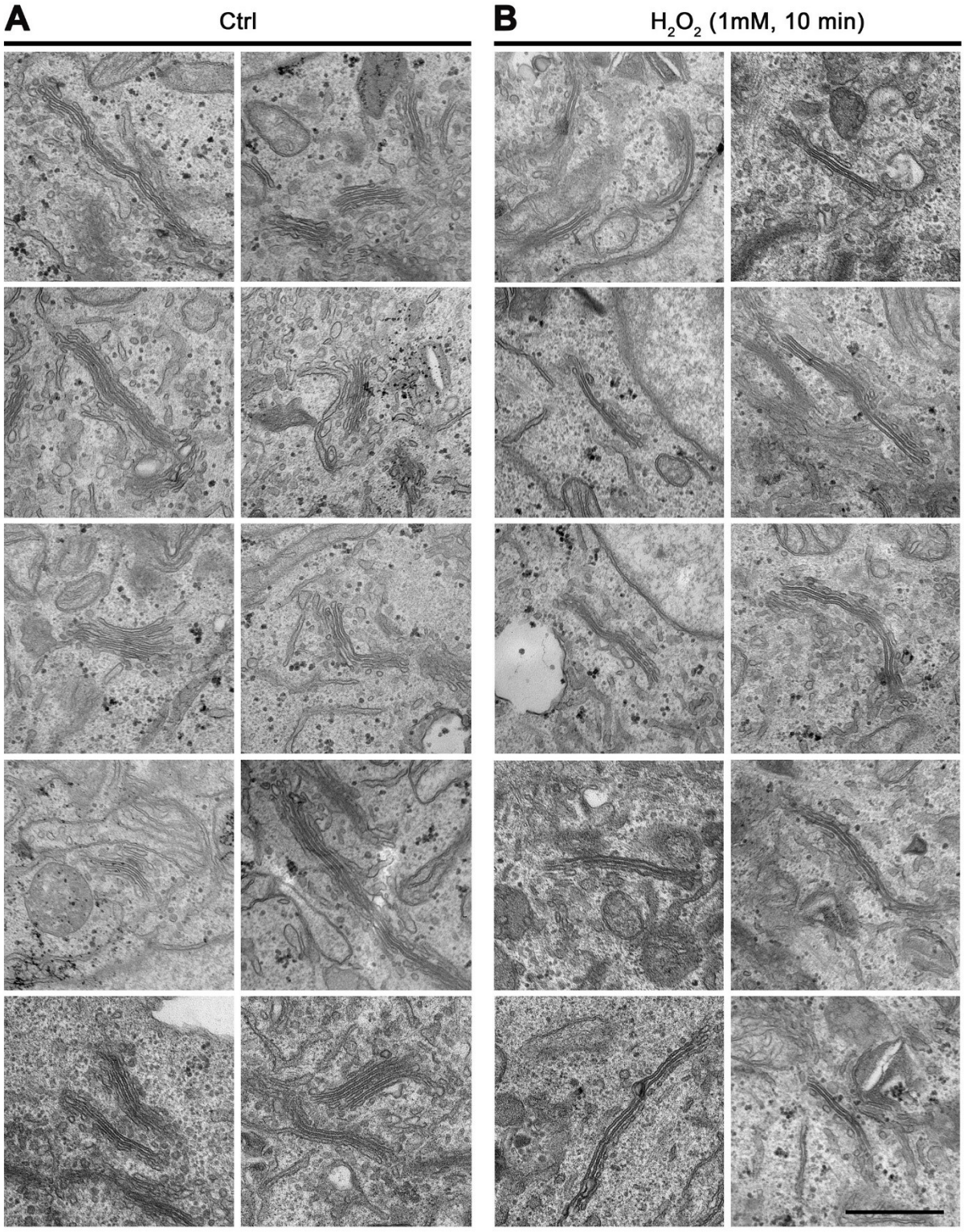

Fig. 3.6 H_2O_2 treatment alters the Golgi structure.
HeLa cells were incubated in growth medium without **(A)** or with 1 mM H_2O_2 **(B)** for 10 min were analyzed by EM. Shown are a collection of electron micrographs representing the two treatments. Consistent aberrations in the Golgi stacks were seen in H_2O_2-treated cells, in

particular a reduction of the cisterna number per Golgi stack, while the cisternal length and the number of vesicles surrounding each stack did not change. Scale bar, 0.5 μm.

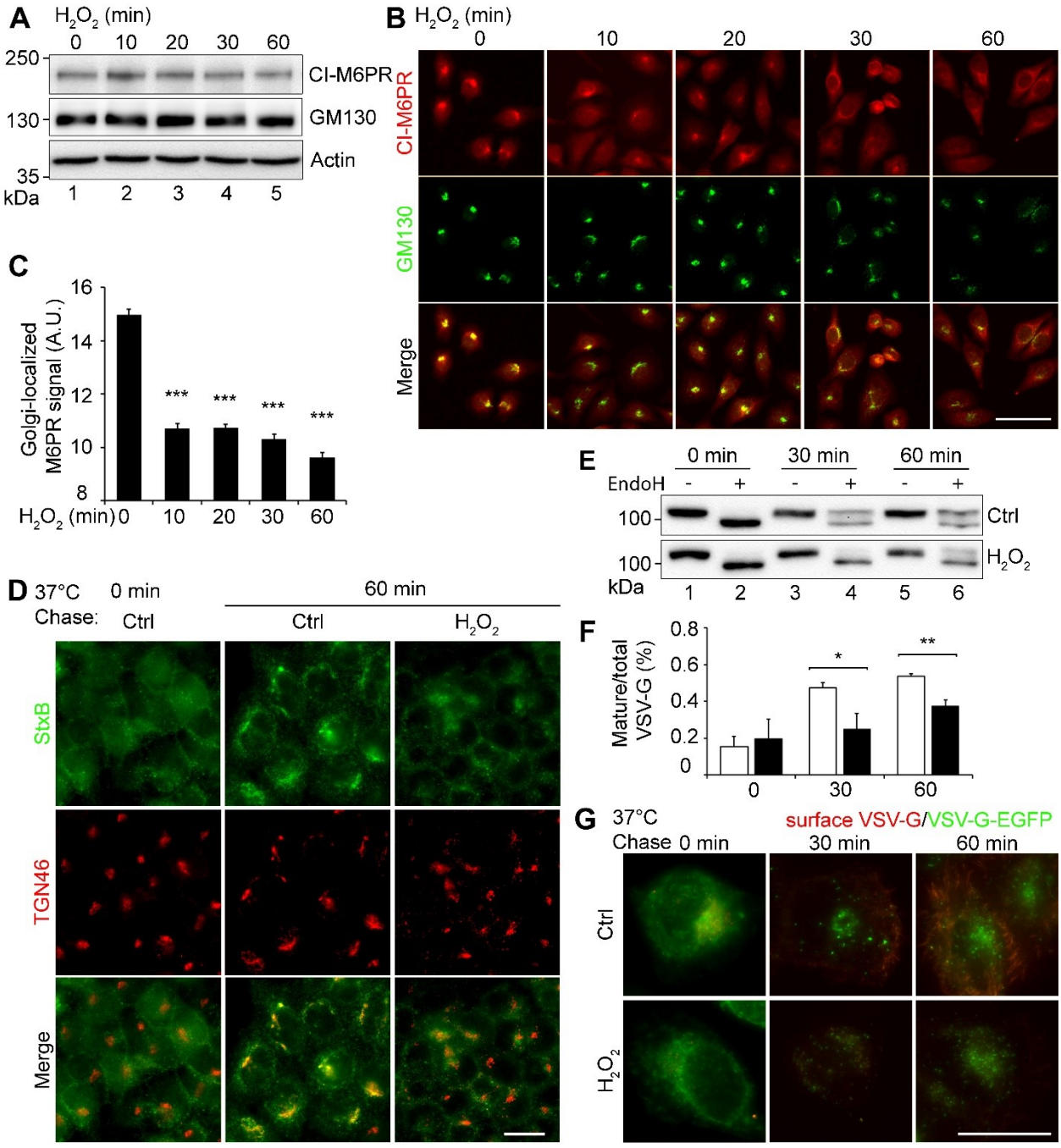

Fig. 3.7 H_2O_2 treatment reduces anterograde and retrograde trafficking
(A) HeLa cells treated with 1 mM H_2O_2 for indicated times were analyzed by Western blotting. **(B)** HeLa cells treated as in **A** were stained for CI-M6PR (red) and GM130 (green). Scale bar, 50 µm. **(C)** Quantitation of the Golgi-localized CI-M6PR intensity in **B**. Statistical analyses were performed using two-tailed Student's *t*-tests in comparison with the control (***, $p \leq 0.001$). Note the decrease in Golgi-localized CI-M6PR along with the unchanging total protein amount in **A**. **(D)** Live cells were incubated with Shiga toxin (StxB) on ice followed by a 60 min incubation at 37ºC to allow StxB trafficking to the Golgi. Cells were fixed and stained for StxB (green) and TGN46 (red). Scale bar, 20 µm. Note the dispersed StxB signals in H_2O_2 treated

cells, which is more concentrated in the Golgi region in control cells. **(E)** VSV-G trafficking assay using the RUSH system. Cells transfected with the Str-li_VSVG wt-SBP-EGFP plasmid were treated with or without 1 mM H_2O_2 for 10 minutes followed by VSV-G release from the ER for indicated times. Cell lysate was treated with or without EndoH and blotted for GFP. **(F)** Bands in **E** were quantified using densitometry analysis. The intensity of the upper EndoH resistant band was divided by that of the total of the upper and lower bands to calculate the mature/total ratio. Results are shown as Mean ± SEM from three independent experiments. Statistical analyses were performed using two-tailed Student's *t*-tests in comparison with the control (*, $p \leq 0.05$; **, $p \leq 0.01$). **(G)** Cells were treated as in **E**, fixed with PFA without permeabilization, and stained with an anti-VSVG antibody that recognizes its luminal domain. Scale bar, 20 μm.

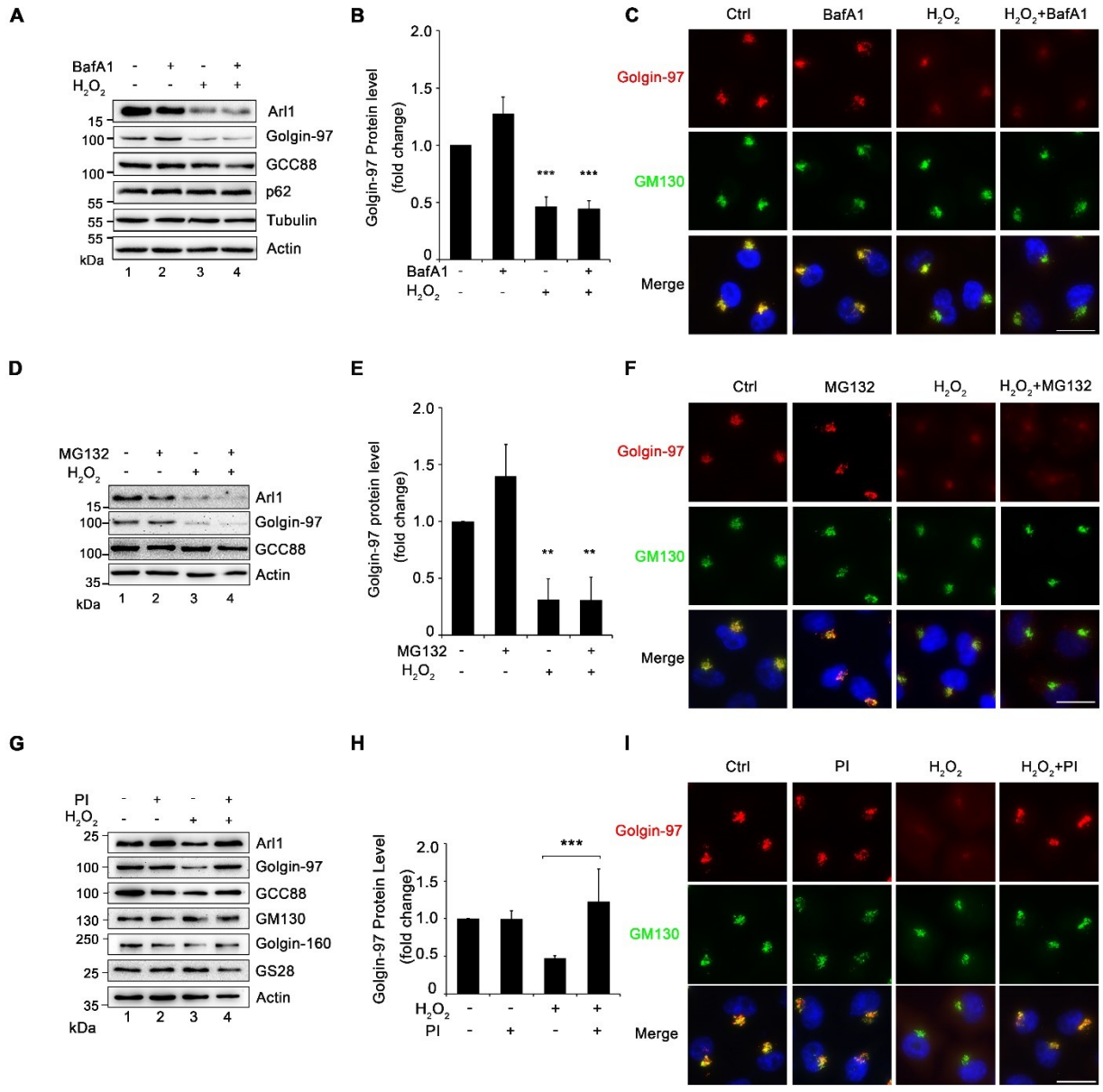

Fig. 3.8 H_2O_2 treatment causes golgin-97 degradation by cytoplasmic proteases.
(A) HeLa cells were treated with 400 nM BafA1 for 2 hours, followed by the addition of 1 mM H_2O_2 in the last 10 min and analyzed by Western blots for the indicated proteins. **(B)** Densitometric analysis of Golgin-97 blots in A from three independent experiments. **(C)** HeLa cells were treated as in **A** and stained for GM130 (green), Golgin-97 (red), and DNA (blue). Scale bar, 20 µm. **(D)** Cells were treated with 20 µM MG132 for 4 hours, followed by the addition of 1 mM H_2O_2 in the last 10 min and analyzed by Western blots for indicated proteins. **(E)** Densitometric analysis of the Golgin-97 protein level on Western blot in **D** from three independent experiments. Results are shown as Mean ± SEM. Statistical analyses were performed using two-tailed Student's *t*-tests (**, $p \leq 0.01$, ***, $p \leq 0.001$). **(F)** HeLa cells were co-treated with MG132 as in **D** and stained for GM130, Golgin-97 and DNA. Scale bar, 20 µm. **(G)** HeLa cells co-treated with or without a protease inhibitor cocktail and 1 mM H_2O_2 for 10

min were analyzed by Western blotting. **(H)** Quantitation of Golgin-97 Western blot in **G** with densitometric analysis. **(I)** Cells treated as in **G** were stained for Golgin-97 (red), GM130 (green), and DNA (blue). Scale bar, 20 μm.Results are shown as Mean ± SEM from three independent experiments. Statistical analyses were performed using two-tailed Student's *t*-tests (***, $p \leq 0.001$).

CHAPTER IV

Conclusions and Future Directions

4.1 Concluding remarks

The conclusion of this research is that the Golgi possesses its own mechanisms to sense and respond to various stresses. It has been commonly thought in the past that Golgi stress is a mere consequence of the expanding capacity of the ER during cellular stress. This, so the theory goes, leads to a failure of the Golgi as it is over-burdened with misfolded or improperly folded proteins, which in turn affect Golgi functions (Oku et al., 2011). However, results do not support this hypothesis for two reasons: First, although three ER stress inducers, TG, Tm and DTT, all induced ER stress, only TG treatment caused Golgi fragmentation. Second, TG induced Golgi fragmentation at a lower dose within a time window when UPR was undetectable. Therefore, Golgi fragmentation occurs independently of ER stress. Furthermore, this study revealed a novel mechanism that coordinates Golgi structure and perhaps function: TG treatment increases cytoplasmic Ca^{2+}, which activates PKCα, that subsequently phosphorylates GRASP55, impairing its function in Golgi structure formation. GRASP55 therefore provides the conceptual link between an extracellular cue on the one hand and Golgi morphological change during stress on the other.

In contrast to some other Golgi stresses such as thapsigargin treatment that triggers Golgi fragmentation (Ireland et al., 2019), H_2O_2 did not cause obvious Golgi fragmentation, nor apoptosis. Here it was revealed that H_2O_2 treatment induced a rapid degradation of Golgi tethering proteins on the *trans*-Golgi, including Arl1, Golgin-97 and Golgin-245. This loss coincided with a stark reduction of the cisternal number per Golgi stack and impaired both anterograde and retrograde trafficking functions. Further results indicate that H_2O_2-stress induced ROS activates a cytoplasmic protease to selectively degrade Arl1, Golgin-97 and Golgin-245 on the *trans*-Golgi. This happened independently of apoptosis and necrosis induced proteolytic activation. In this study we have identified Golgi proteins and Golgi functions as novel targets of ROS-toxicity in cells, in contrast to the fragmentation phenotype seen in **Chapter II**. Furthermore the work has identified specific targets of ROS on the Golgi, Arl1, Golgin-97, and Golgin-245.

The experiments in this study were designed to define intrinsic Golgi stress response mechanisms. It was found that the Golgi indeed is a target to receive physiological inputs from the cell or the environment to increase or decrease functional outputs. Understanding the specific regulatory machinery of the Golgi apparatus during stress can aid in the discovery of ways to manipulate Golgi health and help support cellular homeostasis and organism health.

4.2 Future directions

An outstanding question in the Golgi field has been how GRASP65 and GRASP55 remain segregated into distinct Golgi compartments. The N-terminal GRASP55 domain is 83% similar and 67% identical to that of GRASP65 in human (**Fig. 4.1A**). This has led to the conclusion that

GRASP55 and GRASP65 may stack different regions of the Golgi (Pfeffer, 2001). However, the mechanism controlling this biological distinction remains unsolved.

One possible mechanism of segregations could be palmitoylation of GRASPs. Palmitoylated proteins tend to be trafficked toward the plasma membrane, whereas de-palmitoylated proteins tend to make their way back toward endosomal and Golgi membranes. Palmitoylation is also reversible, unlike myristoylation. Palmitoylation occurs at cysteine residues and less frequently at serine residues within proteins. Human GRASP55 differ in both cysteine and serine residues with its GRASP65 counterpart. It will be interesting to know if one or more of these sites is available for palmitoylation.

Scientific inquiry has had several major shifts over the recent centuries and many of these shifts have involved dramatic improvements in imaging. What is needed next is spatial separation of individual proteins at the ultrastructural level. Super-resolution has brought us closer to achieving this, but electron microscopy will be needed to go further. Utilization of Apex2-GBP, or a derivative technique, will allow cell biologists to label proteins using EM. To that end, a technique was developed for the lab employing apex enzyme labelled Golgi proteins. Some of the progress is shown in **Fig. 4.1B-E**.

The apex tool has the power to directly test the hypothesis that palmitoylation of GRASP homologues controls their segregation within the Golgi. By creating alanine point mutations in the cysteine residues of GRASP proteins and comparing the localization patterns between mutant

and wild type proteins using apex, one could ask if mutants would appear more on the *cis*-Golgi than they normally do.

To continue the work, a researcher in the Wang lab could 1) improve and clarify previous findings that GRASP55 and GRASP65 localize to inter-cisternal spaces of the Golgi stack as previously shown, and 2) identify the mechanism of how GRASP homologues, GRASP55 and GRASP65, separate themselves in different parts of the Golgi stack.

4.3 Figures

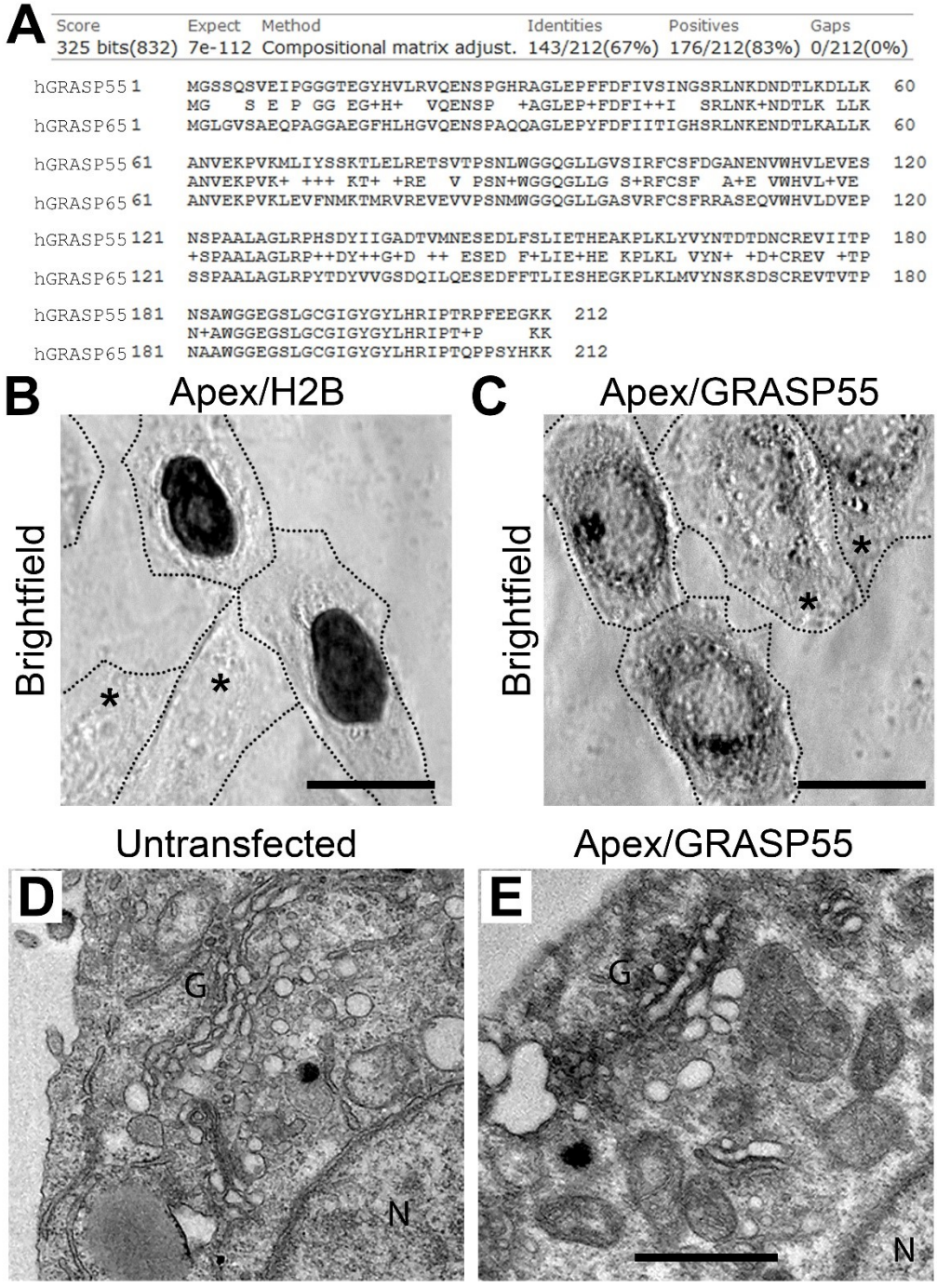

Fig 4.1 GRASP55 localizes to the inter-cisternal spaces of the Golgi stack
(A) BLAST sequence alignment of human GRASP55 and human GRASP65 N-terminus showing the number of identities, mismatches (gaps), and conservative substitutions (+). **(B)**

HeLa cells co-expressing Apex-GBP (Apex) and Histone 2B-GFP (H2B-GFP) after undergoing a DAB reaction. The nucleus exhibits with a high degree of opaque reaction product compared to untransfected cells indicated by the asterisk (*****) (please see section 4.4 for Materials and Methods). **(C)** Co-expression of Apex-GBP and the Golgi structural protein GRASP55-GFP (GRASP55). The Golgi is shown occupying a central position in the cell compared to the H2B control cells in **B**. Scale bar, 20 microns. **(D)** EM visualization of untransfected HeLa cell showing normal Golgi stacks, **G**. Also visible is the nucleus **N**. **(E)** EM visualization of HeLa cell co-transfected with Apex2-GBP and GRASP55-GFP plasmids. The dark, electron dense region within the Golgi, **G**, stacks suggests an inter-cisternal enrichment of GRASP55, whereas light microcopy can never establish this level of detail. Also visible is the nucleus, **N**. Scale bar, 500 nanometers.

4.4 Materials and Methods

Basic Local Alignment Search Tool (BLAST)

Protein BLAST was performed using National Center for Biotechnology Information's (NCBI) online alignment software. Amino acid sequences were obtained by aligning two or more sequences. The first subject sequence was the first 212 positions of human GRASP55 (GORASP2; NCBI Reference Sequence: NP_001188357.1), and the query sequence was the first 212 positions of human GRASP65 (GORASP1; NCBI Reference Sequence: XP_006713364.1).

Reagents and Plasmids

All EM related reagents were from Electron Microscopy Sciences (EMS; Hatfield, PA). The Apex2-GBP plasmid was purchased from Addgene (#67651). The H2B-GFP plasmid was purchased from Addgene (#11680). GRASP55-GFP was made in house using the pEGFP-N1 vector (Zhang et al., 2018)

Cell Culture and Drug Treatments

HeLa were obtained from ATCC (Manassas, VA), cultured in Dulbecco's modified Eagle's medium (DMEM; ThermoFisher) supplemented with 10% fetal bovine serum (FBS; Gemini Bio-Products, Sacramento, CA) and 100 units/ml penicillin-streptomycin at 37°C with 5% CO_2, and routinely screened for mycoplasma contamination. Cells were grown on glass coverslips according to standard tissue culture methods (Tang et al., 2011). Coverslips were pre-coated with poly-lysine (Gibco) to aid in cell attachment.

Apex Electron Microscopy

Hela cells were plated onto 6 cm tissue culture dishes with a coverslip 24 h prior to transfection. Cells were transfected with Apex2-GBP with either mock, H2B-GFP or GRASP55-GFP plasmids for 16 h. Cells were fixed in pre-warmed serum-free DMEM, 20 mM HEPES, pH 7.4, 2% glutaraldehyde at room temperature for 1 h or 4°C overnight as previously described (Tang et al., 2010a; Wang et al., 2005). The DAB reaction buffer was prepared fresh and used immediately (1 mg/mL solution of 3'3-diaminobenzidine tetrahydrochloride (Sigma-Aldrich) in 0.1 M sodium cacodylate). Undissolved precipitate was removed with syringe filtration using a 0.2 μm filter. Cells were washed 2 times with DAB buffer. This initial wash was then replaced with DAB reaction mixture after adding H_2O_2 (5.88 mM), and cells were allowed to incubate for 60 minutes. The cells were next washed 3x with pure 0.1 M cacodylate buffer followed by 10x with ddH_2O. Coverslips were collected and imaged using brightfield (**Fig. 4.1B-C**). Remaining cells were then incubated in 2% filtered uranyl acetate solution at 4°C, and rinsed with water until no traces of yellow remained (about 3 times). The EMBED 812 protocol was used to embed cells and resin blocks were sectioned to 60 nm with a diamond knife and mounted on Formvar-coated copper grids (Tang et al., 2010a).

References

Ahat, E., Li, J., and Wang, Y. (2019a). New Insights Into the Golgi Stacking Proteins. Frontiers in Cell and Developmental Biology *In press*.

Ahat, E., Xiang, Y., Zhang, X., Bekier, M.E., and Wang, Y. (2019b). GRASP depletion-mediated Golgi destruction decreases cell adhesion and migration via the reduction of alpha5beta1 integrin. Molecular biology of the cell *30*, 766-777.

Ahsan, H., Ali, A., and Ali, R. (2003). Oxygen free radicals and systemic autoimmunity. Clin Exp Immunol *131*, 398-404.

Alvarez-Miranda, E.A., Sinnl, M., and Farhan, H. (2015). Alteration of Golgi Structure by Stress: A Link to Neurodegeneration? Front Neurosci *9*, 435.

Araujo, R.L.S., Correa, J.R., and Galera, P.D. (2019). Ultrastructural morphology of goblet cells of the conjunctiva of dogs. Vet Ophthalmol *22*, 891-897.

Baier-Bitterlich, G., Uberall, F., Bauer, B., Fresser, F., Wachter, H., Grunicke, H., Utermann, G., Altman, A., and Baier, G. (1996). Protein kinase C-theta isoenzyme selective stimulation of the transcription factor complex AP-1 in T lymphocytes. Mol Cell Biol *16*, 1842-1850.

Bailey, A.P., Koster, G., Guillermier, C., Hirst, E.M., MacRae, J.I., Lechene, C.P., Postle, A.D., and Gould, A.P. (2015). Antioxidant Role for Lipid Droplets in a Stem Cell Niche of Drosophila. Cell *163*, 340-353.

Barr, F.A., Puype, M., Vandekerckhove, J., and Warren, G. (1997). GRASP65, a protein involved in the stacking of Golgi cisternae. Cell *91*, 253-262.

Basu, S.K., Goldstein, J.L., Anderson, R.G., and Brown, M.S. (1981). Monensin interrupts the recycling of low density lipoprotein receptors in human fibroblasts. Cell *24*, 493-502.

Becker, K.P., and Hannun, Y.A. (2003). cPKC-dependent sequestration of membrane-recycling components in a subset of recycling endosomes. J Biol Chem *278*, 52747-52754.

Bekier, M.E., 2nd, Wang, L., Li, J., Huang, H., Tang, D., Zhang, X., and Wang, Y. (2017). Knockout of the Golgi stacking proteins GRASP55 and GRASP65 impairs Golgi structure and function. Mol Biol Cell *28*, 2833-2842.

Block, E.R. (1991). Hydrogen peroxide alters the physical state and function of the plasma membrane of pulmonary artery endothelial cells. J Cell Physiol *146*, 362-369.

Bock, J.B., Klumperman, J., Davanger, S., and Scheller, R.H. (1997). Syntaxin 6 functions in trans-Golgi network vesicle trafficking. Mol Biol Cell *8*, 1261-1271.

Boncompain, G., Divoux, S., Gareil, N., de Forges, H., Lescure, A., Latreche, L., Mercanti, V., Jollivet, F., Raposo, G., and Perez, F. (2012). Synchronization of secretory protein traffic in populations of cells. Nat Methods *9*, 493-498.

Brockhausen, I., and Stanley, P. (2015). O-GalNAc Glycans. In Essentials of Glycobiology, rd, A. Varki, R.D. Cummings, J.D. Esko, P. Stanley, G.W. Hart, M. Aebi, A.G. Darvill, T. Kinoshita, N.H. Packer*, et al.*, eds. (Cold Spring Harbor (NY)), pp. 113-123.

Capasso, J.M., Keenan, T.W., Abeijon, C., and Hirschberg, C.B. (1989). Mechanism of phosphorylation in the lumen of the Golgi apparatus. Translocation of adenosine 5'-triphosphate into Golgi vesicles from rat liver and mammary gland. J Biol Chem *264*, 5233-5240.

Celsi, F., Pizzo, P., Brini, M., Leo, S., Fotino, C., Pinton, P., and Rizzuto, R. (2009). Mitochondria, calcium and cell death: a deadly triad in neurodegeneration. Biochim Biophys Acta *1787*, 335-344.

Chen, D., Purohit, A., Halilovic, E., Doxsey, S.J., and Newton, A.C. (2004). Centrosomal anchoring of protein kinase C betaII by pericentrin controls microtubule organization, spindle function, and cytokinesis. J Biol Chem *279*, 4829-4839.

Chia, J., Goh, G., Racine, V., Ng, S., Kumar, P., and Bard, F. (2012). RNAi screening reveals a large signaling network controlling the Golgi apparatus in human cells. Mol Syst Biol *8*, 629.

Cole, N.B., Sciaky, N., Marotta, A., Song, J., and Lippincott-Schwartz, J. (1996). Golgi dispersal during microtubule disruption: regeneration of Golgi stacks at peripheral endoplasmic reticulum exit sites. Mol Biol Cell *7*, 631-650.

Colley, K.J. (1997). Golgi localization of glycosyltransferases: more questions than answers. Glycobiology *7*, 1-13.

Cooke, M., Magimaidas, A., Casado-Medrano, V., and Kazanietz, M.G. (2017). Protein kinase C in cancer: The top five unanswered questions. Mol Carcinog *56*, 1531-1542.

Croall, D.E., and DeMartino, G.N. (1991). Calcium-activated neutral protease (calpain) system: structure, function, and regulation. Physiol Rev *71*, 813-847.

Davies, M.J. (2016). Protein oxidation and peroxidation. Biochem J *473*, 805-825.

Deniaud, A., Sharaf el dein, O., Maillier, E., Poncet, D., Kroemer, G., Lemaire, C., and Brenner, C. (2008). Endoplasmic reticulum stress induces calcium-dependent permeability transition, mitochondrial outer membrane permeabilization and apoptosis. Oncogene *27*, 285-299.

Derby, M.C., van Vliet, C., Brown, D., Luke, M.R., Lu, L., Hong, W., Stow, J.L., and Gleeson, P.A. (2004). Mammalian GRIP domain proteins differ in their membrane binding properties and are recruited to distinct domains of the TGN. J Cell Sci *117*, 5865-5874.

Dolman, N.J., and Tepikin, A.V. (2006). Calcium gradients and the Golgi. Cell Calcium *40*, 505-512.

Eisenberg-Lerner, A., Benyair, R., Hizkiahou, N., Maor, R., Kramer, M., Shmueli, M., Zigdon, n., Nudel, N., Lev, M.C., Ulman, A.*, et al.* (2020). Fine-tuning regulation of Golgi organization is mediated by proteasomal degradation. Nature Communications *In press*.

El Homasany, B.S.E.D., Volkov, Y., Takahashi, M., Ono, Y., Keryer, G., Delouvee, A., Looby, E., Long, A., and Kelleher, D. (2005). The Scaffolding Protein CG-NAP/AKAP450 Is a Critical Integrating Component of the LFA-1-Induced Signaling Complex in Migratory T Cells. The Journal of Immunology *175*, 7811-7818.

Farhan, H., Wendeler, M.W., Mitrovic, S., Fava, E., Silberberg, Y., Sharan, R., Zerial, M., and Hauri, H.P. (2010). MAPK signaling to the early secretory pathway revealed by kinase/phosphatase functional screening. J Cell Biol *189*, 997-1011.

Feinstein, T.N., and Linstedt, A.D. (2008). GRASP55 Regulates Golgi Ribbon Formation. Mol Biol Cell *19*, 2696-2707.

Fleischer, B. (1983). Mechanism of glycosylation in the Golgi apparatus. J Histochem Cytochem *31*, 1033-1040.

Fliesler, S.J., and Basinger, S.F. (1987). Monensin stimulates glycerolipid incorporation into rod outer segment membranes. J Biol Chem *262*, 17516-17523.

Fligiel, S.E., Lee, E.C., McCoy, J.P., Johnson, K.J., and Varani, J. (1984). Protein degradation following treatment with hydrogen peroxide. Am J Pathol *115*, 418-425.

Fujita, Y., and Okamoto, K. (2005). Golgi apparatus of the motor neurons in patients with amyotrophic lateral sclerosis and in mice models of amyotrophic lateral sclerosis. Neuropathology *25*, 388-394.

Garrity, A.G., Wang, W., Collier, C.M., Levey, S.A., Gao, Q., and Xu, H. (2016). The endoplasmic reticulum, not the pH gradient, drives calcium refilling of lysosomes. Elife *5*.

Gee, H.Y., Noh, S.H., Tang, B.L., Kim, K.H., and Lee, M.G. (2011). Rescue of DeltaF508-CFTR Trafficking via a GRASP-Dependent Unconventional Secretion Pathway. Cell *146*, 746-760.

Glick, B.S., and Nakano, A. (2009). Membrane traffic within the Golgi apparatus. Annu Rev Cell Dev Biol *25*, 113-132.

Gonatas, N.K., Gonatas, J.O., and Stieber, A. (1998). The involvement of the Golgi apparatus in the pathogenesis of amyotrophic lateral sclerosis, Alzheimer's disease, and ricin intoxication. Histochem Cell Biol *109*, 591-600.

Griner, E.M., and Kazanietz, M.G. (2007). Protein kinase C and other diacylglycerol effectors in cancer. Nat Rev Cancer *7*, 281-294.

Hilditch-Maguire, P., Trettel, F., Passani, L.A., Auerbach, A., Persichetti, F., and MacDonald, M.E. (2000). Huntingtin: an iron-regulated protein essential for normal nuclear and perinuclear organelles. Hum Mol Genet *9*, 2789-2797.

Hu, W.G., and Lu, Q.P. (2014). Impact of oxidative stress on the cytoskeleton of pancreatic epithelial cells. Exp Ther Med *8*, 1438-1442.

Huang, S., and Wang, Y. (2017). Golgi structure formation, function, and post-translational modifications in mammalian cells. F1000Res *6*, 2050.

Ireland, S.C., Ramnarayanan, S., Fu, M., Zhang, X., Emebo, D., and Wang, Y. (2019). Cytosolic Ca²⁺ modulates Golgi structure through PKC-mediated GRASP55 phosphorylation. bioRxiv, 784520.

Ishii, M., Suda, Y., Kurokawa, K., and Nakano, A. (2016). COPI is essential for Golgi cisternal maturation and dynamics. J Cell Sci *129*, 3251-3261.

Ito, Y., Takeda, Y., Seko, A., Izumi, M., and Kajihara, Y. (2014). Functional analysis of endoplasmic reticulum glucosyltransferase (UGGT): Synthetic chemistry's initiative in glycobiology. Semin Cell Dev Biol.

Jackson, C.L. (2003). Membrane traffic: Arl GTPases get a GRIP on the Golgi. Current biology : CB *13*, R174-176.

Jesch, S.A., Lewis, T.S., Ahn, N.G., and Linstedt, A.D. (2001). Mitotic phosphorylation of Golgi reassembly stacking protein 55 by mitogen-activated protein kinase ERK2. Mol Biol Cell *12*, 1811-1817.

Jones, K.T., and Sharpe, G.R. (1994). Thapsigargin raises intracellular free calcium levels in human keratinocytes and inhibits the coordinated expression of differentiation markers. Exp Cell Res *210*, 71-76.

Joshi, G., Bekier, M.E., 2nd, and Wang, Y. (2015). Golgi fragmentation in Alzheimer's disease. Front Neurosci *9*, 340.

Joshi, G., Chi, Y., Huang, Z., and Wang, Y. (2014). Abeta-induced Golgi fragmentation in Alzheimer's disease enhances Abeta production. Proc Natl Acad Sci U S A *111*, E1230-1239.

Joshi, G., and Wang, Y. (2015). Golgi defects enhance APP amyloidogenic processing in Alzheimer's disease. Bioessays *37*, 240-247.

Kajimoto, T., Ohmori, S., Shirai, Y., Sakai, N., and Saito, N. (2001). Subtype-specific translocation of the delta subtype of protein kinase C and its activation by tyrosine phosphorylation induced by ceramide in HeLa cells. Mol Cell Biol *21*, 1769-1783.

Karpati, A., Yoshikawa, T., Nakamura, T., Iida, T., Matsuzawa, T., Kitano, H., Harada, R., and Yanai, K. (2018). Histamine elicits glutamate release from cultured astrocytes. J Pharmacol Sci.

Kellokumpu, S. (2019). Golgi pH, Ion and Redox Homeostasis: How Much Do They Really Matter? Front Cell Dev Biol *7*, 93.

Kiehart, D.P. (1981). Studies on the in vivo sensitivity of spindle microtubules to calcium ions and evidence for a vesicular calcium-sequestering system. J Cell Biol *88*, 604-617.

Kim, H., Zamel, R., Bai, X.H., and Liu, M. (2013). PKC activation induces inflammatory response and cell death in human bronchial epithelial cells. PLoS One *8*, e64182.

Koepke, J.I., Wood, C.S., Terlecky, L.J., Walton, P.A., and Terlecky, S.R. (2008). Progeric effects of catalase inactivation in human cells. Toxicol Appl Pharmacol *232*, 99-108.

Krause, W.J. (2000). Brunner's Glands: A Structural,Histochemical and Pathological Profile. Progress in Histochemistry and Cytochemistry *35*, 255-367.

Lefebvre, T., Guinez, C., Dehennaut, V., Beseme-Dekeyser, O., Morelle, W., and Michalski, J.C. (2005). Does O-GlcNAc play a role in neurodegenerative diseases? Expert Rev Proteomics *2*, 265-275.

Lew, J., Huang, Q.Q., Qi, Z., Winkfein, R.J., Aebersold, R., Hunt, T., and Wang, J.H. (1994). A brain-specific activator of cyclin-dependent kinase 5. Nature *371*, 423-426.

Li, J., Ahat, E., and Wang, Y. (2019a). Golgi structure and function in health, stress and diseases. Springer Nature *Accepted*.

Li, J., Tang, D., Ireland, S.C., and Wang, Y. (2019b). DjA1 maintains Golgi integrity via interaction with GRASP65. Molecular biology of the cell *30*, 478-490.

Lin, P., Fischer, T., Weiss, T., and Farquhar, M.G. (2000). Calnuc, an EF-hand Ca(2+) binding protein, specifically interacts with the C-terminal alpha5-helix of G(alpha)i3. Proc Natl Acad Sci U S A *97*, 674-679.

Lin, P., Le-Niculescu, H., Hofmeister, R., McCaffery, J.M., Jin, M., Hennemann, H., McQuistan, T., De Vries, L., and Farquhar, M.G. (1998). The mammalian calcium-binding protein, nucleobindin (CALNUC), is a Golgi resident protein. J Cell Biol *141*, 1515-1527.

Lin, S.X., Mallet, W.G., Huang, A.Y., and Maxfield, F.R. (2004). Endocytosed cation-independent mannose 6-phosphate receptor traffics via the endocytic recycling compartment en route to the trans-Golgi network and a subpopulation of late endosomes. Mol Biol Cell *15*, 721-733.

Lock, J.G., Hammond, L.A., Houghton, F., Gleeson, P.A., and Stow, J.L. (2005). E-cadherin transport from the trans-Golgi network in tubulovesicular carriers is selectively regulated by golgin-97. Traffic *6*, 1142-1156.

Lu, L., and Hong, W. (2003). Interaction of Arl1-GTP with GRIP domains recruits autoantigens Golgin-97 and Golgin-245/p230 onto the Golgi. Mol Biol Cell *14*, 3767-3781.

Lu, L., Tai, G., and Hong, W. (2004). Autoantigen Golgin-97, an effector of Arl1 GTPase, participates in traffic from the endosome to the trans-golgi network. Mol Biol Cell *15*, 4426-4443.

Luke, M.R., Kjer-Nielsen, L., Brown, D.L., Stow, J.L., and Gleeson, P.A. (2003). GRIP domain-mediated targeting of two new coiled-coil proteins, GCC88 and GCC185, to subcompartments of the trans-Golgi network. J Biol Chem *278*, 4216-4226.

Lupashin, V., and Sztul, E. (2005). Golgi tethering factors. Biochimica et biophysica acta *1744*, 325-339.

Mancini, M., Machamer, C.E., Roy, S., Nicholson, D.W., Thornberry, N.A., Casciola-Rosen, L.A., and Rosen, A. (2000). Caspase-2 is localized at the Golgi complex and cleaves golgin-160 during apoptosis. J Cell Biol *149*, 603-612.

Manoharan, S., Guillemin, G.J., Abiramasundari, R.S., Essa, M.M., Akbar, M., and Akbar, M.D. (2016). The Role of Reactive Oxygen Species in the Pathogenesis of Alzheimer's Disease, Parkinson's Disease, and Huntington's Disease: A Mini Review. Oxid Med Cell Longev *2016*, 8590578.

Matsubara, M., Tamura, T., Ohmori, K., and Hasegawa, K. (2005). Histamine H1 receptor antagonist blocks histamine-induced proinflammatory cytokine production through inhibition of Ca2+-dependent protein kinase C, Raf/MEK/ERK and IKK/I kappa B/NF-kappa B signal cascades. Biochem Pharmacol *69*, 433-449.

McCaughey, J., and Stephens, D.J. (2018). COPII-dependent ER export in animal cells: adaptation and control for diverse cargo. Histochem Cell Biol *150*, 119-131.

Mettlen, M., Chen, P.H., Srinivasan, S., Danuser, G., and Schmid, S.L. (2018). Regulation of Clathrin-Mediated Endocytosis. Annu Rev Biochem *87*, 871-896.

Millarte, V., Boncompain, G., Tillmann, K., Perez, F., Sztul, E., and Farhan, H. (2015). Phospholipase C gamma1 regulates early secretory trafficking and cell migration via interaction with p115. Mol Biol Cell *26*, 2263-2278.

Miyoshi, E., Kamada, Y., and Suzuki, T. (2020). Functional glycomics: Application to medical science and hepatology. Hepatol Res *50*, 153-164.

Mizuno, Y., Hattori, N., Kitada, T., Matsumine, H., Mori, H., Shimura, H., Kubo, S., Kobayashi, H., Asakawa, S., Minoshima, S.*, et al.* (2001). Familial Parkinson's disease. Alpha-synuclein and parkin. Adv Neurol *86*, 13-21.

Mourelatos, Z., Gonatas, N.K., Stieber, A., Gurney, M.E., and Dal Canto, M.C. (1996). The Golgi apparatus of spinal cord motor neurons in transgenic mice expressing mutant Cu,Zn superoxide dismutase becomes fragmented in early, preclinical stages of the disease. Proc Natl Acad Sci U S A *93*, 5472-5477.

Munro, S. (2011). The golgin coiled-coil proteins of the Golgi apparatus. Cold Spring Harb Perspect Biol *3*.

Muschalik, N., and Munro, S. (2018). Golgins. Current biology : CB *28*, R374-R376.

Muto, A., Ohkura, M., Abe, G., Nakai, J., and Kawakami, K. (2013). Real-time visualization of neuronal activity during perception. Curr Biol *23*, 307-311.

Nakagomi, S., Barsoum, M.J., Bossy-Wetzel, E., Sutterlin, C., Malhotra, V., and Lipton, S.A. (2008). A Golgi fragmentation pathway in neurodegeneration. Neurobiol Dis *29*, 221-231.

Nindl, G., Peterson, N.R., Hughes, E.F., Waite, L.R., and Johnson, M.T. (2004). Effect of hydrogen peroxide on proliferation, apoptosis and interleukin-2 production of Jurkat T cells. Biomed Sci Instrum *40*, 123-128.

Nishimoto-Morita, K., Shin, H.W., Mitsuhashi, H., Kitamura, M., Zhang, Q., Johannes, L., and Nakayama, K. (2009). Differential effects of depletion of ARL1 and ARFRP1 on membrane trafficking between the trans-Golgi network and endosomes. J Biol Chem *284*, 10583-10592.

Nishizuka, Y. (1995). Protein kinase C and lipid signaling for sustained cellular responses. FASEB J *9*, 484-496.

O'Connor, E.R., and Kimelberg, H.K. (1993). Role of calcium in astrocyte volume regulation and in the release of ions and amino acids. J Neurosci *13*, 2638-2650.

Oku, M., Tanakura, S., Uemura, A., Sohda, M., Misumi, Y., Taniguchi, M., Wakabayashi, S., and Yoshida, H. (2011). Novel cis-acting element GASE regulates transcriptional induction by the Golgi stress response. Cell Struct Funct *36*, 1-12.

Pajares, M., Jimenez-Moreno, N., Dias, I.H.K., Debelec, B., Vucetic, M., Fladmark, K.E., Basaga, H., Ribaric, S., Milisav, I., and Cuadrado, A. (2015). Redox control of protein degradation. Redox Biol *6*, 409-420.

Pantazopoulou, A., and Glick, B.S. (2019). A Kinetic View of Membrane Traffic Pathways Can Transcend the Classical View of Golgi Compartments. Front Cell Dev Biol *7*, 153.

Petrosyan, A. (2015). Onco-Golgi: Is Fragmentation a Gate to Cancer Progression? Biochem Mol Biol J *1*.

Petrosyan, A., Holzapfel, M.S., Muirhead, D.E., and Cheng, P.W. (2014). Restoration of compact Golgi morphology in advanced prostate cancer enhances susceptibility to galectin-1-induced apoptosis by modifying mucin O-glycan synthesis. Mol Cancer Res *12*, 1704-1716.

Pfeffer, S.R. (2001). Constructing a Golgi complex. J Cell Biol *155*, 873-875.

Pfeffer, S.R. (2010). How the Golgi works: A cisternal progenitor model. P Natl Acad Sci USA *107*, 19614-19618.

Puthenveedu, M.A., Bachert, C., Puri, S., Lanni, F., and Linstedt, A.D. (2006). GM130 and GRASP65-dependent lateral cisternal fusion allows uniform Golgi-enzyme distribution. Nat Cell Biol *8*, 238-248.

Rambourg, A., Clermont, Y., Chretien, M., and Olivier, L. (1993). Modulation of the Golgi apparatus in stimulated and nonstimulated prolactin cells of female rats. Anat Rec *235*, 353-362.

Sahoo, N., Gu, M., Zhang, X., Raval, N., Yang, J., Bekier, M., Calvo, R., Patnaik, S., Wang, W., King, G.*, et al.* (2017). Gastric Acid Secretion from Parietal Cells Is Mediated by a Ca(2+) Efflux Channel in the Tubulovesicle. Dev Cell *41*, 262-273 e266.

Saini, D.K., Karunarathne, W.K., Angaswamy, N., Saini, D., Cho, J.H., Kalyanaraman, V., and Gautam, N. (2010). Regulation of Golgi structure and secretion by receptor-induced G protein betagamma complex translocation. Proc Natl Acad Sci U S A *107*, 11417-11422.

Santos, C.X., Hafstad, A.D., Beretta, M., Zhang, M., Molenaar, C., Kopec, J., Fotinou, D., Murray, T.V., Cobb, A.M., Martin, D.*, et al.* (2016). Targeted redox inhibition of protein phosphatase 1 by Nox4 regulates eIF2alpha-mediated stress signaling. EMBO J *35*, 319-334.

Saraste, J., and Marie, M. (2018). Intermediate compartment (IC): from pre-Golgi vacuoles to a semi-autonomous membrane system. Histochem Cell Biol *150*, 407-430.

Schapiro, F.B., and Grinstein, S. (2000). Determinants of the pH of the Golgi complex. J Biol Chem *275*, 21025-21032.

Schieber, M., and Chandel, N.S. (2014). ROS function in redox signaling and oxidative stress. Curr Biol *24*, R453-462.

Schroder, E., and Eaton, P. (2008). Hydrogen peroxide as an endogenous mediator and exogenous tool in cardiovascular research: issues and considerations. Curr Opin Pharmacol *8*, 153-159.

Selyunin, A.S., and Mukhopadhyay, S. (2015a). A Conserved Structural Motif Mediates Retrograde Trafficking of Shiga Toxin Types 1 and 2. Traffic *16*, 1270-1287.

Selyunin, A.S., and Mukhopadhyay, S. (2015b). A Conserved Structural Motif Mediates Retrograde Trafficking of Shiga Toxin Types 1 and 2. Traffic *16*, 1270-1287.

Sepulveda, M.R., Vanoevelen, J., Raeymaekers, L., Mata, A.M., and Wuytack, F. (2009). Silencing the SPCA1 (secretory pathway Ca2+-ATPase isoform 1) impairs Ca2+ homeostasis in the Golgi and disturbs neural polarity. J Neurosci *29*, 12174-12182.

Sewell, R., Backstrom, M., Dalziel, M., Gschmeissner, S., Karlsson, H., Noll, T., Gatgens, J., Clausen, H., Hansson, G.C., Burchell, J.*, et al.* (2006). The ST6GalNAc-I sialyltransferase localizes throughout the Golgi and Is responsible for the synthesis of the tumor-associated sialyl-Tn O-glycan in human breast cancer. J Biol Chem *281*, 3586-3594.

Singh, M., Sharma, H., and Singh, N. (2007). Hydrogen peroxide induces apoptosis in HeLa cells through mitochondrial pathway. Mitochondrion *7*, 367-373.

Smith, R.D., and Lupashin, V.V. (2008). Role of the conserved oligomeric Golgi (COG) complex in protein glycosylation. Carbohydr Res *343*, 2024-2031.

Sohen, S., Ooe, H., Hashima, M., Nonaka, T., Fukuda, K., and Hamanishi, C. (2001). Activation of histamine H1 receptor results in enhanced proteoglycan synthesis by human articular chondrocyte: involvement of protein kinase C and intracellular Ca(2+). Pathophysiology *8*, 93-98.

Stefan, C.J., Trimble, W.S., Grinstein, S., Drin, G., Reinisch, K., De Camilli, P., Cohen, S., Valm, A.M., Lippincott-Schwartz, J., Levine, T.P.*, et al.* (2017). Membrane dynamics and organelle biogenesis-lipid pipelines and vesicular carriers. BMC Biol *15*, 102.

Stone, J.R., and Yang, S. (2006). Hydrogen peroxide: a signaling messenger. Antioxid Redox Signal *8*, 243-270.

Sundaramoorthy, V., Sultana, J.M., and Atkin, J.D. (2015). Golgi fragmentation in amyotrophic lateral sclerosis, an overview of possible triggers and consequences. Front Neurosci *9*, 400.

Sutterlin, C., Polishchuk, R., Pecot, M., and Malhotra, V. (2005). The Golgi-associated protein GRASP65 regulates spindle dynamics and is essential for cell division. Mol Biol Cell *16*, 3211-3222.

Tan, X., Banerjee, P., Guo, H.F., Ireland, S., Pankova, D., Ahn, Y.H., Nikolaidis, I.M., Liu, X., Zhao, Y., Xue, Y.*, et al.* (2016). Epithelial-to-mesenchymal transition drives a pro-metastatic Golgi compaction process through scaffolding protein PAQR11. J Clin Invest.

Tang, D., and Wang, Y. (2013). Cell cycle regulation of Golgi membrane dynamics. Trends in cell biology *23*, 296-304.

Tang, D., Xiang, Y., De Renzis, S., Rink, J., Zheng, G., Zerial, M., and Wang, Y. (2011). The ubiquitin ligase HACE1 regulates Golgi membrane dynamics during the cell cycle. Nature communications *2*, 501.

Tang, D., Xiang, Y., and Wang, Y. (2010a). Reconstitution of the cell cycle-regulated Golgi disassembly and reassembly in a cell-free system. Nat Protoc *5*, 758-772.

Tang, D., Yuan, H., Vielemeyer, O., Perez, F., and Wang, Y. (2012). Sequential phosphorylation of GRASP65 during mitotic Golgi disassembly. Biology open *1*, 1204-1214.

Tang, D., Yuan, H., and Wang, Y. (2010b). The Role of GRASP65 in Golgi Cisternal Stacking and Cell Cycle Progression. Traffic *11*, 827-842.

Tang, D., Zhang, X., Huang, S., Yuan, H., Li, J., and Wang, Y. (2016). Mena-GRASP65 interaction couples actin polymerization to Golgi ribbon linking. Mol Biol Cell *27*, 137-152.

Thayer, D.A., Jan, Y.N., and Jan, L.Y. (2013). Increased neuronal activity fragments the Golgi complex. Proc Natl Acad Sci U S A *110*, 1482-1487.

Vanoevelen, J., Dode, L., Raeymaekers, L., Wuytack, F., and Missiaen, L. (2007). Diseases involving the Golgi calcium pump. Subcell Biochem *45*, 385-404.

Wang, Y., Satoh, A., and Warren, G. (2005). Mapping the functional domains of the Golgi stacking factor GRASP65. J Biol Chem *280*, 4921-4928.

Wang, Y., and Seemann, J. (2011). Golgi biogenesis. Cold Spring Harb Perspect Biol *3*, a005330.

Wang, Y., Seemann, J., Pypaert, M., Shorter, J., and Warren, G. (2003). A direct role for GRASP65 as a mitotically regulated Golgi stacking factor. Embo J *22*, 3279-3290.

Wang, Y., Wei, J.H., Bisel, B., Tang, D., and Seemann, J. (2008). Golgi Cisternal Unstacking Stimulates COPI Vesicle Budding and Protein Transport. PLoS ONE *3*, e1647.

Witkos, T.M., and Lowe, M. (2015). The Golgin Family of Coiled-Coil Tethering Proteins. Front Cell Dev Biol *3*, 86.

Wong, M., and Munro, S. (2014). Membrane trafficking. The specificity of vesicle traffic to the Golgi is encoded in the golgin coiled-coil proteins. Science *346*, 1256898.

Xiang, Y., Seemann, J., Bisel, B., Punthambaker, S., and Wang, Y. (2007). Active ADP-ribosylation factor-1 (ARF1) is required for mitotic Golgi fragmentation. J Biol Chem *282*, 21829-21837.

Xiang, Y., and Wang, Y. (2010). GRASP55 and GRASP65 play complementary and essential roles in Golgi cisternal stacking. J Cell Biol *188*, 237-251.

Xiang, Y., and Wang, Y. (2011). New components of the Golgi matrix. Cell Tissue Res *344*, 365-379.

Xiang, Y., Zhang, X., Nix, D.B., Katoh, T., Aoki, K., Tiemeyer, M., and Wang, Y. (2013). Regulation of protein glycosylation and sorting by the Golgi matrix proteins GRASP55/65. Nature communications *4*, 1659.

Xie, G., Wang, F., Peng, X., Liang, Y., Yang, H., and Li, L. (2018). Modulation of Mast Cell Toll-Like Receptor 3 Expression and Cytokines Release by Histamine. Cell Physiol Biochem *46*, 2401-2411.

Xu, C., Ma, H., Inesi, G., Al-Shawi, M.K., and Toyoshima, C. (2004). Specific structural requirements for the inhibitory effect of thapsigargin on the Ca2+ ATPase SERCA. J Biol Chem *279*, 17973-17979.

Yadav, S., and Linstedt, A.D. (2011). Golgi positioning. Cold Spring Harb Perspect Biol *3*.

Zampese, E., and Pizzo, P. (2012). Intracellular organelles in the saga of Ca2+ homeostasis: different molecules for different purposes? Cell Mol Life Sci *69*, 1077-1104.

Zhang, X., Cheng, X., Yu, L., Yang, J., Calvo, R., Patnaik, S., Hu, X., Gao, Q., Yang, M., Lawas, M.*, et al.* (2016). MCOLN1 is a ROS sensor in lysosomes that regulates autophagy. Nature communications *7*, 12109.

Zhang, X., Wang, L., Ireland, S.C., Ahat, E., Li, J., Bekier Ii, M.E., Zhang, Z., and Wang, Y. (2019). GORASP2/GRASP55 collaborates with the PtdIns3K UVRAG complex to facilitate autophagosome-lysosome fusion. Autophagy, 1-14.

Zhang, X., Wang, L., Lak, B., Li, J., Jokitalo, E., and Wang, Y. (2018). GRASP55 Senses Glucose Deprivation through O-GlcNAcylation to Promote Autophagosome-Lysosome Fusion. Developmental cell *45*, 245-261 e246.

Zhang, X., and Wang, Y. (2015). GRASPs in Golgi Structure and Function. Frontiers in Cell and Developmental Biology *3*, 84.